INFORMATION TO USERS

This manuscript has been reproduced from the microfilm master. UMI films the text directly from the original or copy submitted. Thus, some thesis and dissertation copies are in typewriter face, while others may be from any type of computer printer.

The quality of this reproduction is dependent upon the quality of the copy submitted. Broken or indistinct print, colored or poor quality illustrations and photographs, print bleedthrough, substandard margins, and improper alignment can adversely affect reproduction.

In the unlikely event that the author did not send UMI a complete manuscript and there are missing pages, these will be noted. Also, if unauthorized copyright material had to be removed, a note will indicate the deletion.

Oversize materials (e.g., maps, drawings, charts) are reproduced by sectioning the original, beginning at the upper left-hand corner and continuing from left to right in equal sections with small overlaps. Each original is also photographed in one exposure and is included in reduced form at the back of the book.

Photographs included in the original manuscript have been reproduced xerographically in this copy. Higher quality 6" x 9" black and white photographic prints are available for any photographs or illustrations appearing in this copy for an additional charge. Contact UMI directly to order.

UMI

A Bell & Howell Information Company
300 North Zeeb Road, Ann Arbor MI 48106-1346 USA
313/761-4700 800/521-0600

BAROTROPIC CIRCULATION VARIABILITY ON CANADIAN ATLANTIC SHELVES

By

Joško Bobanović

SUBMITTED IN PARTIAL FULFILLMENT OF THE
REQUIREMENTS FOR THE DEGREE OF
DOCTOR OF PHILOSOPHY
AT
DALHOUSIE UNIVERSITY
HALIFAX, NOVA SCOTIA
December 10, 1997

© Copyright by Joško Bobanović, 1997

National Library of Canada
Acquisitions and Bibliographic Services
395 Wellington Street
Ottawa ON K1A 0N4
Canada

Bibliothèque nationale du Canada
Acquisitions et services bibliographiques
395, rue Wellington
Ottawa ON K1A 0N4
Canada

Your file Votre référence

Our file Notre référence

The author has granted a non-exclusive licence allowing the National Library of Canada to reproduce, loan, distribute or sell copies of this thesis in microform, paper or electronic formats.

L'auteur a accordé une licence non exclusive permettant à la Bibliothèque nationale du Canada de reproduire, prêter, distribuer ou vendre des copies de cette thèse sous la forme de microfiche/film, de reproduction sur papier ou sur format électronique.

The author retains ownership of the copyright in this thesis. Neither the thesis nor substantial extracts from it may be printed or otherwise reproduced without the author's permission.

L'auteur conserve la propriété du droit d'auteur qui protège cette thèse. Ni la thèse ni des extraits substantiels de celle-ci ne doivent être imprimés ou autrement reproduits sans son autorisation.

0-612-36549-2

Canada

DALHOUSIE UNIVERSITY

FACULTY OF GRADUATE STUDIES

The undersigned hereby certify that they have read and recommend to the Faculty of Graduate Studies for acceptance a thesis entitled "Barotropic Circulation Variability on Canadian Atlantic Shelves"

by Joško Bobanović

in partial fulfillment of the requirements for the degree of Doctor of Philosophy.

Dated: November 28, 1997

External Examiner

Research Supervisor

Examining Committee

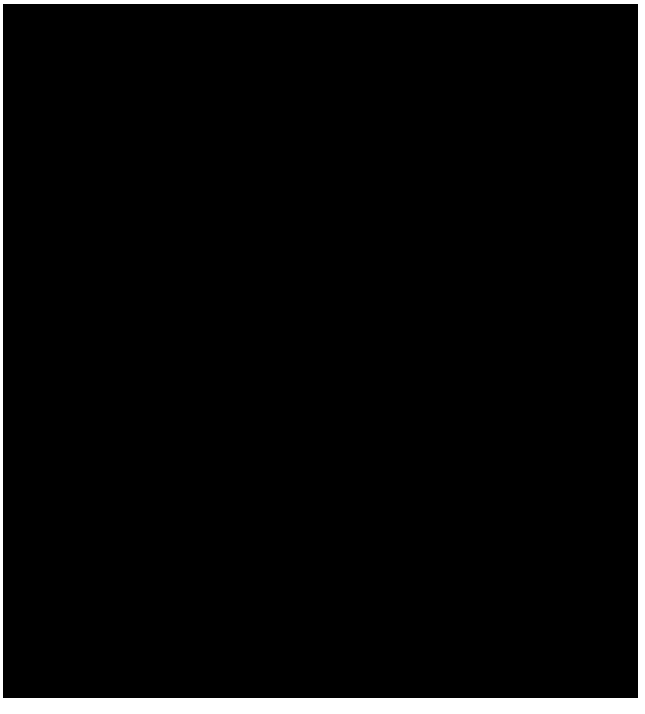

DALHOUSIE UNIVERSITY

Date: **December 10, 1997**

Author: **Joško Bobanović**

Title: **Barotropic Circulation Variability on Canadian Atlantic Shelves**

Department: **Oceanography**

Degree: **Ph.D.** Convocation: **May** Year: **1998**

Permission is herewith granted to Dalhousie University to circulate and to have copied for non-commercial purposes, at its discretion, the above title upon the request of individuals or institutions.

Signature of Author

THE AUTHOR RESERVES OTHER PUBLICATION RIGHTS, AND NEITHER THE THESIS NOR EXTENSIVE EXTRACTS FROM IT MAY BE PRINTED OR OTHERWISE REPRODUCED WITHOUT THE AUTHOR'S WRITTEN PERMISSION.

THE AUTHOR ATTESTS THAT PERMISSION HAS BEEN OBTAINED FOR THE USE OF ANY COPYRIGHTED MATERIAL APPEARING IN THIS THESIS (OTHER THAN BRIEF EXCERPTS REQUIRING ONLY PROPER ACKNOWLEDGEMENT IN SCHOLARLY WRITING) AND THAT ALL SUCH USE IS CLEARLY ACKNOWLEDGED.

Contents

List of Tables

List of Figures

Abstract

Barotropic variability of the Canadian Atlantic Shelf on synoptic time-scales is examined using data analysis, statistical and dynamical models. The main objective is to understand the connections between the subregions and develop models that can be used operationally. Data are used to determine dominant scales, run statistical models and validate dynamical models. Data assimilation is used to infer open boundary conditions for the dynamical models. In the first study synoptic variability of the Labrador Shelf is examined using a limited area model. Wind and upstream boundary forcing are found to be the most important sources of the variability. Based on model results a forecasting scheme is designed and tested. The second subregional study concentrated on the variability in the Gulf of Saint Lawrence. Boundary forcing via Cabot Strait is found to be the dominant source of variability. Data analysis indicates the presence of resonances in the Gulf, some of which can be related to wind and boundary forcing. In the last study, a large scale model of the Canadian Atlantic Shelf forced by wind and air pressure is used to examine connections between the regions. The model showed very good predictive skill for sea level and along-shore coastal currents. The wind driven flow from the Newfoundland Shelf is the most dominant source of remote variability for the Gulf of Saint Lawrence and the Scotian Shelf. High frequency signals from the Newfoundland Shelf can cross the Laurentian Channel and directly force the Scotian Shelf. Non-isostatic pressure forcing within the domain is negligible. The model driven by forecast winds can be run operationally to predict sea level and currents variability or supply boundary conditions for more sophisticated limited area model.

Symbols

English Letters

a	generalized Lagrange multiplier
$\mathbf{B_i}$	dynamical matrix at one model time step
b_i	regression coefficient in the statistical model
C	constant
c	gravity wave speed
c_i	regression coefficient for suboptimal boundary prediction
$\mathbf{D}$	dynamical matrix of the full system
D	length of the strait
d_i	regression coefficient for suboptimal boundary prediction
E	Lagrange multiplier for sea level
e	statistical model error
F	bottom stress (F^{λ},F^{ϕ})
f	Coriolis parameter
g	gravity
$\mathbf{H}$	matrix that maps state variables to observation locations
h	water depth
J	cost function
K	number of lags in the statistical model

k	coefficient
L	Lagrange function
l	radius of the basin
n	number of time steps
P	power spectral density
p	pressure
p_a	surface air pressure
Q	surface area of the basin
R	radius of the Earth
r	friction coefficient
s	forcing vector
T	period
t	time
U	Lagrange multiplier of u component of the flow
u	longitudinal component of depth averaged velocity
V	Lagrange multiplier of v component of the flow
v	latitudinal component of depth averaged velocity
W	width of the strait
w	vertical velocity
$w_{i,j}$	weighting function
$\mathcal{X}$	dynamical matrix mapping forcing to observation points
x	state vector
y	generalized observation
$\hat{y}$	model counterpart of observation y

Greek Letters

α	amplitude at the open boundary
β	amplitude at the open boundary at discrete times
γ^2	measure of model fit
Δ	infinitesimal difference in time or space
η	sea level
θ	generalized forcing term for the adjoint system
κ	coherence
λ	longitude
μ	kinematic viscosity
ρ	density
Σ	covariance matrix
σ	frequency
τ	wind stress ($\tau^{\lambda}, \tau^{\phi}$)
ϕ	latitude
Ψ	structure function for the open boundary
ω	interpolation function

Acknowledgments

Many people contributed to the success of this thesis. Special thanks go to my supervisor Keith Thompson for his help and supervision. He had useful suggestions when the currents shifted, provided the fuel when the sails were down and always pointed to the Pole-star when I lost my compass in these troubled waters. Tony Bowen, Qiang Fu, John Loder and Dan Wright were always on hand to watch my steps, criticise when needed or praise when deserved. Dan Wright often had key comments or some useful reference on hand that helped me understand difficult problems. Dan Kelley and Barry Ruddick attempted to pass some of their knowledge to me during my first years of study. Sheng Jinyu was always open for questions and discussion that helped me make my first modelling steps. Steve Matheson made me understand that computers are not as powerful as I thought. Jackie Hurst helped with so many little things that make life easier.

Many other people made the long Halifax winters seem shorter: Boey Jir Ping is praised for all the sleepless nights we spent together discussing the world, dancing or eating. I'd like to thank comrade Xu Zhigang for excellent food and long and inspiring conversations. Jasmine Bartlett and Christine Pequignet organised most of the social life and cheered a lot of cloudy days. Poppy never lacked good humor and time to discuss problems. Phil MacAulay and Brian May suffered through the same classes with me. I also thank other fellow students Estelle, Karin, Michael, Karen, Dave.

Financial support through research grants from the Department of Fisheries and Oceans Canada and IBM Environmental Research Prediction Programme is gratefully acknowledged.

Chapter 1

Introduction

The Canadian Atlantic Shelf stretches over more than 20 degrees of latitude (Figure 1.1). It is broad and irregular with a number of banks, channels and bays that strongly influence the shelf circulation. The circulation is particularly energetic in the so called meteorological or synoptic band, the periods of two to ten days. The shelf has been long recognized as a guide for shelf waves that are generated by atmospheric systems propagating across the region and also by wind and surface air pressure forcing that acts remotely. Thus, the Canadian Atlantic Shelf is an interesting setting to study synoptic band variability on the continental shelf.

The Canadian Atlantic Shelf consists of several subregions: the Labrador Shelf, Newfoundland Shelf, Gulf of Saint Lawrence, Scotian Shelf and the Gulf of Maine. In recent years we have witnessed an increase in research activity throughout the whole region. A number of field studies (e.g. OLABS, CASP, OPEN, ERP) have provided comprehensive data sets. Most of the research, however, has been local in character (e.g. Smith, 1983; Petrie et al., 1987; Greenberg and Petrie, 1988; Schwing, 1989; Lynch et al., 1996; Thompson and Sheng, 1996), i.e. concentrated on one subregion in isolation. The dynamics of the interactions between the different shelf subregions have not been fully explained. This has left a number of open questions, some of which will be the focus of this thesis.

Modelling has improved our understanding of the shelf circulation (e.g. Davies and Flather, 1978; Hukuda et al., 1989; Lynch et al., 1996). Present day models are highly

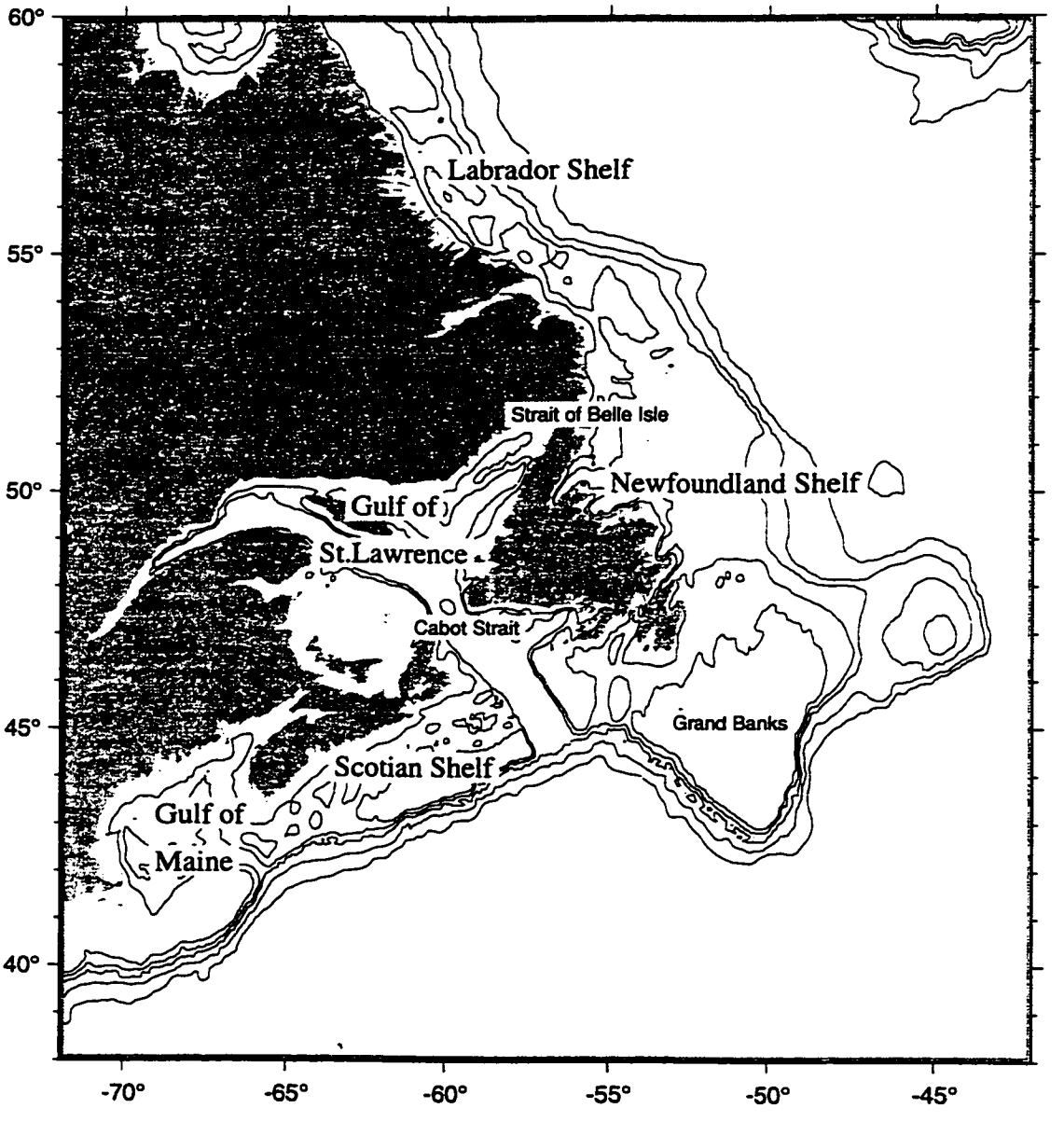

Figure 1.1: Canadian Atlantic Shelf bathymetry. The thin contours correspond to depths of 100, 200, 500, 1500 and 2500 m.

sophisticated and include complex physics (e.g. turbulence closure schemes, density fields that can evolve with the flow). However, the output from these models is generally difficult to interpret. Further, these complex models rely on a large number of observations for initialization and specification of the surface and lateral boundary conditions. In this thesis the emphasis is on simple models that can explain the bulk of the variability in the synoptic band. When considering subtidal variability in the synoptic band on a continental shelf, appropriate information about the open boundaries is of critical importance. The approach taken here is to infer the open boundary conditions by assimilating observations recorded in the interior of the model domain. Data assimilation (Ghil and Rizzoli, 1991; Bennett, 1992) provides a sequence of flow fields that are consistent with both the observations and the underlying dynamics. The variational form of data assimilation used in the present study also allows the testing of hypotheses about the structure and forcing of the circulation.

Two types of problem are addressed through this thesis: scientific questions and operational modelling issues. Scientific questions relate to the connections between the subregions and effects of local and boundary forcing in the synoptic band. The specific questions that apply to each of the subregions are listed in the next section. Apart from the fundamental scientific interest, this region is of growing interest to operational modellers. This is primarily due to intensification of maritime transportation activities that require improved ice predictions and more search and rescue operations; the need for emergency response to oil spills, problems related to fisheries management and numerous aquacultural projects. Therefore, in parallel with the scientific problems, a number of operational modelling issues are addressed. The most important operational application is forecasting the shelf flow. This type of activity is typically associated with limited time availability and thus requires efficient solutions to the open boundary problem. In that context, the use of simple models is advantageous because the number of observations necessary to run and update boundary conditions is small, and validation of the forecasts is much easier. Throughout the thesis, a number of operationally suitable models are developed and tested.

1.1 Objectives of the Thesis

The overall objectives of the thesis are to improve our understanding of the connections between the subregions of the Canadian Atlantic Shelf and to develop models that can be used operationally. These two objectives are complementary because they both require better understanding of the regional physical oceanography and solutions for practical modelling problems.

The objectives are realized by first modelling separately the subregions. This is followed by a large-scale analysis of the whole region. This approach allows the comparison of limited area and large-scale models.

On the Labrador Shelf the synoptic variability in coastal sea level, bottom pressure and currents is examined using a limited area model with data assimilation. A number of questions are addressed: What is the role of local and remote forcing? Can a model with simple dynamics and data assimilation account for the influence of the offshore forcing? Is the southern Labrador Shelf decoupled from the northern shelf? Can we use the results from the model with data assimilation to develop a forecasting scheme for Labrador Shelf circulation? Is the Labrador Shelf an important source of variability for the downstream subregions?

In the second subregional study the following issues related to the circulation of the Gulf of Saint Lawrence are addressed: What are the relative contributions of wind and boundary forcing to the synoptic variability in the Gulf of Saint Lawrence? Can wind and boundary forcing explain some of the resonant frequencies found in the data? This study should improve our knowledge of the synoptic variability of the Gulf of Saint Lawrence and its influence on the Scotian Shelf and the Gulf of Maine.

The two subregional studies are complemented by a large-scale analysis of the Canadian Atlantic Shelf which examines the importance of the connectivity between the subregions. It addresses the following questions: What is the relative importance of the upstream shelves as a source of remote variability for the Gulf of Saint Lawrence and the Scotian Shelf? Does the Laurentian Channel act as a barrier for coastal trapped waves propagating along the Newfoundland Shelf? How much of the variability in sea level and currents is due

to local non-isostatic air pressure forcing? This study should improve our understanding of the interactions between different subregions.

1.2 Thesis Outline

- Chapter 2: An overview of the regional oceanography is presented. Major issues and outstanding problems are discussed.
- Chapter 3: Data sets used throughout the thesis are described. The statistical model used to examine the relationship between the forcing functions and the response is presented. This is followed by a detailed description of the dynamical model and the assimilation scheme used to infer open boundary conditions.
- Chapter 4: Barotropic variability on the Labrador Shelf is examined. Data sets are statistically analysed. The dynamical model is then used to hindcast the flow on the Labrador Shelf. A number of experiments explore different boundary conditions and their effect on model fit. Based on the fully assimilative model runs, a suboptimal prediction scheme is developed and tested.
- Chapter 5: Synoptic variability in the Gulf of Saint Lawrence is examined with a particular emphasis on the resonances of the system. First the effect of local wind is analysed. Different model experiments are used to identify the sources of the resonances found in the observations. A data assimilative model is then used to account for the boundary forcing through the Strait of Belle Isle and Cabot Strait.
- Chapter 6: The entire Canadian Atlantic Shelf is modelled. The model is forced by wind and air pressure fields. The skill of the model is validated against sea level and current observations. Transport variability through the boundaries of the subregions is analysed to determine the connections between the subregions of the model domain. The relative importance of wind forcing over each of the subregions is studied and their contribution to the overall variability quantified. Operational extensions of the large-scale model are then discussed.

- Chapter 7: General conclusions of the thesis and recommendations for future work are given in this chapter.

Chapter 2

Description of Regional Oceanography

The eastern Canadian seaboard is characterized by broad shelves with rugged bottom topography. Along the shelves a chain of shallow banks is interrupted by deep basins and troughs that influence the flow on all scales. The shelves are separated from the deep ocean by a steep continental slope. In addition to bottom variability, several coastline features - gulfs, straits and bays - leave their signature on both the mean flow and its variability. Several large scale circulation features are present in the adjacent northwestern Atlantic, notably the Labrador Current and the Gulf Stream. The shelf region is also exposed to major atmospheric disturbances, propagating both from the continental interior and along the US coast. The forcing mechanisms for the shelf circulation include wind stress and air pressure, buoyancy input, interaction with large scale oceanic features (Smith and Schwing, 1991) and open boundary forcing. The open boundary forcing is comprised of remotely generated tidal forcing, air pressure variations over distant areas (e.g. Hudson Bay), buoyancy input from distant areas, etc. Direct gravitational forcing at tidal frequencies is negligible (e.g. Godin, 1972).

The wind forcing influences the shelf circulation both locally and remotely (Smith, 1983; Thompson et al., 1986; Schwing, 1989). Together with air pressure variations, wind is considered to be a major generating force for the coastal trapped waves that propagate along mid-latitude shelves (Schwing, 1989; Middleton and Wright, 1989; de Young et al., 1995). Isostatic response to pressure variations over Hudson Bay (Wright et al., 1987;

de Young et al., 1995) and the Gulf of Saint Lawrence (Koutitonsky and Bugden, 1991) provides forcing to the Labrador Shelf and Scotian Shelf, respectively. The influence of the large-scale wind field on the sea level variability on the Labrador and Newfoundland Shelves has been demonstrated several times (Thompson et al., 1986; Greatbatch et al., 1990; de Young et al., 1995).

Buoyancy input has a considerable impact on the circulation of the Canadian Atlantic Shelves. The primary source is the fresh water carried by the outflow from Baffin Bay, Hudson Bay and the Saint Lawrence estuary. Most previous research has concentrated on the Labrador Current. It has been studied numerically, theoretically and observationally, starting with the early works of Smith (1937), all the way to recent modelling (Greatbatch et al., 1989) and observational (Lazier and Wright, 1993) efforts. The recent studies suggest that, although the Labrador Current is energetic (Lazier and Wright, 1993), its main branch does not strongly affect the shelf circulation on synoptic time-scales. This might be due to its position along the slope, so the interactions are apparently dominated by baroclinic instabilities (LeBlond, 1982). The inshore branch of the Labrador Current is an important component of the flow on the southern Labrador Shelf (Lazier and Wright, 1993). Sheng and Thompson (1996) in a recent diagnostic calculation of baroclinic currents on the Newfoundland Shelf calculated the seasonal changes in the flow. Little is known about buoyancy forcing on shorter time-scales (e.g. synoptic or weekly variations). Considering the complex topography and a considerable fresh water input along all of the Canadian Atlantic Shelves one could expect that the buoyancy forcing plays a significant role in the currents variability on smaller scales through its interaction with topography (JEBAR), baroclinic instabilities, etc.

2.1 Labrador Shelf

The Labrador Shelf is about 200 km wide and 1000 km long (Figure 1.1). Several banks are separated by deep saddles (for example, Hopedale Saddle reaches a depth of 680 m). The commonly used definition of the shelf break by the 200 m isobath does not apply here,

and I choose to define the offshore edge of the shelf by the 700 m isobath. The fact that the shelf edge is at about 700 m (although not clearly defined by the strong gradient in the topography, as in other shelf regions) is an important point and has a significant impact on the cross-shelf transport and the propagation of coastal trapped waves (Middleton and Wright, 1991).

Garrett et al. (1985) analysed coastal sea level and air pressure variations at Nain and found a significant non-isostatic response on meteorological time scales. This motivated Wright et al. (1987) to examine the effect of Hudson Bay forcing on the northern part of the shelf. They formulated a simple dynamical model and found that wind stress and pressure variations over Hudson Bay could explain the nonisostatic responses found by Garrett et al. (1985). Thompson et al. (1986) examined the response of monthly mean sea level at Nain and were able to separate the responses to local and remote components of the wind forcing. Webster and Narayanan (1988) applied a rigid lid barotropic model and confirmed the importance of Hudson Bay for the coastal trapped signal on the Labrador Shelf. Both Wright et al. (1987) and Webster and Narayanan (1988) showed that the coastal sea level variability at Nain and the depth integrated currents at Saglek Bank were dominated by the first two coastal trapped wave modes. A data set collected between 1985 and 1987 provided the basis for a detailed analysis of coastal trapped waves by Middleton and Wright (1991). They compared variously-forced analytical models and found that most of the variability in coastal sea level can be accounted for by coastal trapped waves. Moving offshore, the bottom pressure variability decreases and the deep ocean forcing seems to have a more significant impact. Middleton and Wright (1989) found a rapid alongshore decrease in amplitude attributed to the complex topography, but the coastal signal persisted as far south as St. John's, Newfoundland. Middleton and Wright (1991) also found large-scale coherence between coastal sea level and near-coastal bottom pressures. Based on statistical analysis of bottom pressure and wind stress Wright et al. (1991) suggested the importance of the offshore forcing on the large scale bottom pressure variations.

A wind driven model of the NW Atlantic was used by Greatbatch et al. (1990) to study the influence of local and remote wind forcing on the seasonal shelf circulation. They

showed that the wind driven model could explain a significant portion of the seasonal sea level variability on the Labrador Shelf. A more sophisticated diagnostic model with a rigid lid that included stratification and JEBAR effects (Sarkisyan and Ivanov, 1971) was applied to the same region by de Young et al. (1992). Middleton and Wright (1989) suggest that the JEBAR term might be important for the cross-isobath transport at the shelf break. De Young et al. (1992) included an 'ad hoc' diagnostic baroclinic term in their model and found that baroclinic forcing of that form did not improve the model predictions for sea level and bottom pressures. The lack of improvement was attributed to the fact that the internal Rossby radius is much smaller than the shelf width (Middleton and Wright, 1989). As a result, de Young et al. (1995) left out density effects and allowed for the free surface. They confirmed that Hudson Bay was a major source of shelf waves on the Labrador Shelf. Its influence decreases as the waves move southwards along the shelf, i.e. away from the source (Gill and Schumann, 1974; Middleton and Wright, 1989). However, it appears clear that the role of the baroclinicity remains an open issue because the model used by de Young et al. (1992) did not allow for the density field to evolve with time.

Despite intensive research, several questions regarding variability on the Labrador Shelf remain unanswered. The relative importance of local wind versus boundary forcing for pressure and currents variability remains to be addressed. More specifically, the dynamical aspects of the offshore influence on synoptic time-scales, addressed statistically by Middleton and Wright (1989), require further exploration. The current variability on synoptic time scales, apart from the study by Webster and Narayanan (1988), has not been addressed. Finally, operational models require a simple, but efficient scheme to predict the time evolution of the open boundary conditions.

2.2 Newfoundland Shelf

The Newfoundland Shelf is an extension of the Labrador Shelf, though significantly broader (Figure 1.1). Its southeastern part is dominated by the Grand Bank, a large shallow bank with depths less than 100 m. Just east of the Grand Bank is Flemish Cap, an isolated

sea mount that splits the Labrador Current into two branches (Greenberg and Petrie, 1988; Hukuda et al., 1989). The western boundary of the Newfoundland Shelf includes two straits - the Strait of Belle Isle and Cabot Strait.

Greenberg and Petrie (1988) examined the circulation on the Newfoundland Shelf using a depth-integrated nonlinear barotropic model. The forcing was provided by two branches of the Labrador Current - an inshore jet and an along-slope jet. They found strong topographic steering of the currents. The results of their steady-state model show quantitative agreement with observations. Steering by the f/h contours was later confirmed by Hukuda et al. (1989) in their steady 3-D model. Hukuda et al. (1989) also separated the influences of the offshore and inshore branches of the Labrador Current. The offshore branch follows the slope and splits in two, one branch going around Flemish Cap, and the other continuing southward. This branch also accounts for the bulk of the coastal flow along the Avalon Channel. Their analysis shows that the inshore branch is only weakly confined to the coast and that most of the water eventually leaks out to the shelf break. The suggestion is that this is due in part to the orientation of the f/h contours. The coastal current flowing through the Avalon Channel continues westward and is joined by the slope branch which then enters the Gulf of Saint Lawrence through the northern side of Cabot Strait. The northern side of Cabot Strait is very deep and the fate of the signal from the Newfoundland Shelf is not known (Koutitonsky and Bugden, 1991). The signal could enter the Gulf of Saint Lawrence via a narrow jet along the northern side of Cabot Strait, part of the signal could enter the Gulf and the other part cross the Laurentian Channel or divert to the open ocean. This question certainly requires further research.

Greatbatch et al. (1990) found that wind forcing may account for the difference between the sea level observed at St. John's and the seasonal steric height anomalies. De Young et al. (1995) used a wind and pressure driven model to predict bottom pressure variability and found the best fit to observations on the Grand Bank. They explained this good fit by the closed isobaths that isolate the Grand Bank from remote influences, such as shelf waves propagating along the Labrador and Newfoundland coast. De Young et al. (1995) did not make an attempt to examine the current variability on synoptic time scales, so that

still remains to be analysed.

2.3 Gulf of Saint Lawrence

The Gulf of Saint Lawrence is a semi-enclosed sea with complex bottom topography (Figure 1.1). It is connected to the shelf through Cabot Strait (500 m depth; 105 km width) and the Strait of Belle Isle (60 m depth; 15 km width). Its topography is dominated by the deep Laurentian Channel that reaches a depth of 550 m. This channel separates the Gulf into two topographically distinct regions: a southern, uniformly shallow plateau - the Magdalene Shallows; and the more complex areas around Anticosti Island and along the Labrador coast.

Buoyancy input by rivers is considered to be the major contributor to the Gulf's estuarine circulation (Koutitonsky and Bugden, 1991). This input is mostly governed by the Saint Lawrence estuary runoff (Trites, 1972), with some impact (83% vs 17%) from other rivers (Koutitonsky and Bugden, 1991). The major variability in the buoyancy forcing is seasonal, although significant interannual variability has been observed. The seasonal variability is associated with the freshwater pulse following the snow-melt in spring. During the summer, the buoyancy fluxes are dominated by the surface heating that results in the thermocline formation (Koutitonsky and Bugden, 1991). Fresh water input, in general, is not highly variable on synoptic time scales (Koutitonsky and Bugden, 1991). When present, typically in spring events, this variability is small, when compared to the wind induced synoptic variability. Trites (1972) found evidence of transient eddy-like features in drifter tracks in the Gaspé region of the lower St. Lawrence estuary that could be attributed to the freshwater pulses by the Gaspé Current.

The Gulf is located on two major storm tracks - 'Northern storms' move eastward over the North American continent and 'Southern storms', move north-eastward along the Atlantic coast of North America (Murty, 1984). Due to the presence of mountains in the Gaspé region and around the lower St. Lawrence estuary, geostrophic calculations of the wind field may have substantial errors in coastal regions (Herfst, 1984). The size of the

Gulf is comparable to that of an atmospheric system, therefore the propagation of storms is expected to generate different responses in the surface Ekman layer around the Gulf (Saunders, 1977). So far, the wind forcing has been recognized as a major contributor to the synoptic variability, but its relative importance, when compared to the open boundary forcing, remains to be determined.

The dynamics of the Strait of Belle Isle was first analysed by Dawson (1907) who examined the influence of the cold and fresh water from the Labrador Shelf. He found that flow through the Strait could be in either direction, last for several days, and was strong enough to reverse the tidal current. His conclusion was that this variability was due to synoptic forcing originating either in the Gulf or on the Newfoundland Shelf. Later, Huntsman et al. (1954) pointed out that an inflow can be found on the northern side and an outflow on the southern side of the strait. Garrett and Petrie (1981) analysed data collected by Farquharson and Bailey (1966) to show that the flow through the strait is associated with a sea level difference across the strait. In other words, the strait is in geostrophic balance. They found the flow to be coherent with the wind stress (not the geostrophic wind), particularly for winds parallel to the west coast of Newfoundland. Using current-meter data and hydrographic observations, Petrie et al. (1988) calculated the net transport to be Gulf-ward and of the order of $0.13 \times 10^6 m^3 s^{-1}$.

Cabot Strait, surprisingly, has received very little attention. It is the Gulf's major connection to the North Atlantic Ocean. It consists of two flow regions: inflow through the deep eastern section and a broader outflow through the shallower western region (Koutitonsky and Bugden, 1991). The Cabot Strait is believed responsible for flushing the intermediate fresh layer through the Laurentian Channel (El Sabh, 1977). It may also act as a remote source of the synoptic variability for the Scotian Shelf (Schwing, 1992).

Remote forcing of the Gulf of Saint Lawrence through the Strait of Belle Isle and Cabot Strait has been primarily studied in terms of steady state or seasonal changes in the flow. The importance of remote forcing at synoptic frequencies remains unclear. Observations show evidence of resonances at periods of 35 and 15 hours that have yet to be examined. The question remains as to whether these resonant responses are due to local wind or

boundary forcing.

2.4 Scotian Shelf

The Scotian Shelf is an approximately east-west oriented shelf off the coast of Nova Scotia. Its northeastern boundary is often defined by the Laurentian Channel (e.g. Schwing, 1989). Its southwestern boundary is defined by the Northeast Channel that separates the Scotian Shelf from the Gulf of Maine. The offshore boundary is defined by a shelf break at 200 m.

The Scotian Shelf is one of the best studied regions off Canada's east coast (e.g. Smith et al., 1978; Smith, 1983; Petrie et al., 1987) . Several major projects (CASP, OPEN, ERP) have helped improve our understanding of subtidal circulation variability in this region. Schwing (1992) used a frequency dependent barotropic model to show that the coastal signal propagates southwestward and that its strength, as expected from theory, decreases offshore. Later Thompson and Sheng (1996) used a 3D barotropic model to examine the influences of the upstream and offshore boundaries as well as the local wind stress. They confirmed the importance of the coastal trapped wave forcing and addressed the possible influences of the offshore boundary, finding that it can have considerable impact away from the coast. This is particularly true for the forcing that originates at the mouth of the Laurentian Channel in the northeastern corner of the Scotian Shelf. Sheng and Thompson (1997) used data assimilation to infer the important boundary conditions that control the variability on the shelf and improve model hindcasts. Based on the results from the data assimilative model, an operational model has recently been developed to forecast the circulation on the Scotian Shelf.

All of the previous studies recognized the importance of the open boundaries for the Scotian Shelf variability. One of the major questions is the interaction of the Scotian Shelf with the upstream regions of the Gulf of Saint Lawrence and the Newfoundland Shelf. Thompson and Sheng (1996) speculate that the form of the upstream forcing may depend on the frequency, but that still remains to be determined. The relative importance of the Gulf of Saint Lawrence and the Newfoundland Shelf wind driven flow is an important issue

that must be addressed when operational modelling is contemplated.

2.5 Summary

Despite intensive research a number of outstanding questions remain regarding the variability on synoptic time-scales. In all subregions, the importance of the boundary forcing has been recognized, however, its importance has not been quantitatively compared to the local forcing. As discussed, the bottom topography of the region is complex, but its effect on the connections between the regions remains unclear.

As stated in the introduction, the models used in this thesis are simple. The focus of interest will be on the connections between the regions and the effects of boundary forcing. Buoyancy forcing and its effects on synoptic variability will not be considered. It is however important to recognize that the density field could play a significant role in generating the small scale variability. Moreover, the buoyancy forcing could play a significant role at synoptic time-scales in the areas of highly-variable topography through JEBAR, baroclinic instabilities, etc.

Chapter 3

Data and Models

One of the most common ways of improving our understanding of shelf circulation has been through the use of models. The models range from conceptually simple statistical models to complex numerical models based on the dynamics of shelf circulation. In this study I will focus on simple dynamical models. As discussed above, they require little data to run and their results are easier to interpret. Moreover, the operational versions of such models are typically easier to implement and require less computation time to run.

Throughout this thesis the observations are an integral part of the modelling effort. They are used extensively to determine the dominant spatial and temporal scales, examine dynamical relationships and validate dynamical model results. The data are also used to infer the time evolving flow through the open boundaries. This is done using the adjoint data assimilation technique that provides a dynamically consistent way of mapping interior observations to the open boundaries of the model.

Two kinds of models are used in this thesis: linear statistical and linear dynamical models. The statistical models are based on regression. They provide a powerful tool when trying to describe the basic relationships between the forcing and response. Conceptually simple and efficient, they help us explore dynamical concepts and guide the development of dynamical models.

Dynamical models are, however, the only way to quantify and understand cause and effect. Once the dynamical models are validated against observations, their results can

be generalized and regional dynamics explored in detail. The fact that both the statistical and dynamical models are linear is of importance here because their predictive skill can be compared if they have the same inputs. The statistical model provides the best linear prediction of a dynamical variable and a large discrepancy between the skill of the statistical and dynamical models should indicate a problem with the dynamical model.

I will now describe the data sets available. This will be followed by a description of the statistical model, and a discussion of its advantages and weaknesses. Finally, the dynamical model and the data assimilation procedure are described.

3.1 Observations

In this section the observations used in the thesis are presented. Their detailed analysis is left for later chapters. (A more detailed description of the observations including their locations, availability and examples of the time series is given in Appendix A.) The data sets are in the form of time series of coastal sea level, bottom pressure, currents, surface wind and air pressure (Figure 3.1).

Most of the oceanographic data (coastal sea level, bottom pressure and currents) were obtained from the Bedford Institute of Oceanography. Additional tide gauge data from the Gulf of Saint Lawrence were supplied by the Marine Environmental Data Service (MEDS). The oceanographic data were analysed for tides and residuals were calculated. Sea level time series were isostatically adjusted to remove the inverse barometer effect. Typical adjusted sea level time series at locations in the Gulf of Saint Lawrence and on the Scotian Shelf are shown in Figure 3.2.

Wind and pressure measurements over the open shelf are sparse and typically not sufficient to resolve the spatial variability. Coastal measurements usually require corrections for local orographic effects and are not representative of the wind field over the shelf. Therefore, it has been common to use model generated wind fields (ECMWF, FNOC, AES) to analyse the response in the ocean or drive the models. Such wind fields usually assimilate

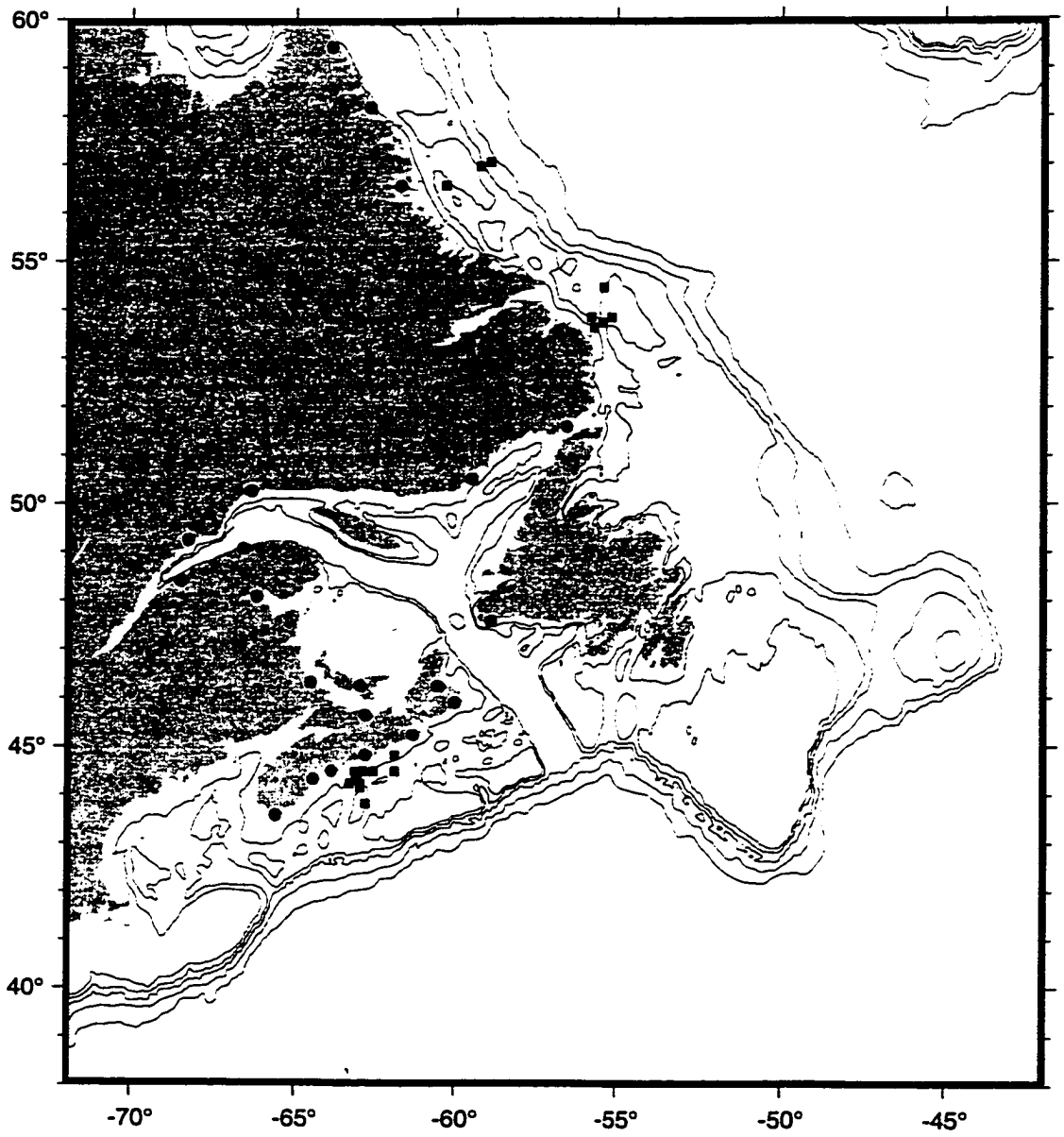

Figure 3.1: Observations locations. Dots mark coastal sea level gauges. Squares mark bottom pressure or current meter locations. Contours correspond to depths of 100, 200, 500, 1500 and 2500 m.

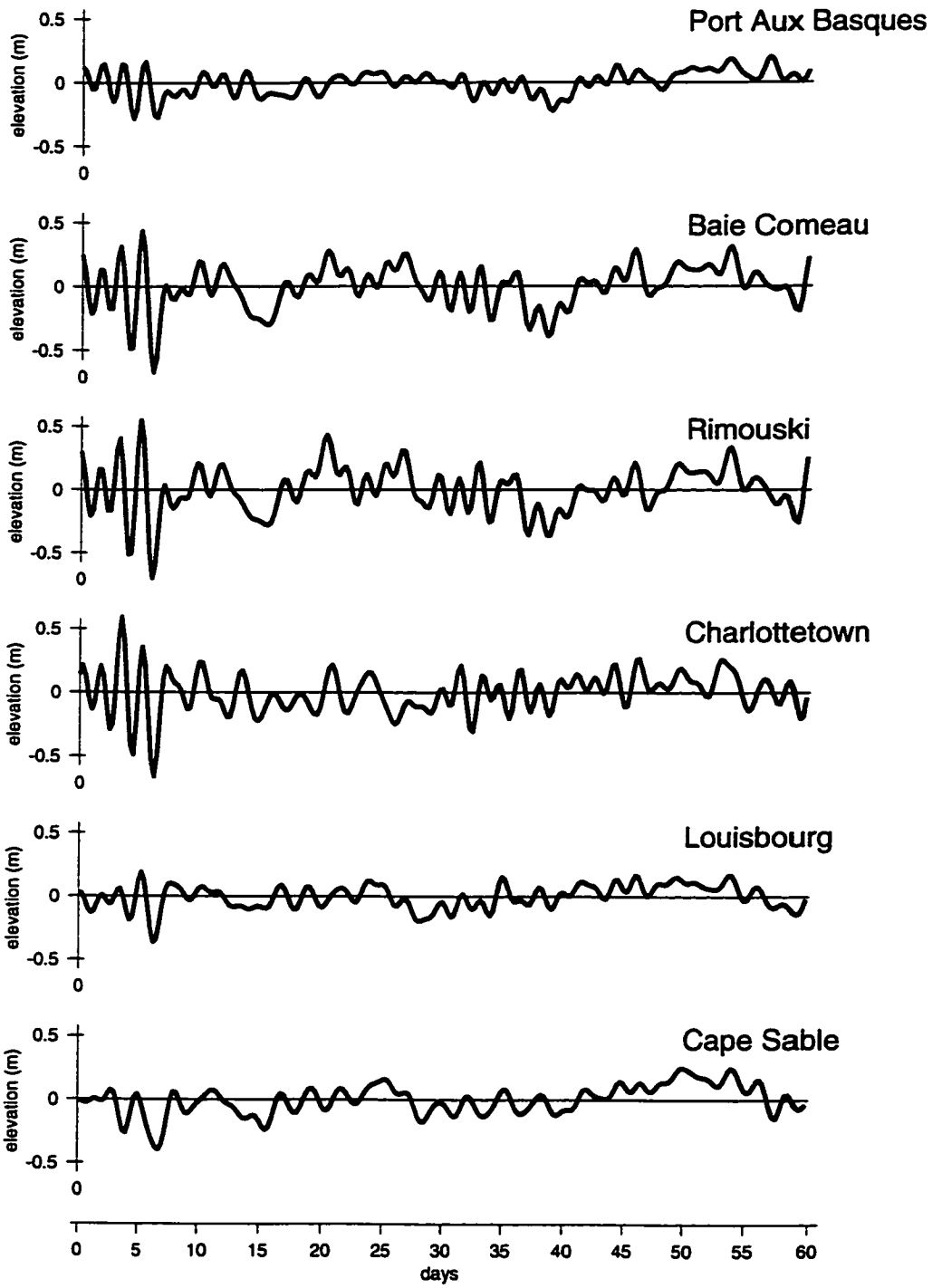

Figure 3.2: Time series of adjusted sea level for January and February 1986. The locations of the tidal gauges are shown on Figure 3.1. The time series have been filtered and periods shorter than 36 hours have been removed.

all the available data and provide dynamically consistent fields that can be considered optimal. In the present study surface wind and pressure data from the European Centre for Medium Range Weather Forecasts (ECMWF) were used, with a spatial resolution of 2.5^o and time step of 12 hours. The wind field was for 10 m above the sea surface. Wind stress was calculated using the Large and Pond (1981) bulk formula, which allows the drag coefficient to depend on wind speed. Both wind stress and surface pressure fields were linearly interpolated to the model grid of $1/12^o$.

The bathymetry was obtained from the ETOPO-5 data set. The resolution was $1/12^o$ (Figure 3.1). Some changes to the deep ocean bathymetry were required to facilitate the modelling and they will be discussed in the later chapters. Otherwise, the original bathymetry was not changed or smoothed except for the coastal areas where some small islands were removed and minimum water depth set to 20 meters.

3.2 Statistical Model

The statistical model is linear and based on regression in the time domain. This kind of model provides a useful and efficient tool that may help us understand the influence of various forcing functions. For example, the statistical model can be used to examine the influence of wind forcing (over different regions) on sea level and current variability on the shelf. The advantage of the statistical model is that it offers a simple way of separating the variance that can be accounted for by different forcing functions. The statistical model, however, can be used only to make predictions at the locations where data are available, i.e. it could not be extrapolated to provide estimates of dynamical variables at other locations. Another problem with the statistical models arises from covariation of the true forcing functions. If, for example, two forcing functions are correlated, say wind and buoyancy forcing, but one of them omitted from the analysis, the statistical model would incorrectly estimate the contribution of the included forcing. That contribution could be either positive or negative, depending on the covariance between the two forcing functions. Finally, the estimation of model parameters needs caution: over-fitting is an ever present concern.

Following Thompson and Sheng (1996), an observation y_t at time t is expressed as

$$y_t = y_t^s + e_t \tag{3.1}$$

where y_t^s, in the general case, is defined by

$$y_t^s = \sum_{k=0}^{K} \sum_i b_k^i s_{t-k}^i \tag{3.2}$$

Here y_t represents any observed quantity, s_{t-k}^i any forcing function (sea level, bottom pressure, wind stress or their combination), b_k^i regression coefficient and e_t a residual incoherent with model inputs. Physically, the model assumes that any observation can be represented as a linear combination of the forcing functions, plus a part that is incoherent with the inputs. The index k stands for the lags used in the model. The number of lags (K) is chosen using the Akaike Information Criterion (AIC; Akaike, 1974). The method involves successive runs of the statistical model with larger number of lags to search for the minimum AIC. Typically, the optimal number of lags span about 3 days. The particular choice of K will be discussed later.

The fit of the statistical model is defined by

$$\gamma_{min}^2 = \frac{var(y_t - y_t^s)}{var(y_t)} \tag{3.3}$$

which is the ratio of the hindcast error variance to the observed variance. In the next section a similar value is defined for the dynamical model. This value represents the relative size of the residual variance, i.e. that proportion of the variability that is completely incoherent with the model inputs. Values of γ_{min}^2 are between 0 and 1, where 0 represents a perfect fit and 1 no predictive skill at all.

As mentioned above, one of the problems with statistical modelling is that forcing functions are usually correlated. Consequently, it becomes increasingly difficult to interpret the physical significance of the changes in the model parameters and fit, as more forcing functions are added or removed from the model.

One of the ways to examine the statistical significance of the fit is by using the phase randomisation procedure described by Thompson and Sheng (1996). Suppose the model is forced by sea level and we want to test if the fit to currents observed at downstream locations is statistically significant. First, the fit is calculated with the original sea level series and the γ^2_{min} value is stored. Then, the sea level series is transformed by calculating its Fourier transform and randomising the phase of the transform. Such a transform is inverted and used instead of the original sea level series to force the statistical model. This procedure is repeated for a large number of realizations (typically 300 is enough) and corresponding values of γ^2_{min} are stored. The result is a distribution for γ^2_{min} that can be compared to the value obtained with the original sea level forcing. If the model fit is significantly different from zero at the 5% level, at least 95% of the γ^2_{min} values from randomized series should be larger (corresponding to poorer fits) than the original value. This procedure can be generalized for the cases where several forcing functions are used. Thus, when a new forcing is added, the improvements in the model fit that arise from adding this new forcing can be estimated by randomising this new forcing function and repeating the procedure as described.

In conclusion, it is clear that statistical models have limitations, however they provide a simple and efficient tool that can help us understand general relationships between the forcing functions and the response. The statistical model cannot provide a definitive result regarding the relative importance of different forcing functions. It does not address the question of the dynamical interactions between the forcing and the response. The only way to address those questions and overcome the limitations of a statistical model is to use a dynamical model.

3.3 Dynamical Model

The dynamical model, unlike the statistical model, provides predictions of dynamical variables at all locations within the model domain. The dynamical model, however, cannot

separate the variance into a part explained and a part not explained. The reason is simply that errors in the dynamical model predictions can remain coherent with the forcing. Specifically, if an observation is given by $y_t = y_t^m + e_t$, the dynamical model variance, unlike the statistical model variance, does not split into two parts because $var(y_t) = var(y_t^m) + var(e_t) + 2cov(y_t^m, e_t)$. Thus, we cannot speak about the proportion of the variance accounted for by the dynamical model. However, if we drive the model with, say, winds, it is possible to talk about the magnitude of the wind effect, which is simply given by $\sqrt{var(y_t^m)}$.

When data assimilation is used, the validation of model results requires particular attention. Due to the character of data assimilation and its goal of minimizing the squared misfit between the model prediction and the data, it is better if an independent data set, not assimilated into the model, is used to validate the model.

Model Formulation

The model used in this thesis is based on horizontal momentum and continuity equations (e.g. Gill, 1982)

$$\frac{d\vec{u}}{dt} + f\hat{z} \times \vec{u} = -\frac{1}{\rho}\nabla p + (\mu \vec{u}_z)_z \tag{3.4}$$

$$w_z = -\nabla \cdot \vec{u} \tag{3.5}$$

The notation is standard (see glossary) with $d\vec{u}/dt$ being total derivative (including advection terms) of horizontal velocity and w vertical velocity. Subscripts indicate differentiation. Csanady (1982) shows that for many shelf problems the advection of momentum, i.e. nonlinear terms in the momentum equations, can be neglected. In other words, the Rossby number (the ratio of the advection to Coriolis term) is small. For the problems considered here, with typical shelf velocities of 0.1 m/s and a horizontal length scale of several tens of kilometers, the Rossby number is at most of order 10^{-1}. Assuming that the fluid is hydrostatic

$$p_z = -\rho g \tag{3.6}$$

and barotropic (no horizontal density gradients), the hydrostatic equation (3.6) can be integrated from the free surface (η) to level z=0 to give the following expression

$$p|_{z=0} = p_a + \rho g \eta \tag{3.7}$$

where p_a is atmospheric pressure at the sea surface. The pressure gradient at z=0 is $\nabla p_a + \rho g \nabla \eta$. The assumption of a barotropic fluid implies that this is the pressure gradient at all depths. The linearized momentum equations can be vertically averaged to yield, in spherical coordinates

$$u_t - fv = -\frac{1}{\rho R \cos\phi} p_\lambda + \frac{1}{h}[\frac{\tau^\lambda}{\rho} - F^\lambda] \tag{3.8}$$

$$v_t + fu = -\frac{1}{\rho R} p_\phi + \frac{1}{h}[\frac{\tau^\phi}{\rho} - F^\phi] \tag{3.9}$$

Here λ and ϕ are longitude and latitude, respectively and (τ^λ,τ^ϕ) and (F^λ,F^ϕ) are the surface and kinematic bottom stress, respectively. It should be noted that the velocity components (u, v) are the depth averaged velocities.

Assuming standard kinematic boundary conditions at the free surface and the bottom, the continuity equation can be integrated from the bottom to the free surface. For subtidal frequencies, the averaged pumping term $\nabla \cdot [\int_0^\eta \vec{u} dz]$ can be neglected and the continuity equation in spherical coordinates reduces to

$$\eta_t + \frac{1}{R\cos\phi}(uh)_\lambda + \frac{1}{R\cos\phi}(vh\cos\phi)_\phi = 0 \tag{3.10}$$

From (3.7) the pressure at z=0 can be re-expressed as $p|_{z=0} = \rho g \eta'$ where η' is adjusted sea level defined by

$$\eta' = \eta + \frac{p_a}{\rho g} \tag{3.11}$$

If adjusted sea level is substituted for the free surface (η), the governing equations take the following form

$$u_t - fv = -\frac{g}{R\cos\phi}\eta'_\lambda + \frac{1}{h}[\frac{\tau^\lambda}{\rho} - F^\lambda]$$

$$v_t + fu = -\frac{g}{R}\eta'_\phi + \frac{1}{h}[\frac{\tau^\phi}{\rho} - F^\phi] \tag{3.12}$$

$$\eta'_t + \frac{1}{R\cos\phi}(uh)_\lambda + \frac{1}{R\cos\phi}(vh\cos\phi)_\phi = \frac{p_{at}}{\rho g}$$

This form of the equations is convenient because the air pressure forcing appears only in the continuity equation. If there is no air pressure forcing, the right hand side of the continuity equation equals zero and the equations are only forced by surface and bottom stresses.

The wind stress is typically calculated using a drag coefficient and the wind velocity at 10 m above the sea surface (e.g. Gill, 1982). Csanady (1982) argues that for most subtidal shelf applications the bottom stress can be parameterized by a linear drag law that defines stress as a function of local velocity, i.e. $\vec{F} = r\vec{u}$, where r is friction coefficient and has the dimension of velocity. This formulation has been successfully used to model the shelf flow (e.g. Scott and Csanady, 1976). The most common value used for r is $10^{-3}ms^{-1}$ although it is recognized it should depend on the strength of the tidal currents and any other unresolved motions.

Given the above simplifications, the governing equations take the following final form

$$u_t - fv = -\frac{g}{R\cos\phi}\eta'_\lambda + \frac{\tau^\lambda}{\rho h} - \frac{ru}{h}$$

$$v_t + fu = -\frac{g}{R}\eta'_\phi + \frac{\tau^\phi}{\rho h} - \frac{rv}{h} \tag{3.13}$$

$$\eta_t' + \frac{1}{R\cos\phi}(uh)_\lambda + \frac{1}{R\cos\phi}(vh\cos\phi)_\phi = \frac{p_{at}}{\rho g}$$

The suitability of these equations for modelling shelf circulation, on both tidal and subtidal time-scales, has been well demonstrated in the past (e.g. Heaps, 1969; Gill and Schumann, 1974). Heaps (1969) showed that such a system can be used to compute storm surges in shallow seas. The system has been used to describe the propagation of the shelf waves excited by wind (Gill and Schumann, 1974) in a homogeneous ocean. Mysak (1980) showed that limiting cases of the system (3.13) can be used to determine the propagation of edge waves and Kelvin waves. Several authors (e.g. Huthnance, 1975; LeBlond and Mysak, 1978; Church et al., 1986; Brink, 1991) showed the shelf waves can be interpreted as a barotropic limit of the coastal trapped waves using the equations presented.

3.3.1 Forcing

The system defined by (3.13) is forced by wind stress and flow across the open boundaries of the domain. The wind field used to drive the model has been described in the data section. For the purpose of these calculations the wind forcing is considered to be exact, i.e. any uncertainties that may be associated with it will be attributed to the unresolvable model error. It is, indeed, possible to treat wind as an uncertain variable (e.g. Nechaev and Yaremchuck, 1994), however that increases the number of unknowns and poses problems with respect to the conditioning of the assimilation problem (see later).

The other forcing is time varying flow across the open boundaries. Usually, it is difficult to specify such boundary conditions. The approach taken here is to infer open boundary conditions from observations in the interior, using the adjoint data assimilation technique. This method has been successfully applied to shelf circulation by several authors (Bennett and MacIntosh, 1982; Griffin and Thompson, 1996; Bogden et al., 1996). The details of the method and its applications are described in the next section.

It is not necessary to force the model through all boundaries. In the area of interest it has been well established that the downstream boundaries (in the sense of coastal trapped

wave propagation) do not play a significant role. For such a boundary Chapman (1985) tested a number of boundary conditions subject to wind and boundary forcing. One type of boundary condition that has shown reasonable behavior is the radiation boundary condition. For example, the flow normal to one of the boundaries could satisfy:

$$u_n = -\sqrt{\frac{g}{h}} \cdot \eta \tag{3.14}$$

where u_n is depth averaged velocity normal to the boundary and h is local depth. This kind of boundary condition is based on gravity wave propagation and it has been successfully used in many shelf applications (e.g. Davies and Furnes, 1980; Sheng and Thompson, 1993). Although shelf waves, unlike barotropic Kelvin waves, do not propagate with $c = \sqrt{gh}$, it has been shown that radiation boundary conditions such as (3.14) allow for the propagation of information out of the domain in both tidal applications (Davies and Furnes, 1980) and wind driven models (Sheng and Thomspon, 1993). On the other hand, reflected topographic waves generated at the forward boundary propagate slowly into the model domain (e.g. Middleton and Wright, 1988) and are dissipated locally, before strongly influencing the main portion of the model domain, which again justifies the choice of the radiation boundary condition. The propagation speed depends on local depth (h) and experiments have shown that boundaries should be set along areas where the bathymetry does not vary dramatically (Sheng, personal communication). The choice of radiation boundary conditions is also convenient because it keeps the model linear, which simplifies the data assimilation procedure. The particular applications of the radiation boundary condition will be discussed later in the context of different model domains.

The model spin-up time is about 30 hours, so after a few days of integration the model "forgets" the initial conditions. Therefore, the initial conditions do not play a major role and the model integration starts from rest.

3.3.2 Assimilation Scheme

The discrepancy between the model results and the data is quantified using a cost function of the form

$$J = \frac{1}{2}\sum_{i,j}(y_i - \hat{y}_i)w_{ij}(y_j - \hat{y}_j) \tag{3.15}$$

where y's are observations, $\hat{y}$'s their model counterparts and w_{ij} weights.

The dominant controls for the shelf flow are time varying flows through the open boundaries. The number of observations available in the interior of the domain rarely exceeds the number of boundary conditions required, if they are needed at each inflow point and model time step. Suppose we express sea level (or equivalently inflow) at the upstream boundary, in the following form

$$\eta(t, \lambda, \phi) = \sum_i \alpha_i(t)\Psi_i(\lambda, \phi) \tag{3.16}$$

where $\alpha(t)$ is an amplitude that varies in time and $\Psi_i(\lambda, \phi)$ is a spatial structure function that is fixed in time. To overcome the problem of ill-conditioning (Thacker, 1988) certain assumptions are necessary. The first is related to the spatial structure of the functions Ψ_i. We assume that the spatial structures at the open boundary are fixed in time. Therefore, at any time the boundary condition is simply defined by the appropriate amplitudes $\alpha_i(t)$. (The particular choices of functions will be discussed later.) The second assumption relates to the temporal resolution of the controls. Since we are considering subtidal flow, and a typical time step in the model is about one minute, it is not necessary to determine the controls $\alpha_i(t)$ at every time step (Griffin and Thompson, 1996). Instead, an interpolation scheme of the following form can be used

$$\alpha_i(t) = \sum_p \beta_{ip}\omega_p(t) \tag{3.17}$$

where β_{ip} is evaluated at $t = 0, \Delta, 2\Delta$ and $\omega_p(t)$ are interpolation functions. For the shelf flow it is sufficient to use Δ between 3 and 6 hours (Griffin and Thompson, 1996). The imposed temporal smoothness of the boundary amplitude again reduces the number of unknowns since the amplitude is evaluated only every Δ hours and interpolated in between using $\omega_p(t)$. For example, if the model is run for two months, its boundaries defined by two structure functions and their amplitudes updated every 6 hours, the total number of unknown parameters would be 480.

The optimal choice of β minimizes the cost function J, i.e. the data-model misfit. The dynamical model is linear and the choice of β is a solution to the regression problem of the form

$$y = \mathcal{X}\beta + \epsilon \tag{3.18}$$

where $\mathcal{X}$ is a dynamical matrix that maps the forcing to the observation points and ϵ is a random error. The details of the regression approach are outlined in the Appendix B.

Typical number of state variables (u, v and η) involved in my shelf circulation models is on the order of $(n \cdot 10^4)$, where n is the number of time steps. This creates computational problems when trying to solve the regression problem and choose the optimal estimates of β. The problems are solved through integration of the adjoint equations of the model that lead to the gradient of the cost function with respect to controls ($\nabla_\beta J$). The adjoint equations are obtained by differentiating a Lagrange function with respect to the state variables. The details of the adjoint model and its derivation are given in Appendix C.

Once the gradient of the cost function is obtained a minimization method is used to update the controls of the system. In this case I use the linear conjugate gradient algorithm (Gill et al., 1981) that requires one run of the dynamical model and one run of the adjoint model to update the controls and the cost function. The new controls are then used to run the dynamical model and the procedure iterated until the solution converges.

To summarize, in order to solve the regression problem, i.e. choose the optimal boundary conditions, the following iterative procedure is used:

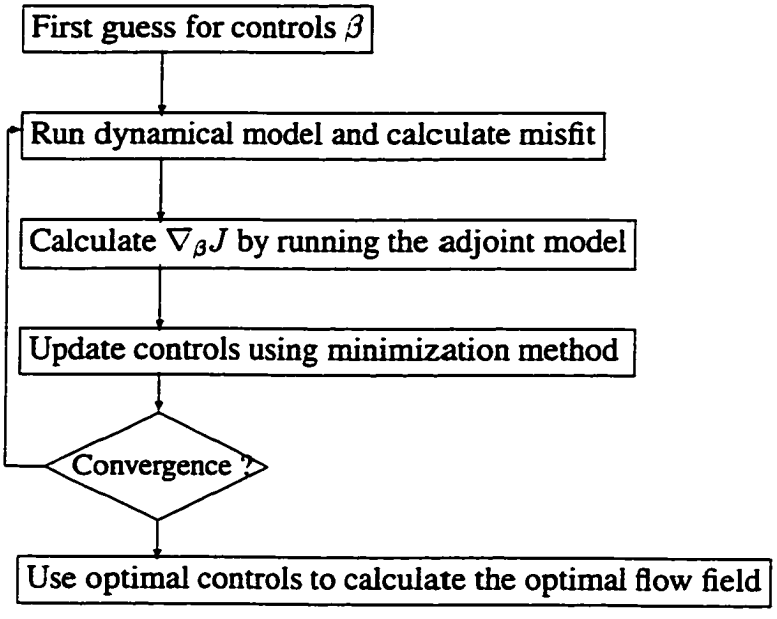

Traditionally data assimilative models are tested by running *identical twin* experiments (Thacker and Long, 1988). First, the dynamical model is used to generate artificial data that are then sampled in the same way as the observations. Second, random noise is added to this *artificial data* that are then used to infer the boundary conditions. This provides a check on the model performance, but can also indicate which observation locations may be more representative for the flow field. A number of such twin experiments were performed for each of the domains used in the thesis. The general conclusion was that the model converges quickly and is able to return the prescribed boundary conditions in less than 10 iterations.

3.3.3 Model Validation

Once the dynamical model hindcasts are obtained, with or without data assimilation, they need to be validated against observations. In the cases when data are assimilated into the

model, the most straightforward way of validation is using an independent set of data that was not assimilated. The procedure of withholding part of the data for validation purposes is particularly useful during the development of the assimilative model. The choice of the data withheld, i.e. the validation subset, is critical for the conclusions about the model performance (Thacker, 1988). Therefore, a suitable experiment would withhold the data from one part of the domain and validate the model based on the assimilation from other parts of the domain. If the model fit at one location is similar for the cases when data were and were not assimilated, one could conclude that the model is robust and that the choice of forcing boundaries was appropriate. The design of validation experiments strongly depends on the domain considered and data available. In this thesis, when data assimilation is used to infer open boundary conditions, current meter data are never assimilated.

The comparison of the skill of the dynamical model against its statistical counterpart is another method of model validation. In a similar fashion as for the statistical model we define γ^2 by

$$\gamma^2 = \frac{var(u_t - u_t^m)}{var(u_t)} \tag{3.19}$$

where u_t^m is now the dynamical model prediction. For the statistical model γ^2_{min} lies between zero and unity, but here γ^2 can have values between zero and infinity. A γ^2 value greater than 1 means that the mean value of the variable is a better predictor than the one produced by the model.

3.4 Summary

The data and models used in the thesis have been described. Two kinds of models were presented. The statistical model provides a simple and efficient tool for the analysis of the shelf response to various forcing functions. The dynamical model however allows for the estimation of complete fields and a dynamical interpretation of the interaction between the forcing and the response. The dynamical model is forced by a spatially varying wind field

and flow through open boundaries. The time-varying flow through the open boundaries is inferred using data assimilation.

If the same measure of the model fit, γ^2, is used for both the statistical and dynamical models, their results can be compared. In the case of the statistical model a γ^2_{min} of 0.3 means that the statistical model can account for 70% of the observed variance. However, in the case of the dynamical model with γ^2 of 0.3 it is incorrect to conclude that 70% of the signal has been accounted for. As discussed, the dynamical model, unlike the statistical model, can not separate the variance into the part explained and a part not explained. For example, imperfections in the dynamical model (e.g. lack of baroclinicity, incorrect drag or bottom friction coefficient) will result in higher value of γ^2 when compared to its statistical counterpart. Therefore, a large discrepancy between γ^2 and γ^2_{min} indicates a problem with the dynamical model. Some improvements can subsequently be made by changing the representation of the open boundaries or adjusting, for example, the friction coefficient.

Chapter 4

Labrador Shelf

The focus of this chapter is synoptic variability of the circulation on the Labrador Shelf (Figure 4.1). Most of the earlier statistical and dynamical modelling studies on synoptic time-scales have concentrated on sea level and bottom pressure. In this study, current data from the southern Labrador Shelf are included in the statistical analysis and used to test the predictions of the dynamical model.

First, the statistical model is used to explore the effects of different forcing functions. The model is forced by wind stress, upstream and offshore sea level. The goal is to estimate the relative importance of different forcing functions on sea level, bottom pressure and current variability. This information will prove useful in the subsequent dynamical model development because it will establish performance limits for any linear model and provide guidance for the specification of the open boundary conditions.

The dynamical model is used to examine the effect of different boundary conditions on the model fit. Upstream and offshore forcing are inferred from sea level and bottom pressure data using the adjoint method of data assimilation. Model results are then validated against the independent set of current observations.

The assimilation runs provide the basis for the development of a suboptimal, but operationally suitable, prediction scheme. The scheme is based on the assumption that only sea level and wind data are available in real time.

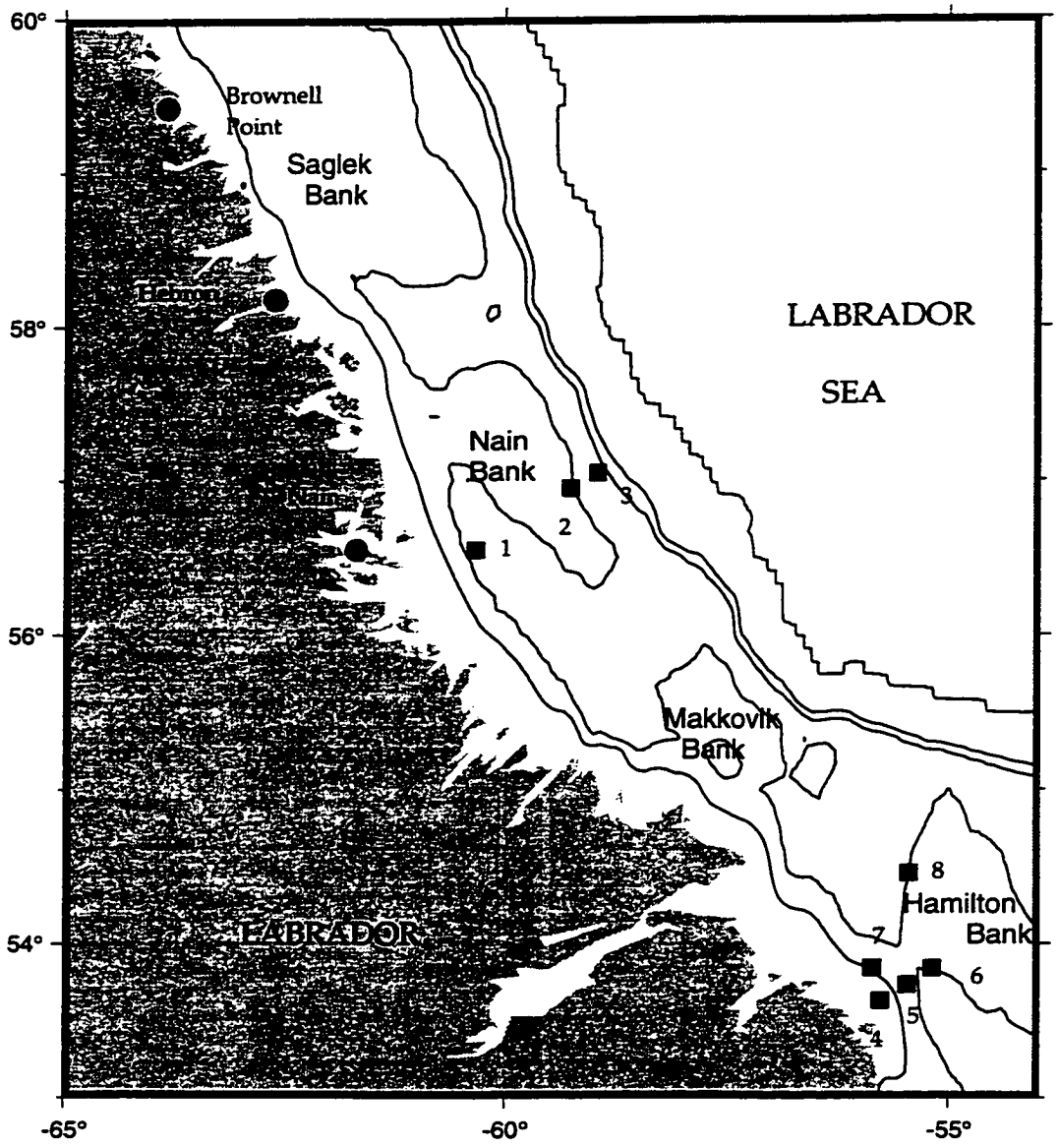

Figure 4.1: Model domain and bathymetry. The resolution of the model is $1/12^{o}$ which corresponds to 9.3 km in the meridional direction. The thin contours correspond to depths of 100, 200, 700, 1000 and 2000 m. The dots mark coastal tide gauges and the squares mark the locations of bottom pressure gauges and current meters. In 1986 coastal sea level data were collected at Brownell Point, Hebron and Nain, bottom pressure data at locations 1, 2, 3, 4 and 6 and current meter data at location 5. In 1987 coastal sea levels were measured at Nain, bottom pressure at locations 1, 2 and 3 and currents at locations 5, 6, 7 and 8.

4.1 Data Analysis

Arrays of bottom pressure sensors, coastal tide gauges and current meters were deployed between 1985 and 1987 on the Labrador Shelf (Figure 4.1). Coastal sea levels were measured on the northern part of the shelf only. Bottom pressure gauges were deployed in lines that ran both cross-shore and along-shore. Current meter data were collected around Hamilton Bank as a part of a long-term monitoring programme of the Labrador Current. All current meters were within 5 m of the bottom.

Power spectra of bottom pressure and currents have energy peaks in the meteorological band (Figure 4.2). Cross-spectra between Brownell sea level (representing the upstream forcing) and downstream bottom pressure gauges p1 and p3 were also calculated (Figure 4.3). The upstream signal from Brownell is coherent with the inshore (p1) pressure gauge at all frequencies with p1 lagging by about 6 hours at periods shorter than 50 hours. The offshore pressure gauge (p3) is coherent with the upstream signal for periods longer than 200 hours. The offshore (p3) also lags by six hours. The bottom pressures from p1 and p3 are highly coherent and in phase for periods longer than 100 hours.

Wright et al. (1991) suggested that the offshore influence is manifested primarily through a spatially uniform, but slow rise and fall of the offshore boundary. It is therefore likely that the coherence at periods longer than 200 hours might be due to offshore forcing. Cross-spectra between the currents from both years and the upstream sea level (not shown here) show significant coherence in the synoptic band. The analysis of the offshore signal (p3) and the current meter data (not presented here) showed that the currents from c5 and c7 were coherent with the offshore signal at periods longer than 100 hours, but the other two current meters (c6 and c8) were not.

Based on spectral analysis only, it is hard to separate the upstream and the offshore signal and their influence on the downstream pressure and currents. I will therefore use a statistical model to try to separate the effects of the various forcing mechanisms. However, it should be noted that cross-spectral analysis and the statistical model, described in Chapter 3, with a single input are very similar. In the limit of infinitely long time series and an infinite number of lags (K) one could calculate γ^2_{min} using the spectral density of the time

series and its coherence with the forcing

$$\gamma^2_{min} = \frac{\int_0^\pi (1-\kappa^2) P_{yy} d\sigma}{\int_0^\pi P_{yy} d\sigma} \tag{4.1}$$

where P_{yy} is the power spectral density of the observation vector y, σ frequency in radians per unit time, and κ coherence.

Current Variability

Before using the statistical model, it is useful to examine the variability of the four current meters deployed during 1987 (c5, c6, c7 and c8, see Figure 4.1). Complex correlation coefficients between all pairs are shown in the first panel of Figure 4.4. Correlations are low (between 0.07 and 0.44), even for the current meters separated by less than 60 km. The phase randomisation procedure described in Chapter 3, was used to determine the significance of the correlations and led to the conclusion that all correlations were statistically significant except for the ones between c8-c5 and c8-c7. The results clearly show that the flow in the vicinity of Hamilton Bank is complex. This is no surprise because previous studies (Lazier and Wright, 1993; Narayanan et al., 1996) have already demonstrated the complexity of the flow in this area. However, additional information is obtained if the flow is decomposed into along and across isobath components. Specifically, for each of the current meters, the along-isobath axis was determined based on the local bathymetry. In Figure 4.4 correlation coefficients for both components of flow are presented. The decomposition shows that the correlations are much higher for the along-isobath component which is presumably part of a larger scale signal. The cross-isobath correlations are much weaker suggesting local generation, perhaps by baroclinic instability. The goal here is to determine the dominant sources of the large-scale synoptic variability and consequently I will concentrate on the along-isobath component of flow.

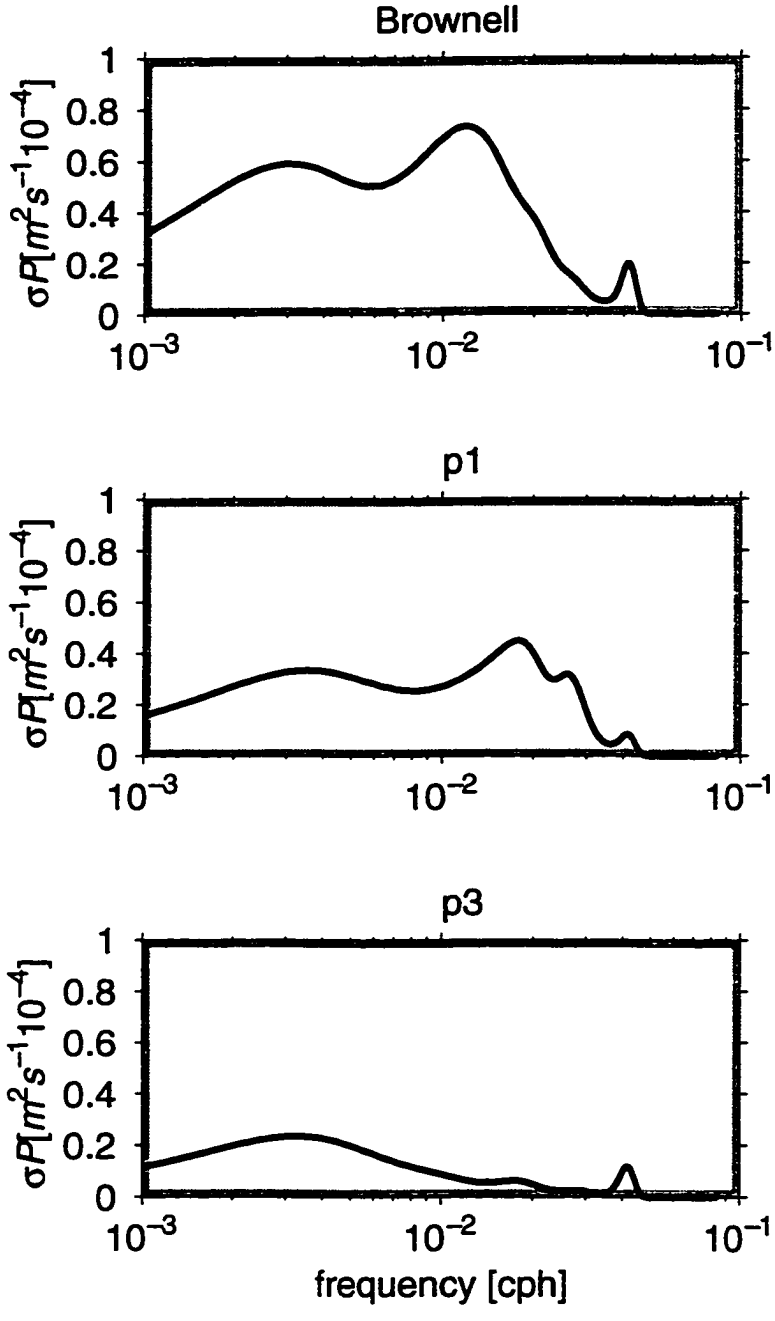

Figure 4.2: Power spectra of sea level at Brownell and bottom pressure at location p1 and p3. The spectra are based on 200 days of data available in 1986. The spectra are shown in variance preserving form.

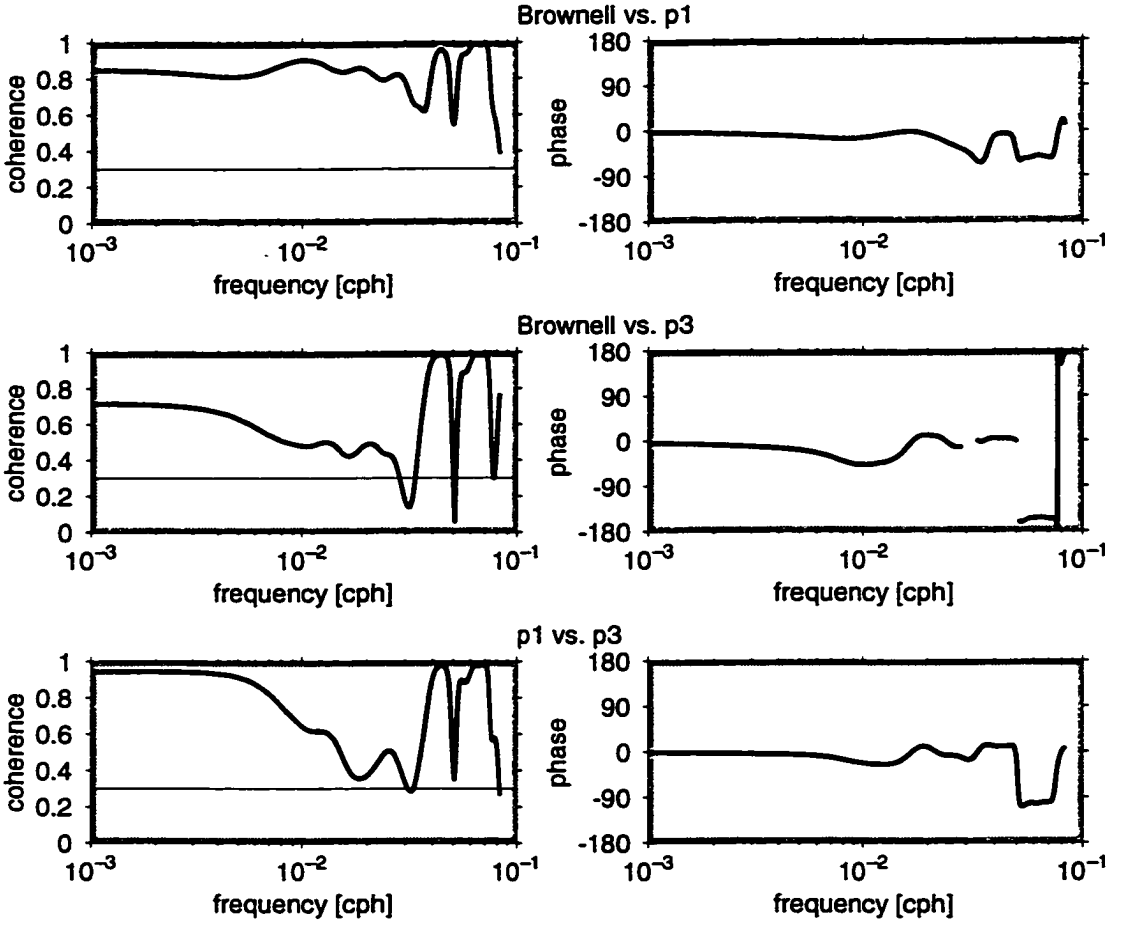

Figure 4.3: Cross-spectra of sea level at Brownell and bottom pressure at stations 1 and 3. The left column shows coherences between the time series. The 5% significance level is shown by the thin line. The right column shows the phase relationship between the time series. The phase is shown only where it is significantly different from zero at the 5% level.

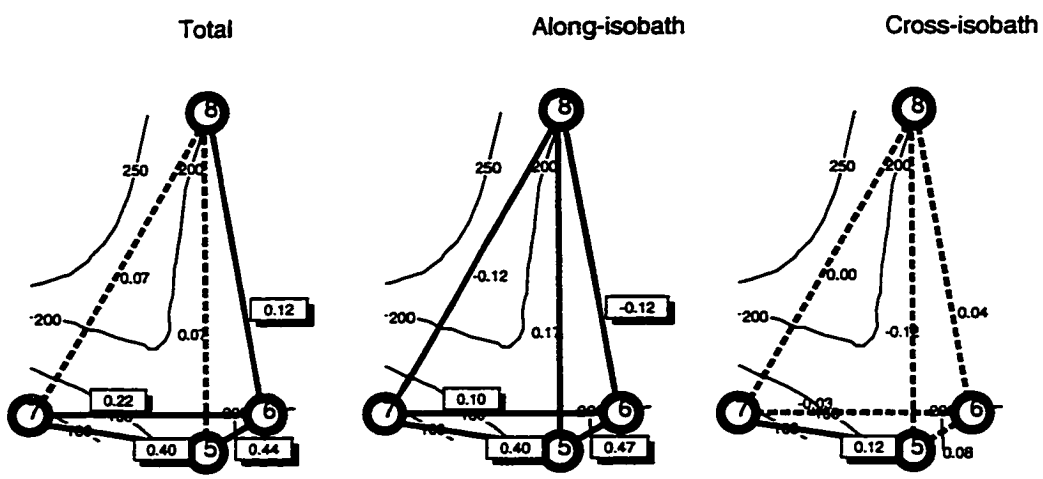

Figure 4.4: Correlation between the currents measured on Hamilton Bank in 1987. The panels show correlations between total flow, local along-isobath and cross-isobath components. Full (dashed) lines denote statistically significant (non-significant) complex correlations. Labels show the magnitude of the complex correlation coefficient for the total flow and correlation coefficient for the along-isobath and cross-isobath component. Boxed coefficients are significantly different from zero at the 5% level.

4.2 Statistical Model

The spectral analysis results indicated that the pressure and current variability at the southern shelf around Hamilton Bank could be related to upstream and offshore variability. In this section statistical models described in Chapter 3 are used to assess the effects of different forcing mechanisms.

For each of the two years a series of statistical models was run with different inputs. The same observation locations were not available each year so the results are not entirely comparable between years. The approach is first to run the statistical models with only one input at a time to estimate the contribution of the particular forcing function to sea level, bottom pressure and current variance. This should give us an idea about the relative importance of the particular forcing function. As discussed before, such a statistical model will also account for the part of the variance that is correlated to some other forcing function. Then, at the end, all of the forcing functions are used to determine the performance limit for a linear model that is driven by wind and sea level. For all models, lags were determined using AIC criterion and the optimal fit was found to be a negative lag of 3 days (positive lags were not considered because they are not physically realizable).

Local Wind Forcing

All data (sea level, bottom pressure and currents) were regressed against two vector wind stresses that were representative of the northern (upper) and southern (lower) portions of the Labrador Shelf. The wind accounts for about 50% of the variance at most of the sea level and bottom pressure stations (Tables 4.1 and 4.2; column Wind). The wind influence is stronger on the southern shelf (stations p4 and p6) which is probably the result of reinforcement of the local wind effect by the wind driven signal from the northern shelf. At the offshore pressure gauges (p2 and p3) the wind accounts for 10-40% of the variance typically 20% less than the variance accounted for at the inshore pressure gauges (p1, p4 and p6). The regression of offshore bottom pressures on the wind stress over the adjacent deep ocean showed that this input could not account for more variance at the offshore locations. The local wind accounts for up to 46% of the along-isobath variance at c5 in 1986.

In the following year wind forcing accounts for only 5-40% of the along-isobath variance. Conclusions based on such a scattered set of results for the currents are difficult, however it appears that the wind is a significant source of current variability closer to the shore (c5 and c6). I note that the along-isobath flow at these two locations had the highest correlation (Figure 4.4), therefore their similar fit is not surprising.

Upstream Forcing

In the next experiment, upstream sea level is taken as forcing function (Tables 4.1 and 4.2; second column). For 1986, I used sea level at Brownell, and for 1987, I used Nain, because no other locations were available. As the upstream signal propagates down the shelf, it is believed to be strongly modified by bathymetry (Middleton and Wright, 1989). In 1986 Brownell sea level accounts for about 80% of the variance at Nain and station p1, but only 40% of the bottom pressure variance on the southern shelf (stations p4 and p6). The Brownell sea level accounts for only 25% of the variability in the along-isobath current at c5. In 1987 the upstream forcing accounts for most of the variability at the inshore pressure gauge p1 and significantly less at the offshore ones. The best fit for the currents was for locations c5 and c6, which is the same as for the wind forced model, and suggested that the signal at these two locations is probably dominated by a coastal trapped wave signal. At current meters c7 and c8 Nain sea level accounted for very little variability. It is interesting to note here that although Nain was used in 1987 as a representative of the upstream signal, the fit for the current meters did not change dramatically. Overall, the results suggest that the upstream signal is an important source of variability, particularly for the sea level and bottom pressure.

Offshore Influence

Middleton and Wright (1991) calculated that the node of the first coastal trapped wave mode in the sea level is located between stations p2 and p3. Therefore, the average bottom pressure from these two stations is taken to represent the offshore forcing for the Labrador Shelf. The statistical model indicates that the offshore signal accounts for a significant part

of the coastal sea level and bottom pressure variance (Tables 4.1 and 4.2; column Off). This result is not surprising because the spectral analysis showed that bottom pressure at p3 is coherent with both sea level and inshore bottom pressures. The offshore signal accounts for only 2-10% of the current variance. This is consistent with the speculation by Middleton and Wright (1991) that the deep ocean influence is manifested through slow changes in the overall level of the adjacent deep ocean. Such changes are expected to have a strong influence on sea level on the shelf.

One of the problems in attempting to quantify the effect of offshore forcing is that it is coherent with the other inputs (e.g. Brownell and p3, Figure 4.3). In the next experiment I assumed that the offshore signal is spatially uniform over the whole shelf and can be removed from all coastal sea levels and bottom pressures by simple subtraction. The average of two offshore pressures (used as forcing in the previous experiment) was taken as the signature of the offshore forcing and subtracted from the sea levels and bottom pressures. Presumably, the dominant part of the signal left after removing the offshore influence will be due to the upstream variability. The fit for the sea level and bottom pressure was calculated using the corrected observations, i.e. the subtracted signal was not added back in. The γ^2_{min} (Tables 4.1 and 4.2; columns B-Off and N-Off) show that the model fit improves at some current meters in 1987 and does not deteriorate at others. This result is encouraging because it suggests that the simple subtraction of the deep ocean level could lead to some improvements in current predictions using the dynamical model.

Summary

The statistical model suggests that the local wind is the most important contributor to the current variability on the Labrador Shelf, particularly the southern shelf. The upstream signal affects the sea levels and bottom pressures, but not currents. Considering the upstream forcing together with the wind forcing (not shown in the table) reduces γ^2_{min} for the currents by an additional 5-10% relative to experiments with one input. The direct offshore forcing affects the pressure signal, but has little influence on the currents. The removal of the offshore signal generally led to slightly improved current predictions.

γ^2_{min}	Wind	Brow	Off	B-Off	All
Brownell	0.52	-	0.59	-	-
Hebron	0.41	0.34	0.84	0.37	-
Nain	0.45	0.21	0.65	0.29	-
p1	0.41	0.28	0.43	0.42	-
p2	0.59	0.54	0.11	0.83	-
p3	0.62	0.62	0.14	0.83	-
p4	0.27	0.64	0.77	0.76	-
p6	0.47	0.64	0.72	0.79	-
c5	0.54	0.76	0.90	0.79	0.28

Table 4.1: Fit of the regression of adjusted sea level, bottom pressure and along-isobath currents in 1986 on various inputs. The numbers are values of γ^2_{min}. The station numbers correspond to locations given on Figure 4.1. Letters *p* and *c* stand for bottom pressure and currents. The inputs to the statistical model are as follows: *Wind*, two wind stresses representative of the upper and lower shelf; *Brow*, coastal sea level at Brownell; *Off*, average of the offshore bottom pressure time series at p2 and p3; *B-Off*, coastal sea level at Brownell corrected for the offshore influence by subtracting the average of the bottom pressure time series at p2 and p3; *All*, all sea levels, bottom pressures and wind stresses.

Overall, the model with the wind, sea level and bottom pressure as inputs can account for between 20% and 70% of the variability in currents (Tables 4.1 and 4.2; columns All). The better fit for the currents in 1986, when all data were considered, is probably the result of using bottom pressure from p4 and p6 as inputs: they capture effectively the geostrophic balance at location c5. If these two pressure gauges are left out, the model accounts for only about 40% of the current variance. In 1987 when all pressure data are used to force the model, less than 50% of the signal was accounted for, which is in accord with the complex character of the currents around Hamilton Bank. The results from the last columns (All) correspond to the fit of the dynamical model runs that assimilate all sea level and bottom pressure data. As previously discussed, they provide a lower bound for the dynamical model performance.

γ^2_{min}	Wind	Nain	Off	N-Off	All
Nain	0.56	-	0.54	-	-
p1	0.61	0.09	0.45	0.15	-
p2	0.77	0.34	0.15	0.53	-
p3	0.90	0.79	0.26	0.53	-
c5	0.60	0.65	0.89	0.62	0.49
c6	0.83	0.71	0.92	0.70	0.57
c7	0.93	0.97	0.98	0.98	0.60
c8	0.95	0.92	0.98	0.90	0.78

Table 4.2: Fit of the regression of adjusted sea level, bottom pressure and along-isobath currents in 1987 on various inputs. The numbers are values of γ^2_{min}. The station numbers correspond to locations given on Figure 4.1. Letters *p* and *c* stand for bottom pressure and currents. The inputs to the statistical model are as follows: *Wind*, two wind stresses representative of the upper and lower shelf; *Nain*, coastal sea level at Nain; *Off*, average of the offshore bottom pressure time series at p2 and p3; *N-Off*, coastal sea level at Nain corrected for the offshore influence by subtracting the average of the bottom pressure time series at p2 and p3; *All*, all sea levels, bottom pressures and wind stresses.

4.3 Dynamical Model Results

In this section, the dynamical model is used to hindcast circulation on the Labrador Shelf. I choose to concentrate on two winter months (January and February) in both years. This period is chosen because the conditions are more likely to be barotropic. Severe winter weather results in a well mixed water column, so the use of the depth integrated circulation model is easier to justify (away from the baroclinic boundary currents). The numerical experiments examine the importance of different forcing functions that are introduced in the same order as for the statistical model. First, the influence of wind stress on bottom pressure and currents is assessed. Different combinations of boundary conditions are then used to examine the importance of the upstream and offshore forcing.

4.3.1 Model Setup

The dynamical model is described in Chapter 3. Here, some details of its application on the Labrador Shelf are presented. The model domain is shown on Figure 4.1. It is defined by the 53°N and 60°N parallels and the 53°W meridian. As discussed in Chapter 2, the bottom topography of the Labrador Shelf is rugged and the classical definition of the shelf break at 200 m does not hold. The shelf break is defined by the 700 m isobath. The topography of the adjacent deep ocean is flattened at 700 m, i.e. all depths are clipped at 700 m. It should be noted that the flattening of the deep ocean may have a significant influence on the shelf flow. The reason is that shelf flow is in general decoupled from the deep ocean in the barotropic limit (Wang, 1982), but the flattening allows for stronger deep ocean influence. This choice is primarily made to increase the computational efficiency of the model. Thus, for the case of a deep ocean at 700 m, the model time step is 40 seconds. If the deep ocean was flattened at 2000 m to allow for more realistic topography the numerical stability criteria would require a model time step of 20 seconds. Considering the iterative character of the assimilation procedure this choice was not computationally feasible. With the deep ocean depth set to 700 m a model run with 6 iterations needed 2 days to run.

Conditions along the 53°N and 54°W open boundaries are radiative (Equation 3.14). The upstream boundary is defined along 60°N (Figure 4.5). A linear setup, controlled by the sea level at the coast and a node at the shelf break, is used to represent the upstream forcing (dashed line in Figure 4.5). In the geostrophic limit this boundary condition is equivalent to uniform flow along the shelf. Statistical analysis has already shown that the character of the offshore forcing might be very complex. In the model the offshore influence is accounted for by forcing the model at its northern boundary in the deep water, i.e. east of the shelf break. The boundary condition is defined by a linear setup that is zero in the northeast corner of the domain and is controlled by the amplitude at the shelf break (Figure 4.5). Therefore, if only the upstream boundary is used, the node at the shelf break is set to zero (dashed line in Figure 4.5). If both upstream and offshore forcing are used, the slope of the upstream boundary is defined by two points: coastal and shelf-break amplitudes (1 and 2 in Figure 4.5). Dynamically this combination of boundary conditions

allows uniform flow along the shelf and another uniform flow of different strength across the northern deep ocean boundary. This choice of the offshore boundary is not an attempt to represent what really happens in the deep water: the dynamics there are probably much more complex. Rather it is an attempt to include an offshore influence to which the shelf can adjust. During model development different forms of the offshore forcing were considered, but the general result was that a boundary too close to the shelf (e.g. boundary condition along the shelf break) caused spurious flows.

4.3.2 Local Wind Forcing

The model is run for the first two months of both 1986 and 1987 with spatially variable wind fields over the shelf. No boundary forcing was imposed. The results are presented in the first column of Tables 4.3 and 4.4.

The wind driven model does not show good skill for the sea level - the residual variances are larger than 57%. The fit improves as we move downstream along the shelf, so the sea level at Nain shows the best fit in both years. The bottom pressure fit varies spatially, but a general feature is that the inshore pressure gauges (p1, p4 and p6) fit better than the offshore ones. The same spatial pattern was obtained for the statistical model, however the γ^2 values for the wind driven model are much higher. The better fit for the downstream pressure gauges shows that the local wind is an important source of the coastal trapped wave energy on the Labrador Shelf. The result is consistent with the Gill and Schumann's (1974) theory of shelf waves and Csanady's (1982) theory of arrested topographic waves, both of which predict the intensification of wind effects at downstream locations.

The fit for the along-isobath currents varies significantly with location and year. The best fit for currents is found at location c5 which is consistent with the statistical model results. The statistical model indicated that the wind is probably the most important source of current variability at the lower Labrador Shelf, but also demonstrated the complexity of the flow around Hamilton Bank. The residual variance at c5 is 68% for 1986, but higher at most locations in 1987. In an attempt to assess the skill of the model on the large scale I averaged the flow at c5, c6 and c7 and the residual variance is now similar to the one

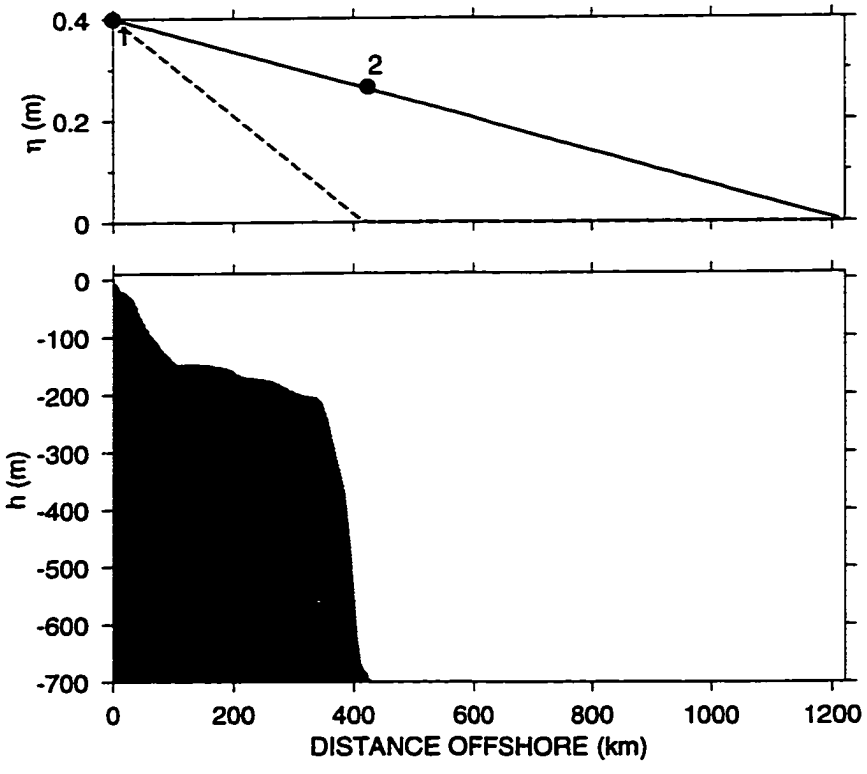

Figure 4.5: Structure functions for the open boundaries on the Labrador Shelf. The dashed line shows the case where model is forced only by the upstream boundary condition, i.e. sea level at the coast (1). The full line shows the case where model is forced by upstream and offshore boundary condition and controlled by the sea level at the coast (1) and on the shelf break (2).

obtained by the statistical model. Considering the relatively coarse wind field used and the lack of stratification and non-linear effects, one can not expect the model to resolve the small scale variability. Therefore, the result for the average of the three current meters is consistent with the statistical model results and close to optimal ($\gamma^2_{min} = 0.70$ for wind driven statistical model).

The model was also forced by the wind acting over the deep water (not presented here), i.e. I allow for the wind field not only over the shelf but over the whole model domain. The rationale was that although the statistical model did not show much sensitivity to offshore winds, it is possible that the offshore wind field might improve model predictions at the shelf break and around Hamilton Bank. This was not the case. One of the reasons might be that the offshore wind forcing is not important for the shelf. More likely, the use of false bottom in the deep ocean affected the exchange between the deep ocean and the shelf.

In summary, I conclude that wind forcing acting over the model domain can not resolve the complete variability on the Labrador Shelf. A wind field with better spatial resolution might slightly improve the model predictions, however it appears necessary to account for the effect of open boundary forcing and probably more realistic offshore topography.

4.3.3 Upstream Forcing

The model is now forced by the wind and a sea level setup across the shelf along 60°N using the upstream boundary condition described earlier. There is no offshore forcing in this experiment (the amplitude at the shelf break is set to zero). The upstream boundary is inferred by assimilating all coastal sea level and bottom pressures. Currents, as mentioned previously, are withheld for model validation. The wind field is set to zero in the deep water. This introduces an artificial curl of the wind stress, however, its effects seem to be negligible as they appear only on one grid cell scale, over the shelf break. This was tested by running the model with and without deep water winds.

The results for 1986 are presented in Figure 4.6 and for both 1986 and 1987 in Tables 4.3 and 4.4. The fit for coastal sea level improves dramatically. This is not surprising given the sea level data were assimilated. In 1986, the γ^2 values are between 0.1 and 0.25, while

γ^2	Wind	W+U	W+U+O	W+U-D
Brownell	**0.98**	0.25	0.18	0.21
Hebron	**0.84**	0.10	0.04	0.05
Nain	**0.75**	0.16	0.12	0.16
p1	**0.88**	0.45	0.15	0.35
p2	**1.14**	0.91	0.49	-
p3	**1.05**	0.79	0.12	-
p4	**0.47**	0.25	0.08	0.14
p6	**0.64**	0.35	0.07	0.20
c5	**0.68**	**0.75**	**0.82**	**0.74**

Table 4.3: Skill of the circulation model for the adjusted sea level, bottom pressure and currents in 1986. The numbers are values of γ^2 (bold for data that were not assimilated). The station numbers correspond to locations given on Figure 4.1. Letters *p* and *c* stand for bottom pressure and current meter. The circulation model fit is presented for the model forced in the following ways: *Wind*, model forced by the wind field over the shelf; *W+U*, model forced by the wind field over the shelf and the upstream boundary condition inferred by assimilating all sea level and bottom pressure data; *W+U+O*, model forced by the wind field over the shelf and the upstream and offshore boundary conditions inferred by assimilating all sea level and bottom pressure data; *W+U-D*, model forced by the wind field over the shelf and upstream and offshore boundary conditions inferred by assimilating all sea level and bottom pressure data that were corrected by the offshore signal, as described in the text.

in 1987 the fit at Nain has a γ^2 value of only 0.05.

The results for bottom pressures improve compared to the wind driven case. The inshore stations (p1, p4 and p6) fit better and the model at some locations leaves as little as 10% of the variability unaccounted for. The fit is also better at stations p4 and p6 on the lower shelf. There are probably two reasons: First, the bottom pressures were assimilated and, second, the local wind and remote forcing effects reinforce on the southern part of the shelf. The model fit for 1987 is typically 30% better than the model fit in 1986 at pressure gauges p1, p2 and p3. One possible reason is that the offshore influence is stronger in 1986. This possibility is addressed in the next section when explicit offshore forcing is considered.

The fit to the along-isobath currents on Hamilton Bank shows large variability. The fit deteriorates at c5 in 1986 with the addition of upstream forcing, but improves in 1987. The model predictions at c7 improve dramatically in 1987, to the point that the residual variance is 75% of the observed variance. At locations c6 and c8 the inclusion of the upstream forcing does not improve the model fit. The dynamical model results are somewhat different from the statistical model where in 1987 the upstream forcing had the largest contribution to the variance at c5 and c6, while the dynamical model prediction improves at c5 and c7, but deteriorates at c6. This represents additional evidence of the complexity of the flow in the vicinity of Hamilton Bank. However, when the average flow at c5, c6 and c7 is considered, the inclusion of the upstream forcing did not significantly change the model fit (Tables 4.3 and 4.4).

4.3.4 Offshore Forcing

As mentioned, the offshore sea level is thought to be a broad, large-scale signal that influences the whole shelf. Therefore, one could expect that the model predictions for the bottom pressure gauges at the shelf break would improve if we account for the offshore forcing. Based on the statistical model results, allowing for an offshore influence should not change dramatically the fit to currents or inshore pressure gauges.

The model is now forced by two open boundaries. In the deep water, the boundary

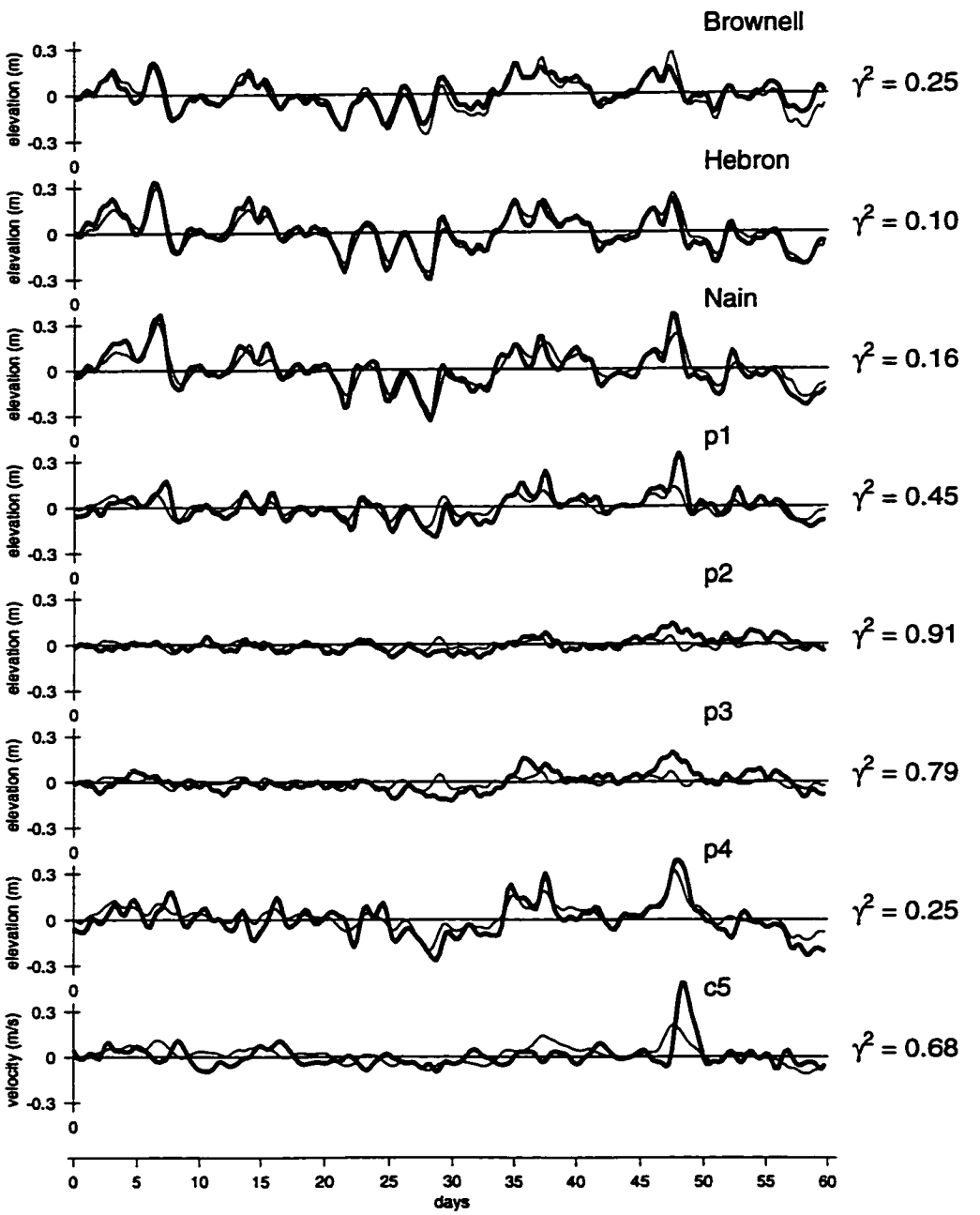

Figure 4.6: Comparison of observed adjusted sea level, bottom pressure and currents and predictions from the model driven by wind and the upstream boundary. The boundary conditions were obtained by assimilating all sea level and bottom pressure data. The thick (thin) line shows observed (predicted) sea level at Brownell, Hebron and Nain and bottom pressure at stations 1, 2, 3, 4 and along-isobath currents at station 5. The period covered is January and February 1986. The value of γ^2 shown to the right of each graph is the variance of the difference between observation and prediction divided by the variance of the observations (Table 4.3, column W+U).

condition described above is controlled by its amplitude at the shelf break (Figure 4.5). The other forcing boundary is cross-shelf setup, as in the previous experiment. As discussed, this combination of boundary conditions does not attempt to resolve the physics in the deep waters of the Labrador Sea, but rather it attempts to provide some approximation of the offshore boundary and assess its potential influence. The wind field is again set to zero in the deep water, so only shelf wind forcing is included. Other model boundaries remain radiative as before. The model is run for the first two months in 1986 and 1987 and the results are presented in Tables 4.3 and 4.4 and Figure 4.7.

As expected, the model fit improves at all sea level locations. The values for γ^2 are now everywhere below 18%. The model accounts for almost all of the variability at Nain in 1987. The fit improves at all bottom pressure locations, particularly at the offshore locations p2 and p3. The model fits better at the downstream bottom pressure gauges as well. This result is not surprising because the statistical model showed that the offshore pressure signal is related to both sea level and inshore bottom pressure. However, the main reason is that the dynamical model now has more free parameters (two time varying open boundary conditions) and the fit should not deteriorate for data that were assimilated into the model.

The most important result is obtained for the fit of the model to data that were not assimilated. The fit to along-isobath currents deteriorates in both years, except for c6 in 1987. Based on the statistical analysis we could have anticipated that the inclusion of offshore forcing would not improve the current predictions.

The improved fit to bottom pressures p4 and p6, but worse fit for the currents, suggests that the assimilation model has been over-fit. It is important to note that the assimilation procedure can give an improved fit even though the dynamics are incorrect. Therefore, as discussed in Chapter 3, it is sometimes critical to have an independent set of observations (currents in this case) to validate the model results.

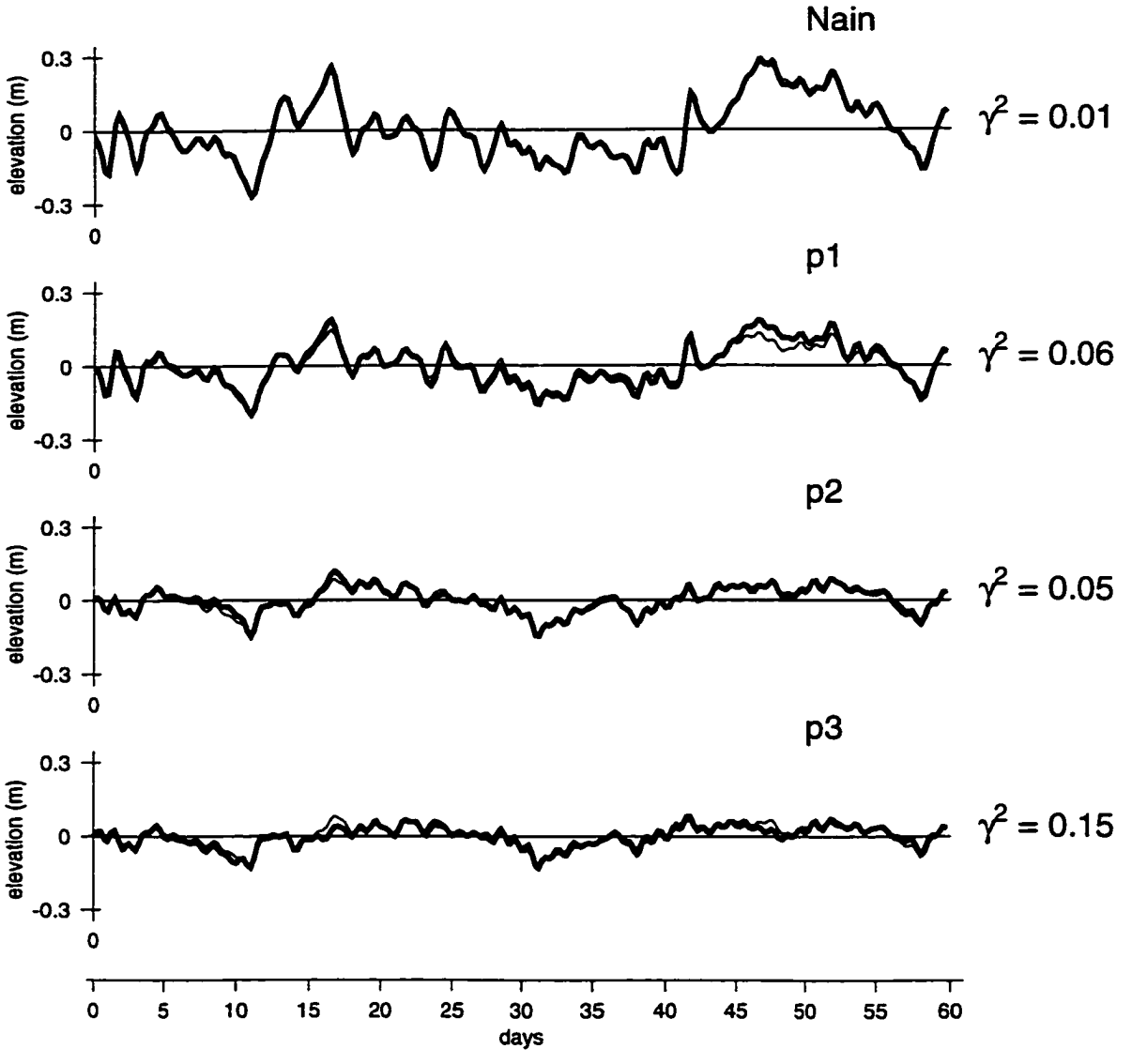

Figure 4.7: Comparison of observed adjusted sea level and bottom pressure and predictions from the model driven by wind and the upstream and offshore boundaries. The boundary conditions were obtained by assimilating all sea level and bottom pressure data. The thick (thin) line shows observed (predicted) sea level at Nain and bottom pressure at stations 1, 2 and 3. The period covered is January and February 1987. The value of γ^2 shown to the right of each graph is the variance of the difference between observation and prediction divided by the variance of the observations (Table 4.4, column Off).

γ^2	Wind	W+U	W+U+O	W+U-D
Nain	**0.57**	0.05	0.01	0.04
p1	**0.93**	0.10	0.06	0.46
p2	**1.09**	0.38	0.05	-
p3	**1.11**	0.45	0.14	-
c5	**1.01**	**0.90**	**0.96**	**0.77**
c6	**1.49**	**1.99**	**1.73**	**1.50**
c7	**1.19**	**0.75**	**0.77**	**0.90**
c8	**1.27**	**1.27**	**1.27**	**1.14**
c5+c6+c7	**0.77**	**0.79**	**0.80**	**0.58**

Table 4.4: Skill of the circulation model for the adjusted sea level, bottom pressure and currents in 1987. The numbers are values of γ^2 (bold for data that were not assimilated). The station numbers correspond to locations given on Figure 4.1. Letters *p* and *c* stand for bottom pressure and current meter. The circulation model fit is presented for the model forced in the following ways: *Wind*, model forced by the wind field over the shelf; *W+U*, model forced by the wind field over the shelf and the upstream boundary condition inferred by assimilating all sea level and bottom pressure data; *W+U+O*, model forced by the wind field over the shelf and the upstream and offshore boundary conditions inferred by assimilating all sea level and bottom pressure data; *W+U-D*, model forced by the wind field over the shelf and upstream and offshore boundary conditions inferred by assimilating all sea level and bottom pressure data that were corrected by the offshore signal, as described in the text.

4.3.5 Offshore Correction

The previous experiment showed that the offshore effects can improve predictions for the sea level and bottom pressure data, but that the dynamics behind those improvements might be incorrect. As mentioned, Wright et al. (1991) suggest that the offshore influence is manifested through spatially uniform variability of the sea level along the shelf break. If that is the case we should be able to 'remove' the offshore influence from all pressure gauges, as was done for the statistical model. The average of the two pressure gauges at the shelf break (p2 and p3) is subtracted from all remaining sea level and bottom pressure time series. It should be noted that dynamically, subtracting a spatial mean from the observed sea level and bottom pressure does not affect pressure gradients, and therefore will have no effect

on the horizontal momentum balance. The new time series are assimilated in the model. The model is again forced by upstream and offshore boundary condition. If the removal of the offshore influence was successful, the amplitude of the offshore forcing is expected to be very small. The model is run for the same period as in previous experiment with wind forcing over the shelf. All corrected sea levels and bottom pressures are assimilated.

The model predictions are summarized in the last column of Tables 4.3 and 4.4 and current meter time series for 1987 are shown on Figure 4.8. The γ^2 values are computed using 'corrected' observations. One could as well add the subtracted offshore signal back to the model predictions and compare them to the original observations. This choice is not critical for the model validation, because the best verifications of the model performance comes from the current meter data that are not affected by this correction.

The direct comparison of γ^2 values for sea level is not correct because different time series were used to compute them. Hence, only fits within W+U-D columns can be compared, but they were assimilated into the model. Previous experiment showed the danger of over-fitting, so the fit for the assimilated data is not discussed. Better estimate of the model performance comes from the current meters. The fit for the currents improves at c5 and c6 in 1987 and does not change significantly at other locations. The fit for the average current at c5, c6 and c7 improves significantly. This is an important result for two reasons: First, as discussed before, one can not resolve the small scale variability with the barotropic model, so the γ^2 value for the average current is more relevant. Second, the results show that the subtraction of the offshore signal can lead to improved model predictions for the currents on the southern Labrador Shelf. Considering the complexity of the flow in the deep water of the Labrador Sea and possible importance of the baroclinic flow, the subtraction of the offshore signal seems to be a feasible solution to the problem of the offshore influence. In the case of the model used here, this choice is even more justified because of the false bottom set at 700 m, which, as discussed, influences the cross-shelf exchange.

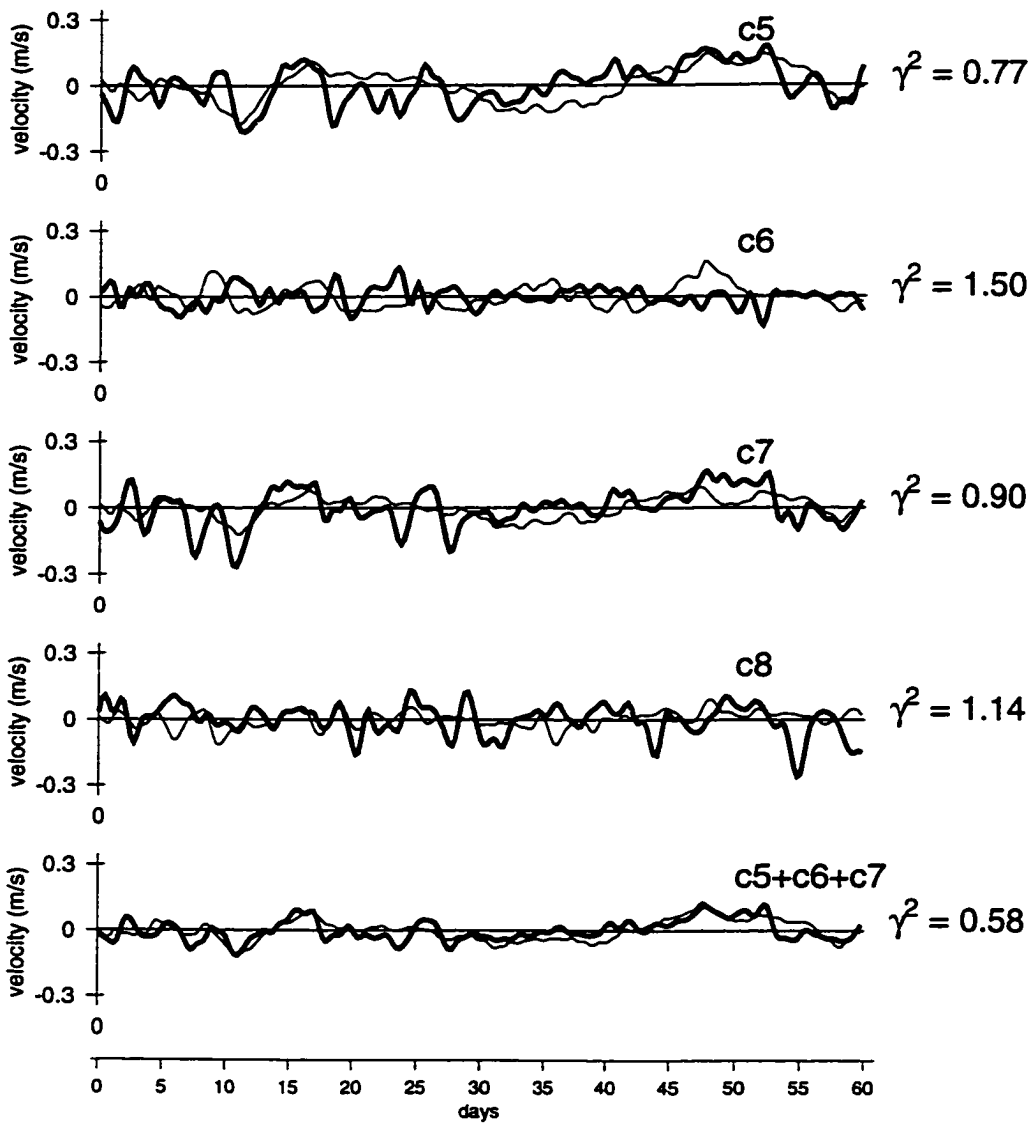

Figure 4.8: Comparison of observed along-isobath currents and predictions from the model driven by wind and the upstream and offshore boundaries. The last panel (c5+c6+c7) shows the average observed and predicted along-isobath current at locations c5, c6 and c7. The boundary conditions were obtained by assimilating the sea level and bottom pressure data after correcting for the offshore signal, as described in the text. The thick (thin) line shows observed (predicted) along-isobath currents at stations 5, 6, 7 and 8. The period covered is January and February 1987. The value of γ^2 shown to the right of each graph is the variance of the difference between observation and prediction, divided by the observation variance (Table 4.4, column W+U-D).

4.4 Suboptimal Prediction Scheme

One of my interests is operational modelling of the circulation on the Labrador Shelf. In the previous section the advantages of the assimilative approach to estimate open boundary conditions were demonstrated. In this section a suboptimal, but operationally suitable scheme for the prediction of open boundary conditions is formulated and tested. It is based on results from the assimilative run described in the previous section (4.3.3). The idea here is to estimate the boundary conditions at some later time without actually running the full assimilation model. The scheme is suboptimal because it does not include explicit dynamical constraints, but rather assumes that the relationship between the forcing and variables in the interior is time invariant.

Tide gauge data and wind forecasts are available in near real time and this is the information used in the suboptimal prediction scheme. The prediction scheme is based on the assimilation experiment that used wind and upstream boundary forcing (Section 4.3.3). An attempt to infer the offshore forcing using only tidal gauge data would probably not succeed.

Let us denote the boundary control by β, as described in Chapter 3 and Appendix B. The vector β consists of amplitudes that are associated with the linear setup across the shelf used to represent the upstream forcing in Section (4.3.3). The β was estimated by assimilating the data from the interior using a linear model. Thus, β is a linear combination of all the data used to run the model (coastal sea levels, bottom pressures and wind field). For the suboptimal scheme I approximate this by a linear combination of three coastal sea levels and two representative wind stress series. Therefore, at some time t, the boundary control is

$$\beta_t = \sum_{k=0}^{K} [\sum_i c_k^i \eta_{t-k}^i + \sum_j d_k^j \tau_{t-k}^j] \tag{4.2}$$

where η is coastal sea level and τ is wind stress. To estimate the regression coefficients (c_k^i and d_k^j) coastal sea levels at Brownell, Hebron and Nain, and two wind stresses were regressed against the boundary forcing (β) obtained from the two month assimilative run.

The maximum number of lags K was equivalent to 3 days. The prediction scheme was validated using sea level and wind stress data for a period of 75 days (March 1 to May 15 1986) that immediately followed the assimilation period in 1986. Using the coefficients c_k^i and d_k^i the boundary conditions for the new period are calculated and used to run the model for 75 days. Therefore, this new suboptimally predicted boundary condition is only a function of coastal sea level and wind stress as defined by (4.2).

The model predictions are shown in Figure 4.9. The model clearly has significant skill for coastal sea level. This result could be expected because coastal sea levels were used to predict the boundary conditions. The best fit is at Hebron where $\gamma^2 = 0.10$, similar to the γ^2 realized by the fully assimilative model run.

Even though bottom pressure gauges were not used in the suboptimal assimilation scheme (see (4.2)) they are predicted with the same skill as before. The inshore locations have residual variance ratios between 0.3 and 0.5 (Figure 4.9). The model, as one could expect, does not predict the offshore variability very well (the γ^2 values at p2 and p3 were 0.8 and 1.0). Good predictive skill for the pressure is probably the consequence of the high coherence of the inshore pressure with the upstream signal, as discussed in the data analysis section.

Most encouragingly, the fit for the along-isobath current at c5 is very similar to the fully assimilative model. It should be noted that this result was realized with only tidal gauge and wind stress data. The assimilative run from the previous section uses information from pressure gauges p4 and p6 that provide the geostrophic balance for the current meter at c5. The suboptimal model has no information from those two pressure gauges but the fit is of similar quality.

4.5 Discussion

A linear, barotropic, depth-averaged circulation model with data assimilation was used to hindcast the circulation on the Labrador Shelf. The data analysis showed the relative importance of the wind driven flow and the boundary forcing for the synoptic coastal sea level,

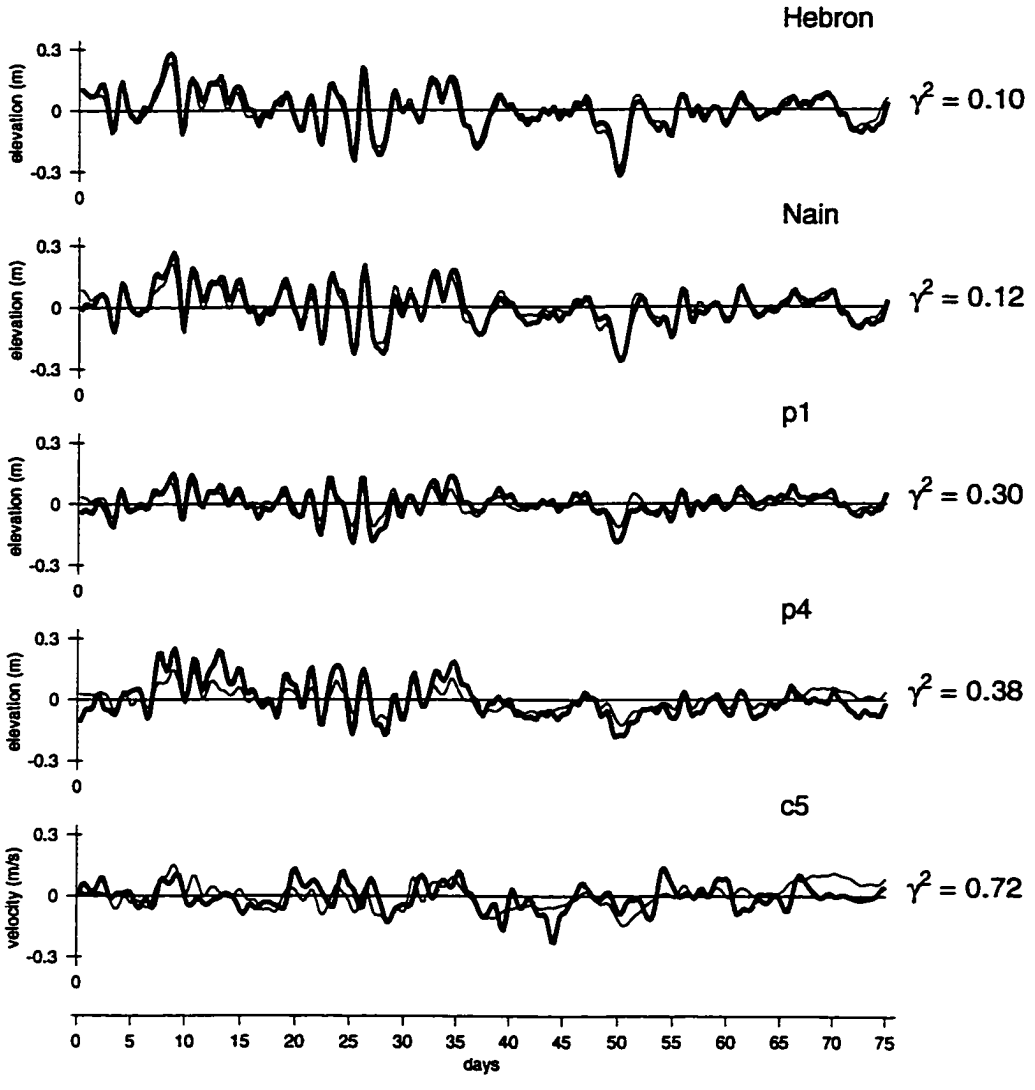

Figure 4.9: Comparison of observed adjusted sea level, bottom pressure and along-isobath current and predictions from the model driven by wind and suboptimally predicted upstream boundary conditions. (The upstream boundary condition was obtained from equation 4.2, based on suboptimal assimilation of the coastal sea level at Brownell, Hebron and Nain and two wind stress series representative for upper and lower shelf.) The thick (thin) line shows observed (predicted) sea level at Hebron and Nain, bottom pressure at stations 1 and 4 and along-isobath current at station 5. The period covered is March 1st to May 15th 1986, a total of 75 days. The value of γ^2 shown to the right of each graph is the variance of the difference between observation and prediction divided by the variance of the observations.

bottom pressure and current variability. Model results confirm that upstream boundary and wind forcing are dominant sources of the variability on the Labrador Shelf. The model used data assimilation to infer open boundary conditions.

Statistical analysis showed that the currents in the vicinity of Hamilton Bank are very complex. Individual current meters are correlated when the along-isobath component of the flow is considered, but those correlations are not always high. The cross-isobath component of the flow shows much local variability. The dynamical model used here is not capable of resolving this small scale variability. On average, when the offshore influence is subtracted the model leaves about 60% of the variance unaccounted for. Although this value for the γ^2 is relatively high it is close to optimal for a linear model forced by winds and sea level data. This demonstrates that the model has predictive skill, but the discrepancies between individual current meters and their model counterparts could be due to problems with the bathymetry, depth of the current meters, baroclinic effects, etc. Considering the complexity of the flow and the potential importance of the baroclinic forcing, the results are on a level similar to that realized by a similar model on the Scotian Shelf (Thompson and Sheng, 1996). The analysis presented here suggests that future models should include 3-D dynamics, nonlinear terms in the momentum equations and allow density to evolve with the flow. That would be the only way to incorporate the effects due to baroclinic instabilities, interaction of density with topography and other effects that comprise the part of the variance that could not be accounted by a linear barotropic model.

At this point, one might attempt to estimate the required contribution of the density effects to subtidal currents. Typical current residuals in the model were of the order of 0.1 m/s. Taking thermal wind relationship, the change of current Δu over $\Delta z = 20$ m of depth can be expressed in terms of spatial density gradients over distance $\Delta\lambda$. The change in velocity is given by $\Delta u = (g\Delta z)/(f\Delta\lambda) \cdot (\Delta\rho/\rho)$. Over spatial scale of $\Delta\lambda = 20$ km, the density anomaly $(\Delta\rho/\rho)$ of 0.1% results in Δu of 0.1 m/s. Temperature and salinity records from the current meters separated roughly by 20 km suggest that this kind of density anomalies are realistic for the period considered (Wright et al., 1988).

One of the goals of this study was to assess the role of the offshore in driving circulation

variability on the shelf. The offshore forcing used in the model was not realistic, but rather an attempt to allow for the offshore influence to which the shelf can adjust. The increased number of boundary controls resulted in model over-fitting. The model predictions improved at the locations where data were assimilated, but the underlying model formulation was presumably incorrect. This again demonstrated the danger of over-fitting when data assimilation is used and, also, the importance of the current meter data that were withheld from the assimilation for validation purposes.

The subtraction of the offshore signal from the inshore bottom pressures and coastal sea levels resulted in improved fits for along-shore currents on the southern Labrador Shelf. Considering the complex dynamics in the Labrador Sea, the form of the offshore forcing that was used and the flattening of the bathymetry at 700 m, the removal of the offshore signal is probably a better choice when using a barotropic model.

A separate set of questions, that was not addressed in this thesis, concerns the origin of the offshore forcing. It is useful, at this point, to extend the data analysis a little further to indicate possible directions for future research of this problem. I therefore calculated the correlation coefficients between the time series of bottom pressure at the shelf break (p3) and the large-scale North Atlantic wind field. The results are shown in Figure 4.10 where the vector components are determined by the correlation coefficient between the longitudinal or latitudinal component of the wind and the bottom pressure at p3. This analysis revealed that the offshore signal could be related to the large scale wind field in the North Atlantic. Considering the low frequency of the response at the shelf break bottom pressure (e.g. Figure 4.6), the dynamics of this correlation are probably associated with the cyclonic circulation in the Labrador Sea and the large scale atmospheric variations of the Icelandic Low and Azores High. This analysis is beyond the scope of this model, but it should be noted that de Young et al. (1995) used the complete North Atlantic wind field and were not able to account for the variability at the shelf break. Their model, as discussed in Chapter 2, was barotropic and the proper modelling of the dynamics at the shelf break at synoptic time scales would probably require a nonlinear prognostic model where density evolves with the flow. An attempt to use a diagnostic model where density is fixed was not

successful (de Young et al., 1992).

The suboptimal prediction scheme shows significant skill. The upstream boundary condition is predicted using a statistical relationship between the wind and sea level, and the open boundary predicted by the assimilation model. The transfer function (i.e. regression coefficients) is effectively time invariant for the validation period that was chosen. The model with the suboptimally predicted boundary condition shows good agreement with the pressure data that were not used to predict the boundary conditions. This result gives us confidence that the transfer function used here is reasonable. The predictions for the along-isobath currents are of similar quality to those achieved in fully assimilative runs. This result is encouraging because the suboptimal scheme uses only wind stress and tide gauge information. The suboptimal model could be used for operational modelling of sea level and provide guidance regarding alongshore current variability.

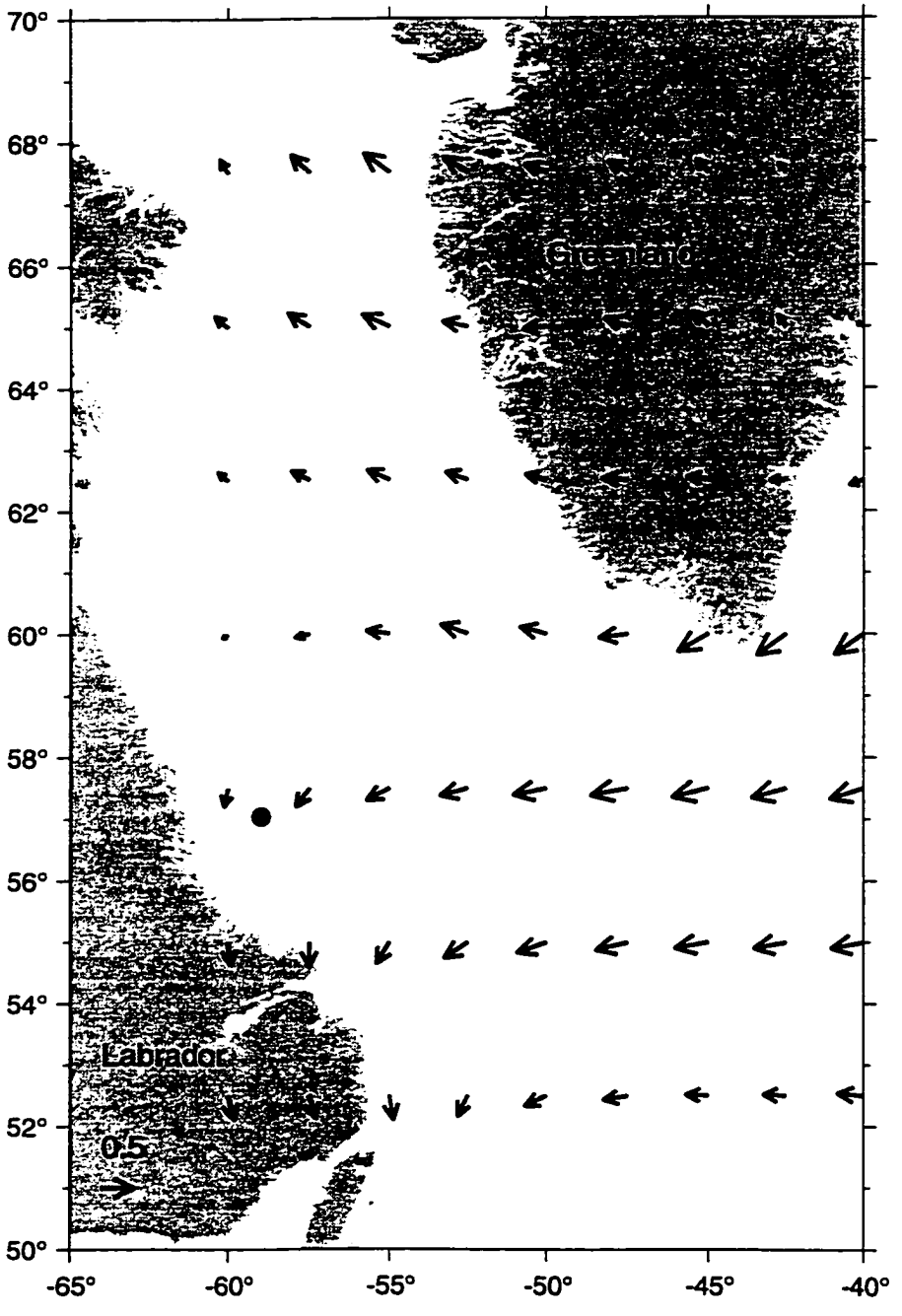

Figure 4.10: Correlation coefficients between the offshore bottom pressure at p3 (denoted by black dot) and the large scale Northwest Atlantic wind field. The arrows represent correlation coefficients between the longitudinal or latitudinal component of the wind field and the offshore bottom pressure at p3.

Chapter 5

Gulf of Saint Lawrence

This chapter focuses on the synoptic variability in the Gulf of Saint Lawrence (Figure 5.1). The Gulf is one of the world's largest semi-enclosed ocean basins and one of the most important maritime transportation routes. Research on the Gulf has been directed mainly at its basic estuarine circulation and little is known about the variability at synoptic periods. Moreover, the potential resonant behaviour of the Gulf and its free modes has not been addressed with a numerical model. Thus, in this chapter both data and a numerical model are used to explore the causes of synoptic variability and explain the resonances that can be found in coastal sea level records. The data analysis is based on sea level data collected at the permanent tide gauges around the Gulf of Saint Lawrence shown in Figure 5.1 and the model used is described in Chapter 3.

A statistical model forced by wind and coastal sea level close to the Gulf's boundary is used to examine the influence of wind and boundary forcing on synoptic time scales. Then, the dynamical model is used to quantify the wind and boundary driven variability in the Gulf. First, the model is run with wind forcing to estimate the contribution of the spatially variable wind field to sea level variability in the Gulf. The boundary forcing is then added to account for the remote forcing through Cabot Strait and the Strait of Belle Isle. The evolution of the open boundaries is inferred using data assimilation.

Resonances in the Gulf are first examined using statistical analysis. Then, a review of the theory of free oscillations in closed and semi-enclosed basins is presented. The data

are analysed using complex empirical orthogonal functions to find if energy peaks found at individual time series are present throughout the Gulf and can be explained by the free mode theory. The numerical model is then used to relate some of the periods found in the data to wind and boundary forcing. Both wind and boundary models are run with random forcing for a long time to establish a representative record. Model results are then analysed to identify and interpret some of the periodicities found in the data.

5.1 Data Analysis

Hourly tide gauge data from several locations around the Gulf of Saint Lawrence were obtained from MEDS (Marine Environmental Data Service) for 1986 and 1987. Most of the tide gauges had periods during which they malfunctioned: only the Charlottetown record is complete. Examples of 12-hourly wind stress data and sea level from Charlottetown and Riviere au Renard are shown in Figure 5.2. Based on one year of data at Charlottetown and Riviere au Renard power spectra were calculated. (None of the other locations have a complete record that would cover the whole year and thus capture a complete seasonal cycle.) For the same one year period, the wind stress spectrum at the representative location, shown on Figure 5.1, was calculated. The spectra are shown in Figure 5.3. The wind stress spectrum shows that most of the energy is at synoptic periods between 2 and 10 days. Sea level spectra, however, show much more variability at shorter periods with distinct peaks at around 35, 21 and 15 hours at both locations. Some residual energy at diurnal and semi-diurnal tidal periods is evident at both locations. At this point it is hard to estimate if the residual energy at tidal periods is the result of some weaknesses in the tidal analysis package or if it is the result of some other processes that might be present.

Although the Gulf of Saint Lawrence, as a semi-enclosed basin, has a strong potential for resonances, there has not been much research of the resonances in the Gulf. The spectral analysis of the one year records from Charlottetown and Riviere au Renard suggests that some of the energy peaks, in particular those at shorter periods, might be the result of resonances. To address this issue, the sea level data from 10 locations and for a period of

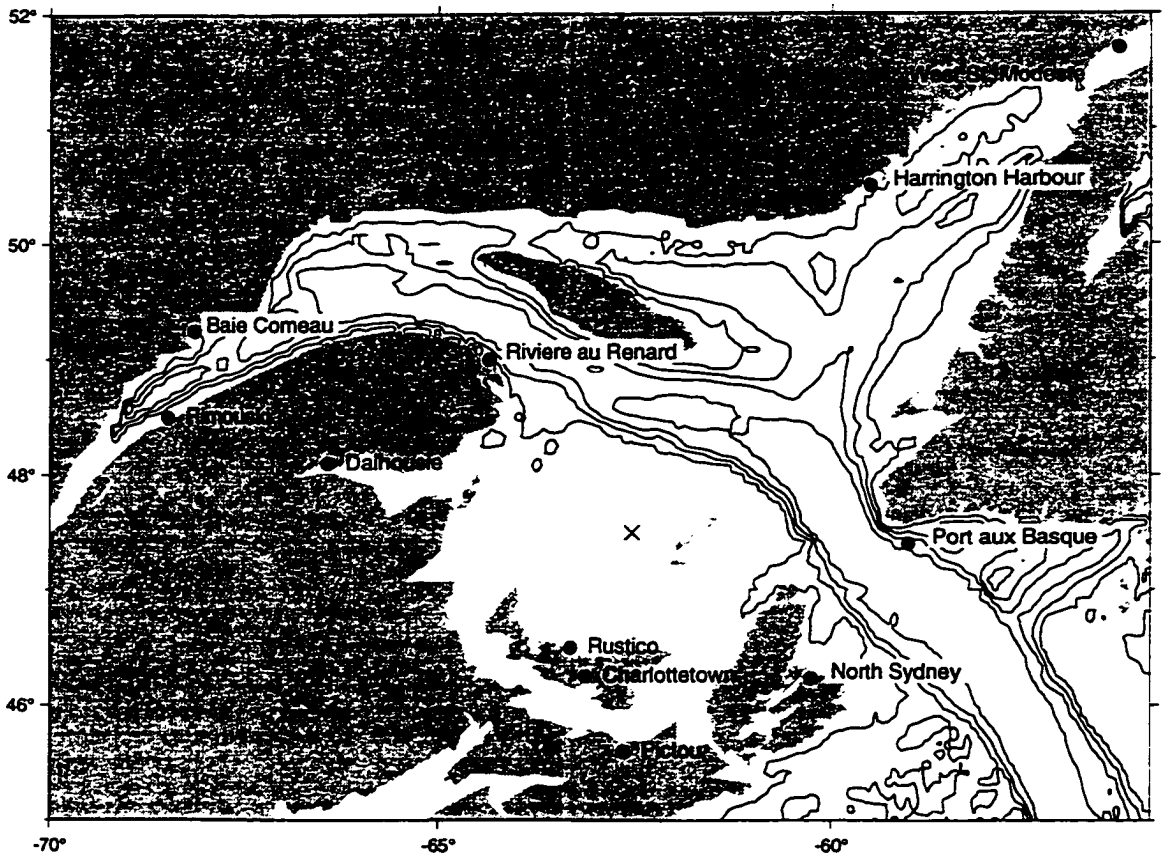

Figure 5.1: Model domain and bathymetry. The resolution of the model is 1/12° which corresponds to 9.3 km in the meridional direction. The thin contours correspond to depths of 100, 200, 300 and 400 m. The dots mark tidal gauges. In January and February of 1986 sea level data were available at all locations except Rustico. In January and February 1987 sea level data were available at all locations except Port aux Basque, West St. Modeste, Rimouski and North Sydney. The cross marks the location of the wind stress series that was taken to be representative of the whole Gulf.

2 months were examined. Although two months of data are not long enough to be fully representative of the system, it was the best compromise between the record length and data coverage. From the sea level data a cross-spectral matrix was estimated and complex empirical orthogonal functions were calculated. The results are presented in Figure 5.4. Most of the variability in the sea level data is captured by the first mode: it accounts for 95% of the variance summed over all frequencies. Although the record is short and not fully representative of the system, energy peaks are found at similar periods as for the long records at individual tidal gauges (Figure 5.3). This result suggests that the system might be resonant at those frequencies. Therefore, eigenvector elements were plotted in the complex plane for periods of 35 and 21 hours (Figure 5.4). The positive angle that increases with time is defined as counter-clockwise (cyclonic) around the Gulf, so that the direction of the arrows denotes phase. In both cases the eigenvector elements show the cyclonic propagation of the signal around the Gulf of Saint Lawrence. This is particularly evident at the 21 h period where the speed of propagation is greater and the phase differences more obvious.

5.1.1 Theory of Resonances

At this point, it is useful to briefly review the theory of resonances in closed and semi-enclosed basins. The subject has been studied extensively by a number of authors and theoretical solutions exist for simple idealized cases. Lamb (1932) considered free oscillations of a circular basin with constant depth. The solution to the problem is represented in terms of modes. Rao (1966) and LeBlond and Mysak (1978) discuss the use of different modes and show that, for the idealized cases (circular and rectangular basins), only lowest modes are of interest for oceanographic analysis, as they appear at frequencies that might be excited by tides or atmospheric effects. Thus, Lamb (1932) for the non rotational case of a circular basin finds the frequency of the first mode to be $\sigma = 1.84 \cdot c/l$, where $c = \sqrt{gh}$ and l is the basin radius. If we take the radius of the Gulf of Saint Lawrence to be l =250 km and an average water depth of h =50 m (the same values are used in all subsequent examples), the period of oscillation of the first mode is T =10.5 h.

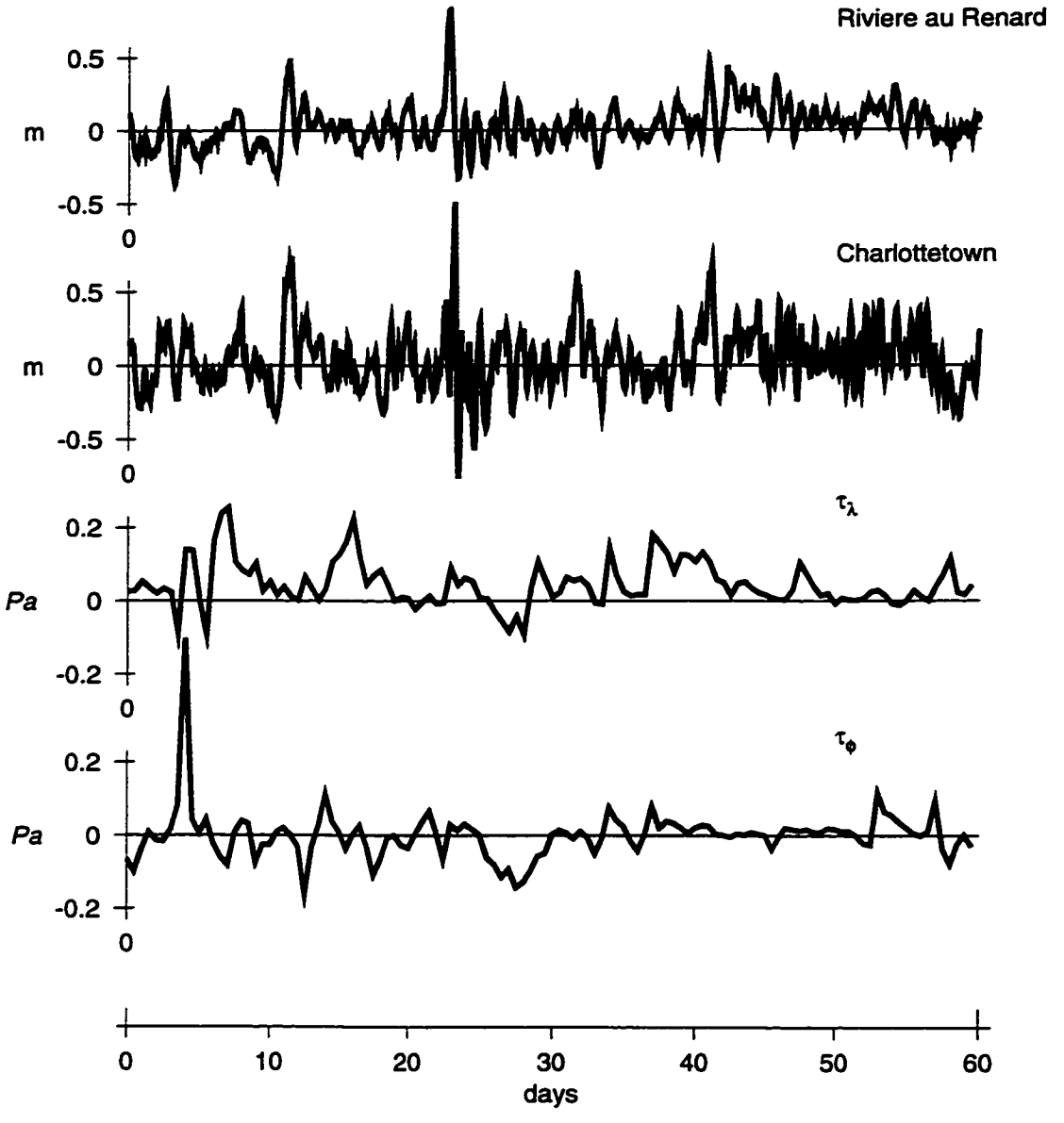

Figure 5.2: Time series of sea level at Riviere au Renard and Charlottetown and wind stress at a selected location in the central Gulf of Saint Lawrence (see Figure 5.1). The period covered is 60 days starting on January 1st 1987. Sea level time series are detided and sampled every hour and wind stress time series are sampled every 12 hours.

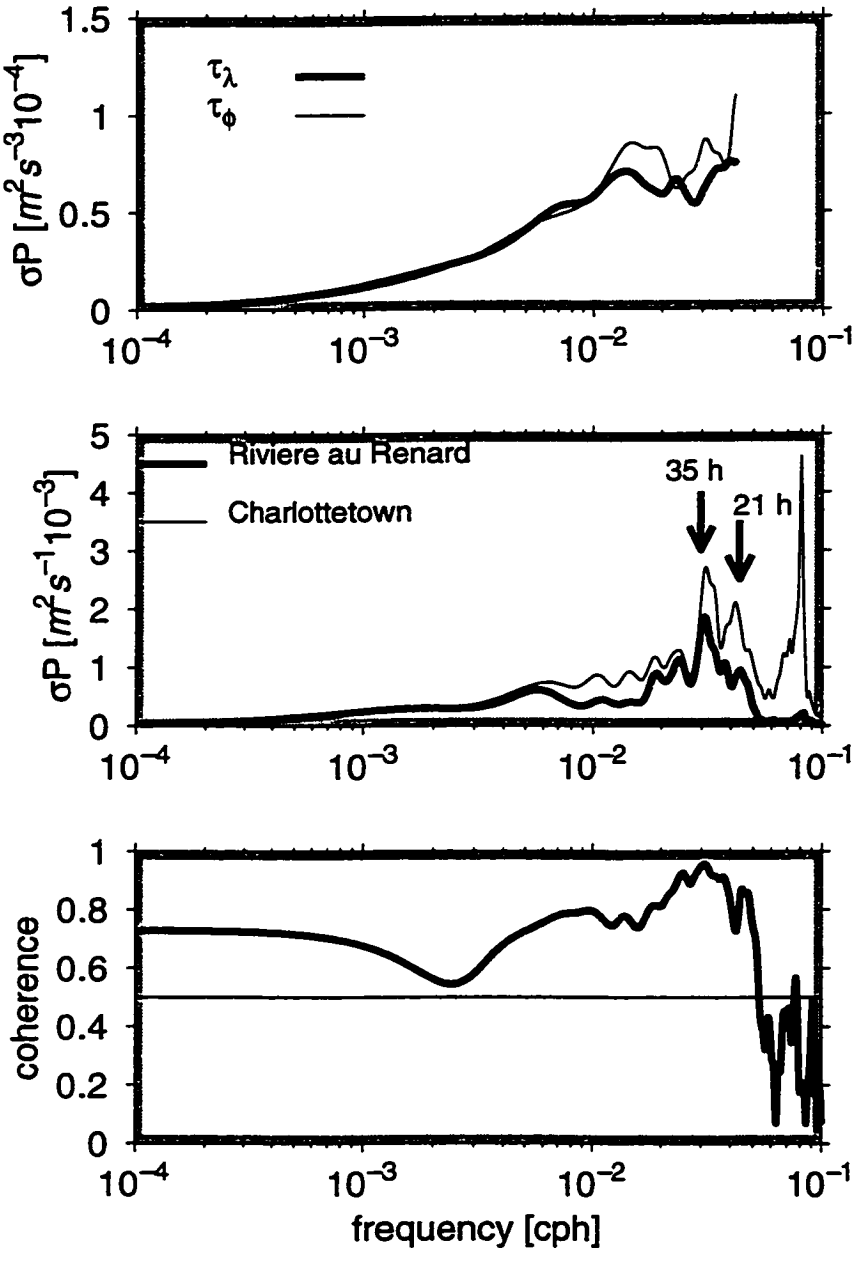

Figure 5.3: Power spectra of wind stress data and sea level at Riviere au Renard (thick) and Charlottetown (thin) and coherence between the two sea levels. Wind and sea level power spectra shown in variance preserving form are based on one year of data starting on June 1st 1986. The 5% significance level for coherence is shown by the thin line in the lowest panel.

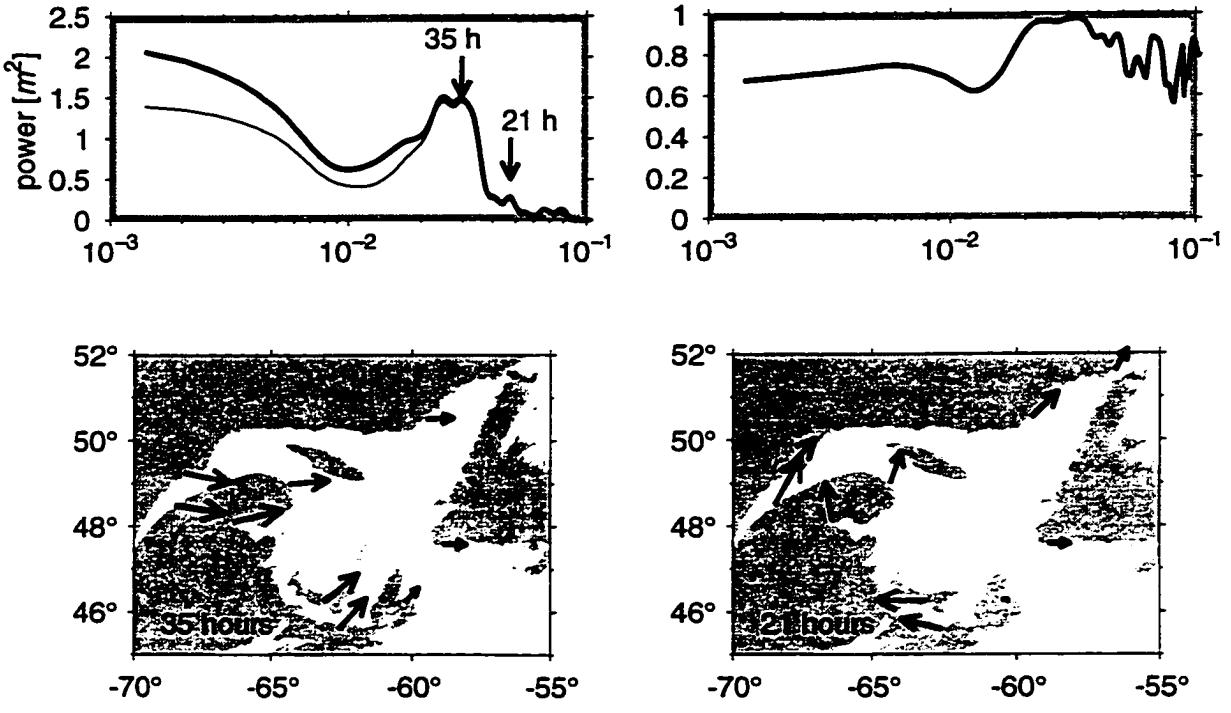

Figure 5.4: Complex empirical orthogonal function for sea level. The results are based on 2 months of data for January and February 1986. The upper left panel shows the trace of the cross-spectral matrix (thick line) and the first eigenvalue (thin line), both as a function of frequency. Upper right panel shows the ratio between the two lines on the left. The lower row shows eigenvector elements in the complex plane (arrow direction denotes phase) for two periods (35 h–left panel and 21 h–right panel) at which higher energy was found.

When rotation is included, the changes in the free period depend on the ratio between the Rossby radius and the radius of the basin. Csanady (1982) discussed Lamb's solution for a circular basin forced by steady wind stress and showed that for a very large basin, where the Rossby radius exceeds the radius of the basin, the frequency of the oscillations approaches the inertial frequency. For the Gulf of Saint Lawrence the Rossby radius is close to the basin radius ($\sqrt{gh}/f$ =210 km). According to Lamb (1932) and Rao (1966) the frequency of the first mode should be about 60-80% higher than the inertial frequency (for the Gulf the inertial period is $T_i = 2\pi/f$ =16.44 h) which gives periods between 9.13 h and 10.27 h. The result is consistent with the results of Platzman (1972) who numerically calculated free periods for the Gulf of Mexico and found that rotation only slightly decreased the period of the first free mode.

The Gulf of Saint Lawrence is not a closed basin, so the influence of the straits needs to be considered as well. Platzman (1972) calculated fundamental modes for the Gulf of Mexico with open and closed straits and found that the fundamental period shortens once the straits are opened (for the rotational case 7.36 h as opposed to 6.34 h when straits were open), but the spatial structure of the modes does not change dramatically. When the basin is open, another mode needs to be considered. It corresponds to a mode that has no nodal points in the basin and is generally called the Helmholtz mode. Miles (1971) has studied the response of harbours to excitation by tsunamis and tidal forcing. If the simple case of a basin of depth h, with surface area Q connected with the open sea via a strait of width W and length D is considered without rotation (LeBlond and Mysak, 1978), the frequency of the response is given by $\sigma^2 = gWh/QD$. If applied to the Gulf of Saint Lawrence with the surface area of 400 000 km^2, and taking Cabot Strait to have W =100 km and D =50 km, the Helmholtz period is T=34.88 h. Platzman (1972) shows that when rotation is included the period will shorten, by an amount depending on the ratio between inertial frequency and the non-rotational Helmholtz period.

Considering the geometry of the Gulf of Saint Lawrence and its bottom topography dominated by the Laurentian Channel, another type of resonances needs to be discussed as well. One of the simplest theoretical concepts is the so called quarter-wave resonator for

a channel of length D open at one end. The lowest period of oscillation is given by $T = 4D/\sqrt{gh}$. If applied to the Laurentian Channel with the length of 1100 km (measuring from its mouth at the shelf break), and mean depth of 300 m, the period is $T = 22$ h. Similarly, quarter-wave periods could be calculated for the small bays (e.g. Baie de Chaleurs) that are present in the Gulf of Saint Lawrence.

All of the theories discussed so far are for flat bottomed basins. The bottom topography of the Gulf is, however, highly variable and it certainly affects the resonant periods of the basin. Lamb (1932) extended his analysis of the circular basin by considering a variable bottom topography using an idealized parabolic shape. As before, for the non rotating case the frequency is given by $\sigma = 1.4c/l$, where $c = \sqrt{gh_0}$ and h_0 is the deepest point of the parabolic bottom. Taking for example h_0 to be 200 m, the period of the lowest mode would be 7 hours. If the bottom slopes more gently (h_0=100 m), the corresponding period would lengthen to 9.8 h. The rotation has the same effect as it did for the flat bottom case, i.e. the rotation shortens the period of the first mode. The topographic effects in semi-enclosed and closed elliptical basins were considered by Gratton and Le Blond (1986) and Mysak (1985). In both cases, the so called 'second class oscillations' (topographic waves) were considered. They found that depending on the geometry of the basin and shape of the bottom, the topography can induce a wide range of oscillations with periods from 2 to 30 days. Gratton (1983) used a parabolic bottom shape in a circular lake with coastal depth of $h_c = 100$ m and depth at the lake center of $h_0 = 300$ m and calculated the period of the first mode to be on the order of 10 days. The coastal depth of 100 m used in Gratton's (1983) calculation is clearly not realistic for the Gulf of Saint Lawrence. Mysak (1985) considered elliptical lakes and showed that if the ratio between the coastal depth and the depth at the lake center (h_c/h_0) decreases, the period of the first mode shortens. For an elliptical lake with small aspect ratio (width/length=1.1) and idealized bottom with $h_c/h_0 = 0.1$, Mysak(1985) calculated the period of the first mode to be 2 days. The small aspect ratio is realistic for the Gulf of Saint Lawrence, however the h_c/h_0 ratio is probably too large because typical coastal depths in the Gulf are about 20 m and the depth near the Gulf center is about 400 m. Hence, as discussed above, the period for the smaller h_c/h_0

will be shorter than 2 days. Hence, it is also possible that some of the observed periods are due to topographic effects.

The theoretical results are restricted to idealized basins. However, when typical values are considered the periods obtained show that some of the energy peaks present in the data could be due to the resonances in the Gulf of Saint Lawrence. In the later sections the dynamical model is used to relate some of the observed frequencies to wind and boundary forcing.

5.2 Statistical Model

Most of the forcing in the Gulf of Saint Lawrence at synoptic frequencies is probably due to local wind and open boundaries. In this section a statistical model is used to estimate the relative importance of wind and boundary forcing on the sea level variability in the Gulf of Saint Lawrence. Complex empirical orthogonal functions show that, at synoptic frequencies, sea level at Port aux Basques and West St. Modeste tend to lead other sea levels around the Gulf. Thus, it is reasonable to assume that sea level at Port aux Basques and at West St. Modeste can be taken as representative of the boundary forcing of the Gulf of Saint Lawrence.

One of the problems in the analysis of wind and sea level data is their different sampling intervals. For the purpose of the statistical analysis it is assumed that the wind stress over the Gulf can be represented by one wind stress series whose location is shown on Figure 5.1. This choice is made because although the wind field is spatially variable, the wind stress series are coherent, so multiple regression would probably result in model over-fitting. The wind stress series is temporally interpolated to match the sea level sampling interval of one hour.

All of the sea level time series were regressed on the wind stress to estimate how much of the variability in the sea level could be accounted for by the wind forcing. The optimal fit was found for the range of lags of 0 to 6 hours, determined using the AIC criterion. Given the temporal interpolation of the wind stress, the optimal lag of only 6 hours suggests that

the Gulf responds almost instantaneously to the wind forcing. The wind can account for about 20-30% of the variability in the Gulf of Saint Lawrence (Table 5.1; column Wind). These γ^2_{min} values would probably have been lower if the sea level series had been filtered and subsampled to match the wind data. However, the prefered choice was to use hourly sea level data and temporally interpolate the wind stress.

The residual of the regression on the wind series is the signal that is due to other uncorrelated forcing mechanisms. If the wind stress used in the regression is indeed representative of the wind forcing over the Gulf, the residuals should not be correlated to the wind field over the Gulf. In fact, the correlation coefficients for each of the available wind stress series and sea level residuals were small and in general statistically insignificant. The wind field over the Gulf is not uniform, but the wind stresses are correlated, so once lagged winds were considered the regression model, as discussed, probably accounts for the part of the signal coherent with other wind stress series. Therefore, we can assume that the residual time series have the wind signal removed from them. Similarly, the wind signal was removed from two stations (Port aux Basques and West St. Modeste) that are taken to be representative of the boundary forcing for the Gulf of Saint Lawrence.

In the next experiment the importance of the boundary forcing via Cabot Strait and the Strait of Belle Isle is estimated. Each of the wind-corrected sea level time series is regressed against wind-corrected sea level series from Port aux Basques and West St. Modeste. The sea levels used as forcing (Port aux Basques and West St. Modeste) now represent the distant forcing that is completely incoherent with the Gulf winds. The results are presented in the second and third column of Table 5.1. Overall it appears that the Cabot Strait signal can account for 40-70% of the wind corrected variance, while the Belle Isle signal accounts for only 15-40% of the variability. This result is not surprising considering the difference in the cross-sectional areas of the straits.

These two simple statistical considerations suggest that Cabot Strait is a more important source of variability in the Gulf of Saint Lawrence than the local wind. The statistical model offers only partial answers about the importance of wind and boundary forcing. In this case, the large scale wind is probably correlated to the boundary forcing and their covariances

Station	Wind	Cabot St.	Belle Isle
Harrington H.	0.76	0.34	0.62
Baie Comeau	0.72	0.37	0.87
Rimouski	0.73	0.49	0.85
Riv au Renard	0.79	0.35	0.76
Dalhousie	0.67	0.44	0.81
Charlottetown	0.82	0.59	0.84
Pictou	0.82	0.64	0.81
North Sydney	0.78	0.58	0.67

Table 5.1: Fit of regression of adjusted sea level on lagged winds and boundary forcing. The numbers are values of γ^2_{min} for the statistical model. The stations are listed anti-clockwise around the Gulf of Saint Lawrence. The regression fit is presented for the model forced by winds (Wind) and boundary forcing via Cabot Strait (Cabot St.) and the Strait of Belle Isle (Belle Isle). The values used to calculate γ^2_{min} in columns Cabot St. and Belle Isle are corrected for the wind as described in the text.

are not accounted by the statistical model. Therefore, in the following sections I will use a dynamical model to offer more definitive dynamical explanations of these interactions.

5.3 Dynamical Model

In this section a dynamical model is used to analyse synoptic variability in the Gulf of Saint Lawrence. Wind forcing is considered first to examine how much of the variability can be accounted for by the spatially variable wind field. The possibility of wind driven resonances is also explored. Finally, the boundary forcing is inferred using data assimilation and the model run with both wind and boundary forcing. At the end, the effects of boundary forcing on resonances are examined.

5.3.1 Model Setup

The model is forced by wind stress and flow across the open boundaries of the model. As described above, wind fields were available on a 2.5° × 2.5° grid. The Gulf of Saint

Lawrence has two open boundaries: the Strait of Belle Isle and Cabot Strait. The open boundary conditions are defined along 55° W and 45° N. Moving the boundaries away from the region of interest results in more realistic flow in the interior of the domain. The time variability of the open boundaries is inferred using data assimilation, as described in Chapter 3.

The boundary forcing is defined at the following boundaries as sketched in Figure 5.5. A spatially uniform flow is specified through the Strait of Belle Isle. Along the southern Newfoundland coast between Newfoundland and St. Pierre Bank a spatially uniform boundary flow is defined. Finally, a spatially uniform flow is specified in the southeastern corner of the model domain along the eastern side of the Laurentian Channel. All other parts of the open boundaries are radiative. During the development stage of the model, a number of inflow boundaries were considered and this combination provided the best agreement with the data.

5.3.2 Wind Driven Circulation

The statistical analysis of Section 5.1 suggests that only a small portion of the variability in the sea level can be accounted for by wind forcing. However, those results were based on regression and did not take into account the spatial variability of the wind field. In this section the wind driven model is used to hindcast the flow in the Gulf of Saint Lawrence. All boundaries are radiative and no boundary forcing is prescribed.

The model is run for both 1986 and 1987, using the spatially variable wind field described in Chapter 3. The results for January and February of 1986 are presented in Figure 5.6. The ratio between model error variance and the observation variance (γ^2) for the wind driven model is typically around one. Similar results were obtained for the 1987 run. This indicates that local wind forcing cannot account for much of the synoptic variability in the Gulf of Saint Lawrence. The result is consistent with the regression analysis where wind could account for only about 25% of the variability in the data. The difference in the fit between the statistical and dynamical model, as discussed, is also expected because of imperfections in the forcing field, drag coefficient, etc.

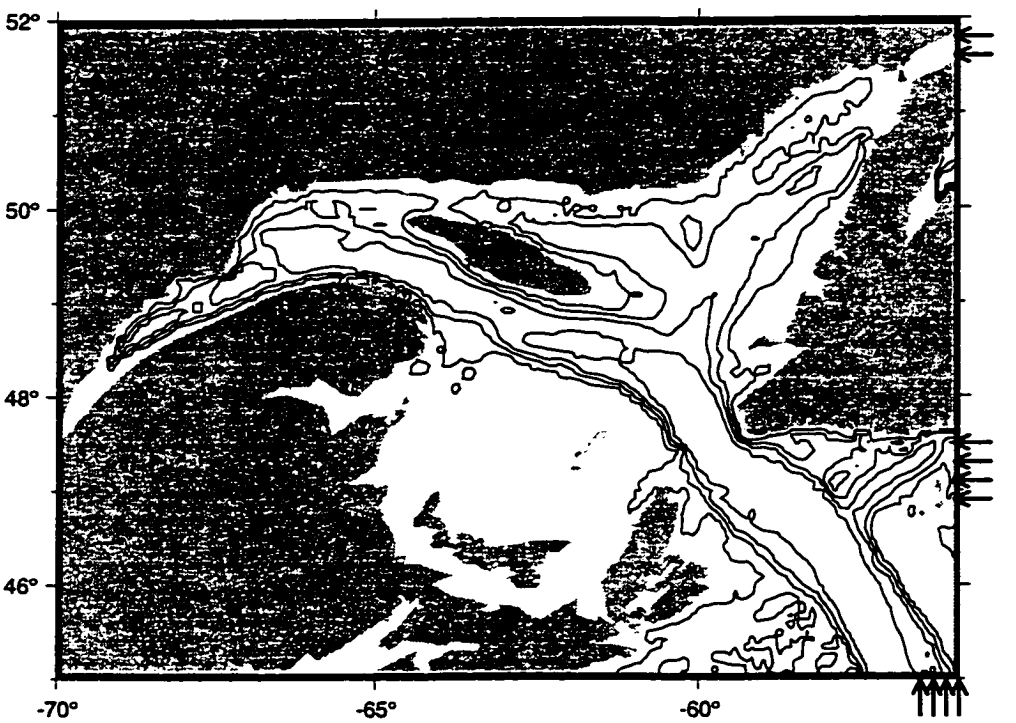

Figure 5.5: Forcing boundaries for the Gulf of Saint Lawrence model. The arrows represent parts of the boundary where inflows are prescribed. The number of arrows is schematic and does not represent the number of inflow points. The evolution of the open boundaries is inferred using data assimilation.

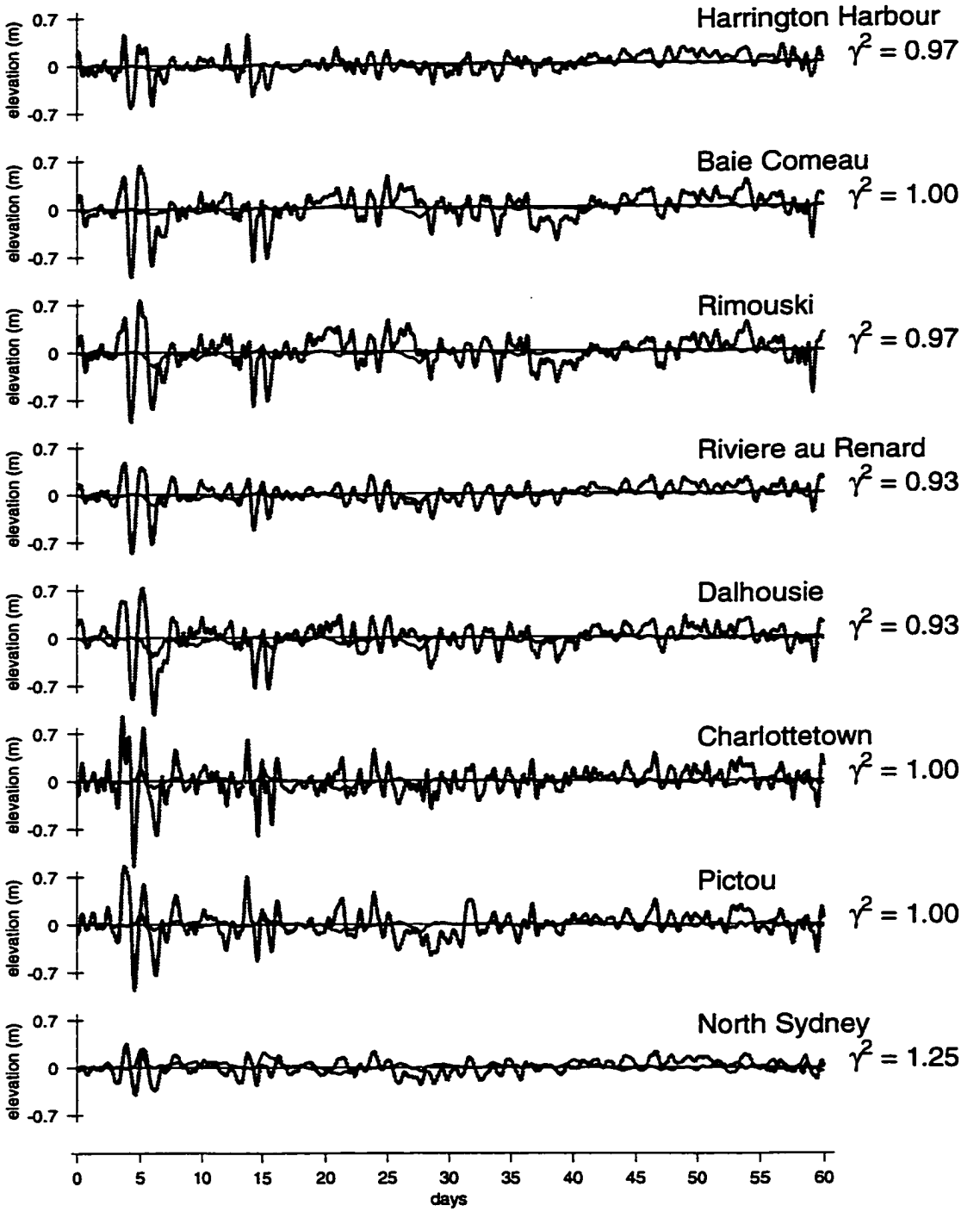

Figure 5.6: Comparison of observed adjusted sea level and predictions from the wind driven model. The thick (thin) line shows observed (predicted) adjusted sea level at 8 locations in the Gulf of Saint Lawrence. The period covered is 60 days starting on January 1st 1986. The value of γ^2 shown to the right of each graph is the variance of the difference between observations and predictions divided by the observation variance.

Data analysis shows energy peaks at some frequencies which may be due to resonances in the Gulf. Some of these resonances might be induced by the wind. Therefore, an experiment was designed in which random wind forcing was considered and the response analysed to see if more energy was present at particular periods. The model was run for two years, forced by a spatially uniform wind field whose direction and amplitude changed randomly every 12 hours and were linearly interpolated in between. The choice of the 12-hourly time interval used here is, from the statistical point of view, arbitrary, but was made for the following reasons: First, the interval chosen should roughly represent the changes that occur on synoptic time scales. Second, if a shorter interval is used, the response is dominated by high frequencies, which is not consistent with the observed spectra (see Figure 5.3).

Although the model predicts sea level and currents at all locations, it is not feasible to calculate the complex empirical orthogonal functions on the complete model output. Therefore, a number of locations were selected around the Gulf and the predicted sea level was sampled hourly at these locations. Then, the complex empirical orthogonal functions were calculated in the same fashion as for the data in Section 5.1. The results (Figure 5.7) show that the random wind forcing does not induce particularly distinct energy peaks in sea level. The analysis of eigenvector elements at a period of 35 hours suggests signal propagation around the Gulf, but the signal is very weak.

When individual spectra for the locations around the Gulf are considered some locations show energy peaks at shorter periods. For example, the spectrum for sea level at Dalhousie, which is located in the Baie des Chaleurs, shows a peak at around 9 hours. This period corresponds to a quarter-wavelength period of the bay which is estimated to be 9.4 hours. Similar, but less distinct, energy peaks could be found at locations in the St. Lawrence estuary (e.g. Rimouski) and around Prince Edward Island (e.g. Charlottetown and Pictou), probably the result of local modes of the estuary and Magdalene Shallows, respectively.

The model was also used to find the typical response of the Gulf of Saint Lawrence to wind forcing that is suddenly turned off. The experiment corresponds to the situation when the wind blows in one direction for a time sufficiently long that the Gulf is in quasi-steady

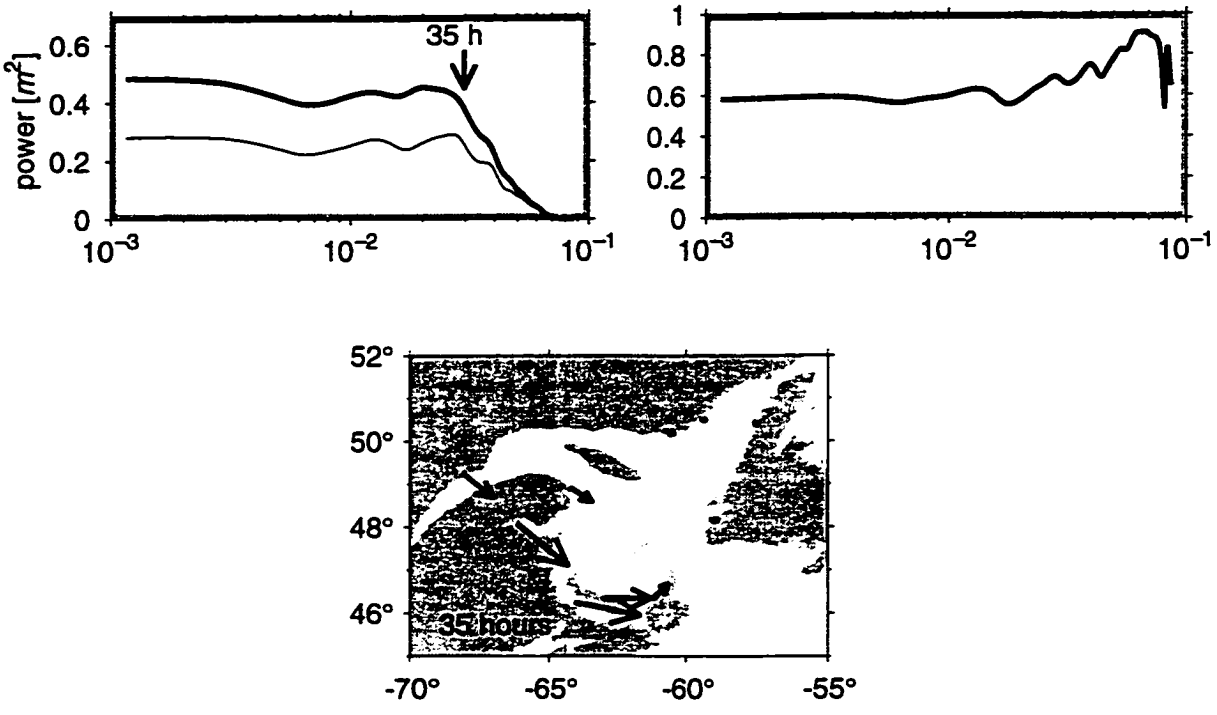

Figure 5.7: Complex empirical orthogonal functions for the sea level based on the model forced by a spatially uniform wind that changed randomly every 12 hours and was linearly interpolated. The upper left panel shows the trace of the cross-spectral matrix (thick line) and the first eigenvalue (thin line), both as a function of frequency. Upper right panel shows the ratio between the two lines on the left. The lower row shows eigenvector elements in the complex plane for periods of 35 hours.

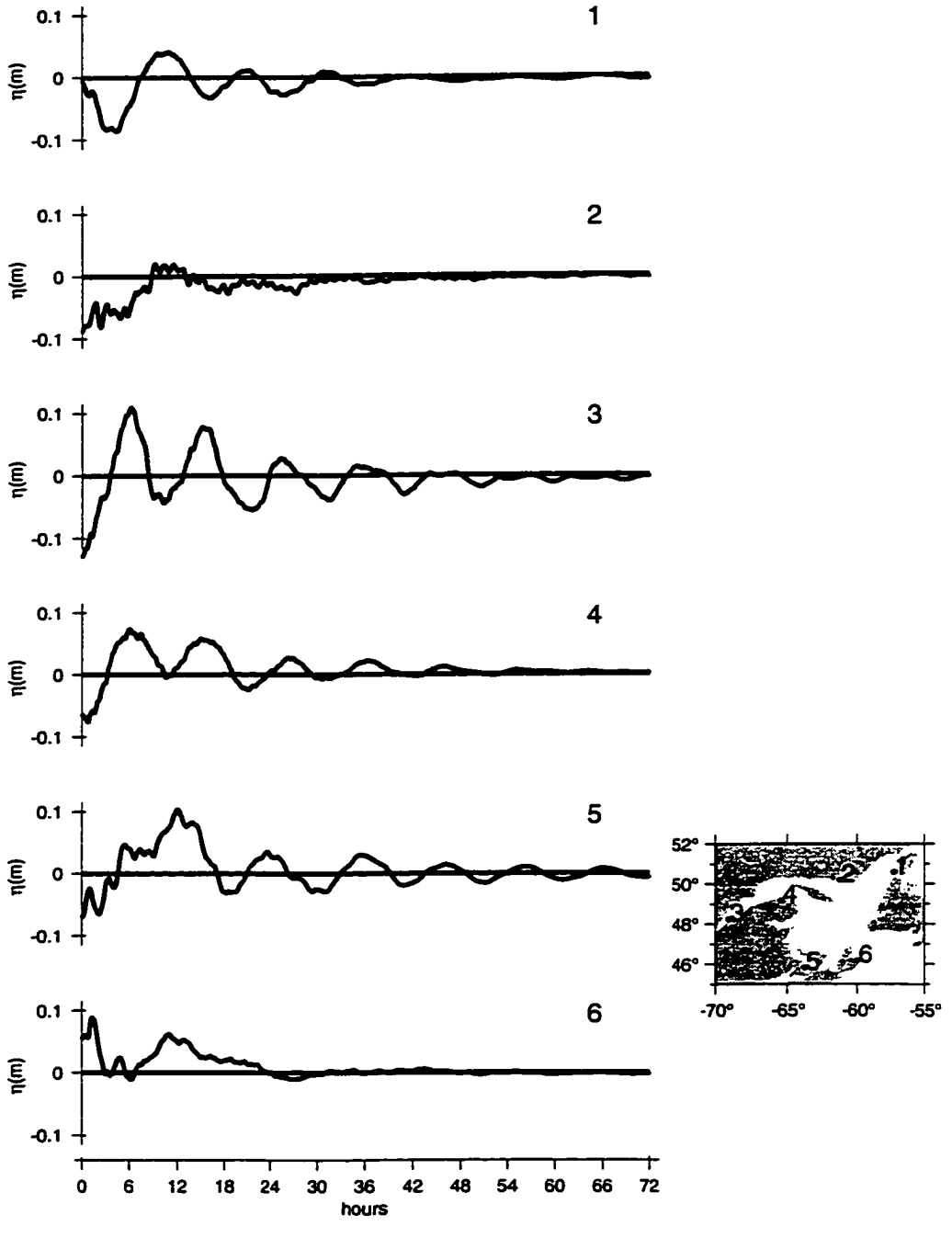

Figure 5.8: Sea level response at selected locations to an eastward wind that was suddenly turned off at t=0. The locations of the tide gauges are shown on the small map to the right of the time series plots. The magnitude of the wind stress used to drive the model into the steady state was 0.4 Pa.

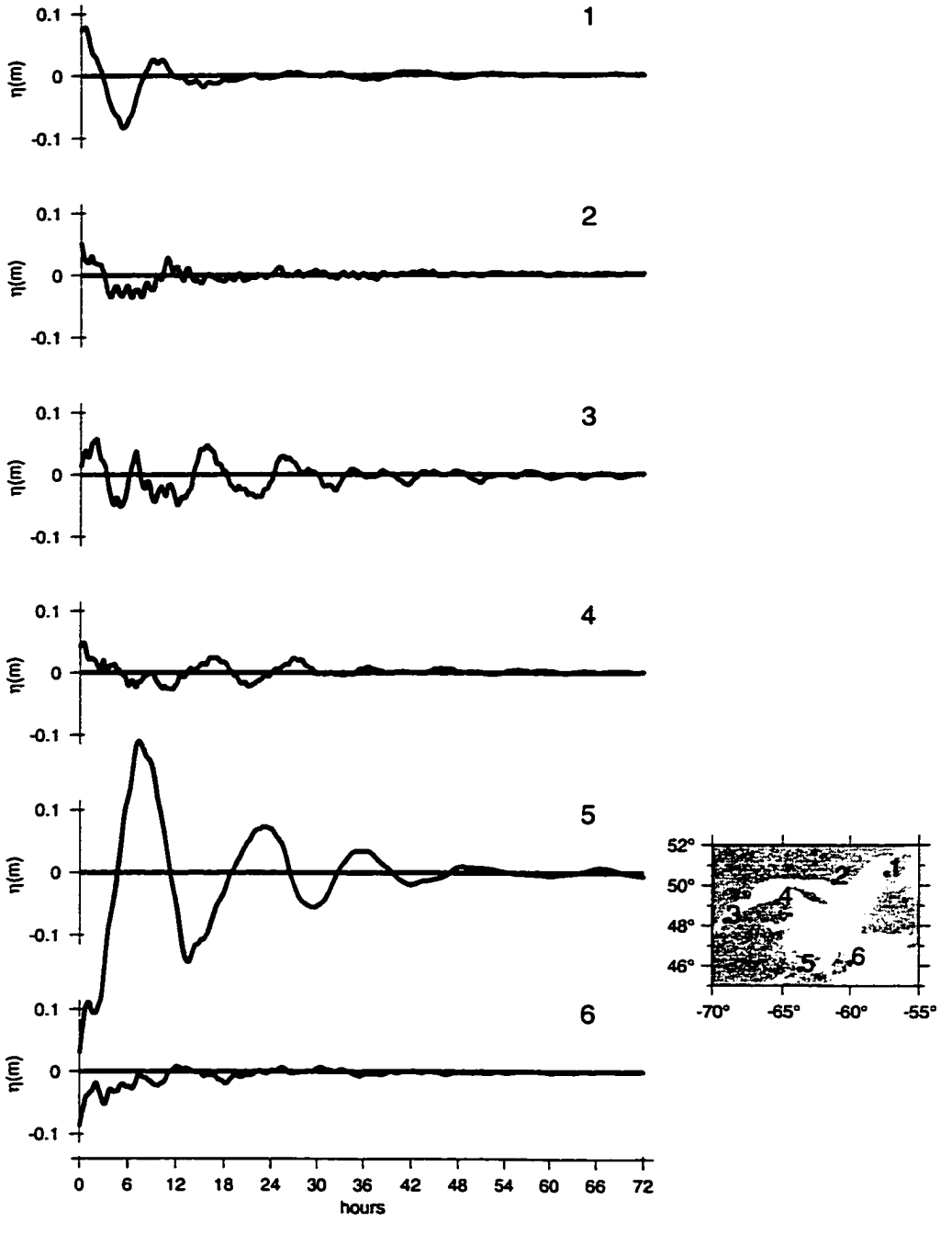

Figure 5.9: Sea level response at selected locations to a northward wind that was suddenly turned off at t=0. The locations of the tide gauges are shown on the small map to the right of the time series plots. The magnitude of the wind stress used to drive the model into the steady state was 0.4 Pa.

state. When the wind suddenly subsides, free oscillations are excited in the Gulf. Platzman (1972) showed that for a basin that has dimensions similar to the Gulf of Saint Lawrence we need to consider both longitudinal and latitudinal components of the flow as well as rotation. Therefore, as demonstrated in the data analysis section, it is rather difficult to use theoretical formulae to calculate the response of the Gulf, and a numerical calculation seems more appropriate.

The model was run for two cases: latitudinal and longitudinal (eastward and northward) wind forcing. In both cases a wind stress of 0.4 Pa was used to drive the model for 10 days after which it was effectively in a steady state. Then, the wind was suddenly turned off. The sea level response at selected locations around the Gulf is shown on Figures 5.8 and 5.9. The response in both cases is spatially very complex, both in sea level and currents.

The strongest response in both cases is in the shallow areas around Prince Edward Island, in the lower St. Lawrence estuary and in the approaches to the Strait of Belle Isle. The dominant periods of the response for both eastward and northward wind cases are at periods between 9 and 10 hours depending on the location. At most places more than one period is present. This is probably due to a number of small bays and inlets that typically have their own periods of response, as was the case with random wind forcing.

In conclusion, the local wind forcing can account for only a small part of the sea level variability. The origin of the energy peaks present in the data was explored by running a model forced by a spatially uniform, but temporally random wind field. The results indicated that the wind field that changed randomly every 12 hours could not induce much energy at the observed periods. The response of the Gulf of Saint Lawrence to step changes in the wind is spatially complex. Analysis of the sea level shows variability at periods around 9-10 hours that are also found in the data and are close to theoretical calculations for a circular basin.

5.3.3 Boundary Driven Flow

The statistical analysis of Section 5.2 suggested that the effects of boundary forcing are important for the sea level variability in the Gulf. Therefore, in this section I account for

the forcing through the open boundaries of the model domain. The evolution of the open boundaries will be inferred using the assimilation scheme described in Chapter 3.

The results from wind and boundary driven model runs for January and February of 1986 and 1987 are shown on Figures 5.10 and 5.11. The fit of the sea level improves at all locations and the γ^2 values are typically 0.2. The fit of the model does not change dramatically when data from more than 3 locations are assimilated into the model. These results are comparable to the statistical model that showed the dominance of the boundary forcing for the synoptic variability in the Gulf of Saint Lawrence.

The theoretical formula for the Helmholtz resonance considered earlier suggests that some of the energy peaks might be explained by boundary forcing of the Gulf of Saint Lawrence. Hence, as in the previous section, boundary forcing as a possible source of resonances in the Gulf is explored. Similarly to the wind-forced case, the model was run for two years and forced with random boundary forcing that changed every 12 hours. For this experiment the model was forced only through the Laurentian Channel using the same inflow structure as before. The Strait of Belle Isle carries little transport, so it is less likely that it could cause resonances in the whole Gulf. A test where both Laurentian Channel and southern Newfoundland boundaries were used was not different from the one with only Laurentian Channel as the control boundary.

Figure 5.12 shows the complex empirical orthogonal functions based on predicted sea level at the same locations as for the random wind case. The results show that some of the energy peaks found in the data might be due to the resonances induced through the open boundaries of the system. Energy peaks are present at periods of 35 and 21 hours. Eigenvector elements plotted for these two periods (Figure 5.12) show cyclonic propagation of the signal. The model derived phases (vector angles in Figure 5.12) are comparable to those obtained from the data analysis. The period at 35 hours is close to the theoretical calculation for the Helmholtz period. The pure Helmholtz oscillation, however, is a standing wave and should not be propagating around the Gulf. On the other hand, theoretical calculation suggested that topography might be responsible for the oscillations with periods shorter than 2 days. To explore the possible role of topography, the model was also

run with a flat bottom in the Gulf of Saint Lawrence only (realistic bottom topography was kept in the rest of the model domain). Although, this kind of experiment may not be very realistic, it showed that in the case of a flat bottom, an energy peak at 35 hours was not present any more. This demonstrates that the topography probably plays an important role in generating resonant response in the Gulf.

Evidence of a potential resonance event with the period of 35 hours could be found around day 5 of the 1986 sea level series, when the sea level shows large variation with amplitude of 1 m. The wind driven model (Figure 5.6) does not reproduce the event; however, when boundary forcing (Figure 5.10) is included, the model can reproduce this oscillation. This result suggests that the oscillation at 35 hours is due to boundary forcing.

Considering the complex geometry of the Gulf, it is hard to estimate the origin of the energy peak at 21 hours. A theoretical estimate of the quarter-wavelength period of the Laurentian Channel gave a period of 22 hours. Individual sea level power spectra indeed suggest that there is more energy at periods around 21 hours at locations in the lower estuary. The phase propagation for those locations is similar to the observed one. However, the spatial structure of the first mode obtained through complex EOFs does not correspond to a quarter wave resonance. In addition, the model used here did not include the whole of the Laurentian Channel and the theoretical formula is based on the full channel length. Thus it is difficult to draw any definitive conclusions about the origin of the resonance at this period.

5.4 Discussion

A linear, barotropic, depth-averaged model with data assimilation was used to study the response of the Gulf of Saint Lawrence to local and remote meteorologically induced variability. Both data analysis and model show that twice daily winds cannot account for much of the variance of the sea level around the Gulf of Saint Lawrence: residual error variances with wind forcing were typically of order $\gamma^2 = 1.00$ When boundary forcing was included and evolution of the open boundaries determined by data assimilation, the residual variance

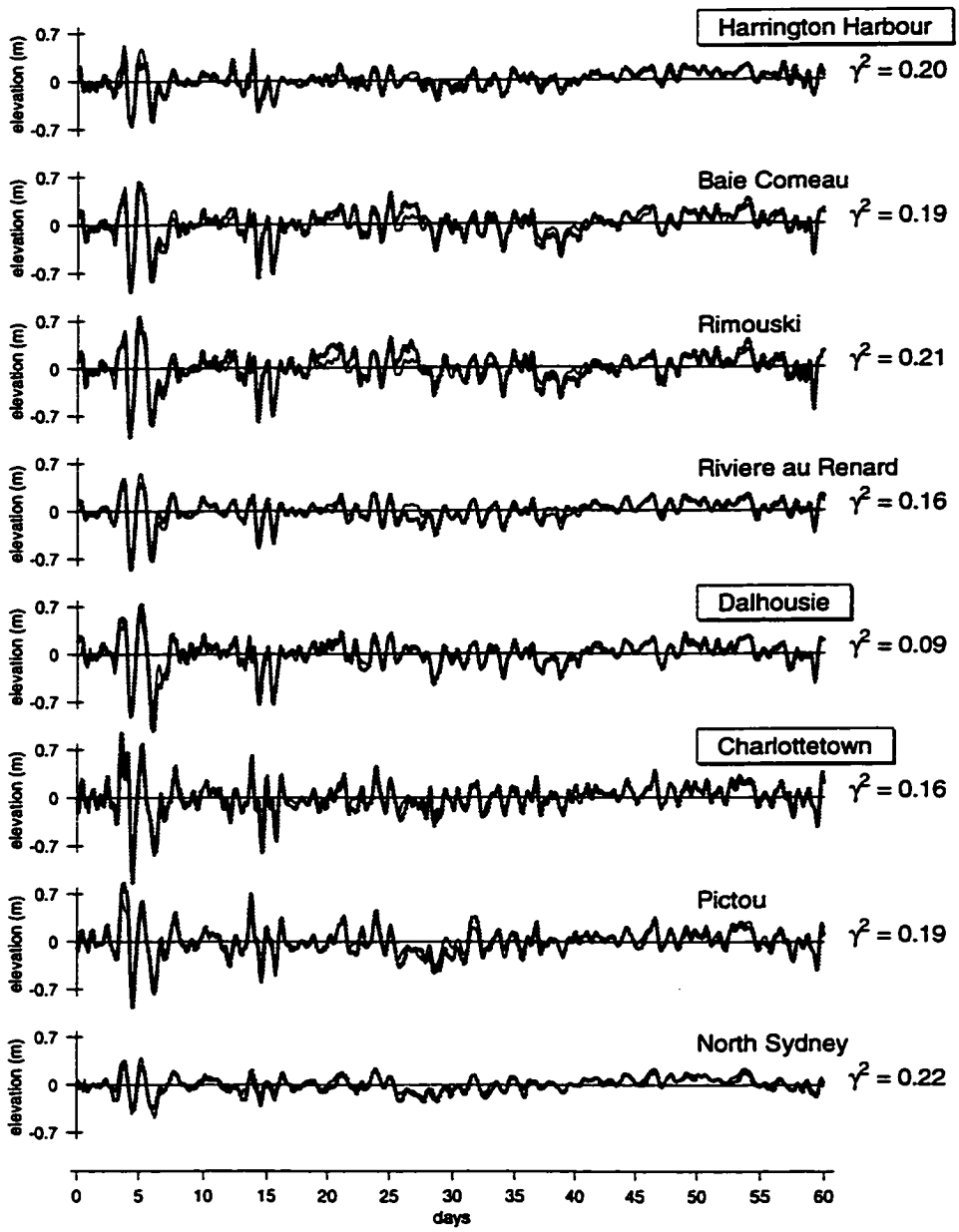

Figure 5.10: Comparison of observed adjusted sea level (thick) and predictions from the model (thin) driven by the observed wind and boundary forcing through the Strait of Belle Isle, along the southern Newfoundland coast and through the Laurentian Channel. The boundary conditions were obtained by assimilating sea level from Harrington Harbour, Dalhousie and Charlottetown (shown by boxed labels). The thick (thin) line shows observed (predicted) adjusted sea level. The period covered is 60 days starting on January 1st 1986. The value of γ^2 shown to the right of each graph is the variance of the difference between observations and predictions divided by the observation variance.

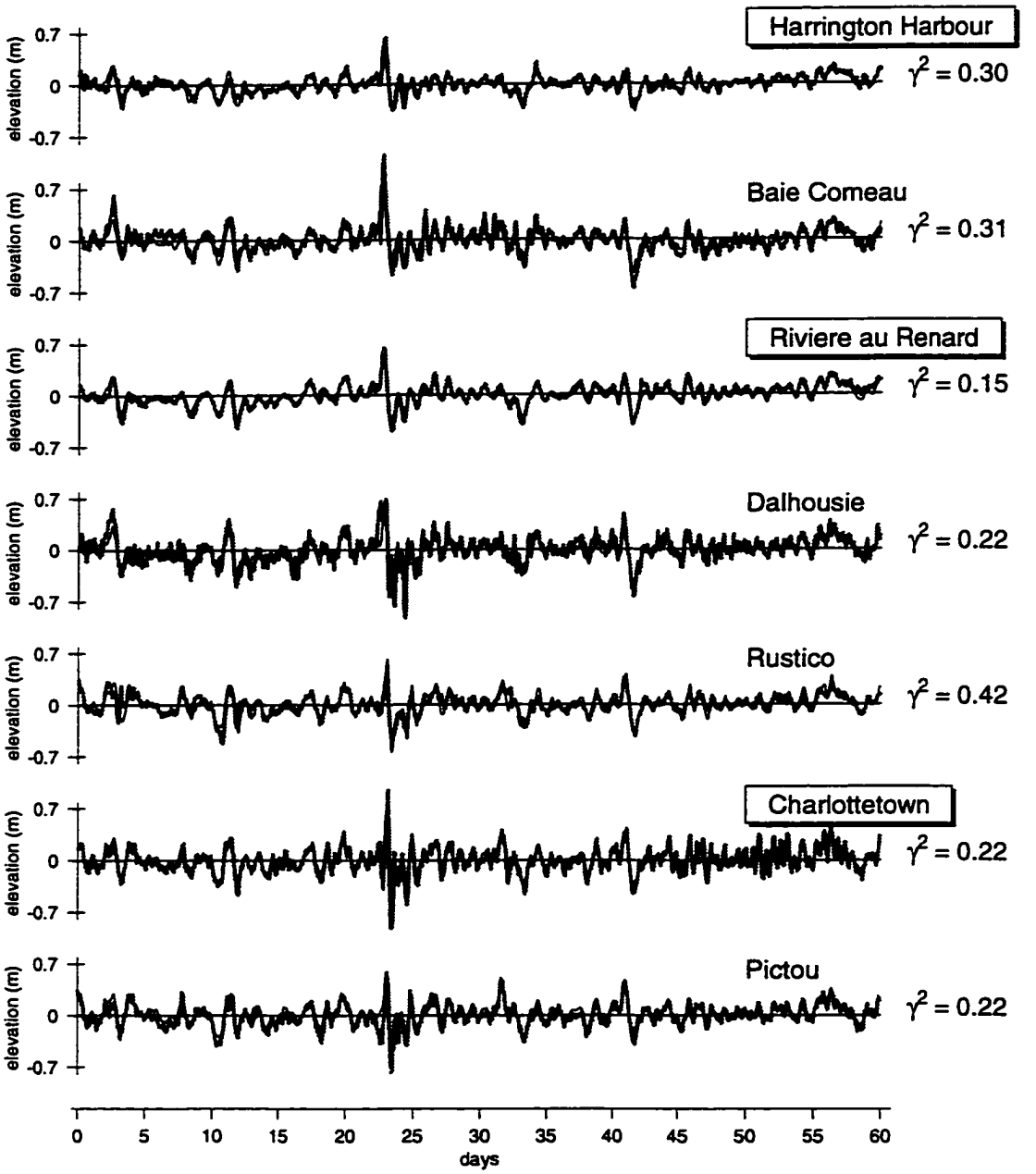

Figure 5.11: Comparison of observed adjusted sea level (thin) and predictions from the model (thick) driven by the observed wind and boundary forcing through the Strait of Belle Isle, along the southern Newfoundland coast and through the Laurentian Channel. The boundary conditions were obtained by assimilating sea level from Harrington Harbour, Riviere au Renard and Charlottetown (shown by boxed labels). The thick (thin) line shows observed (predicted) adjusted sea level. The period covered is 60 days starting on January 1st 1987. The value of γ^2 shown to the right of each graph is the variance of the difference between observations and predictions divided by the observation variance.

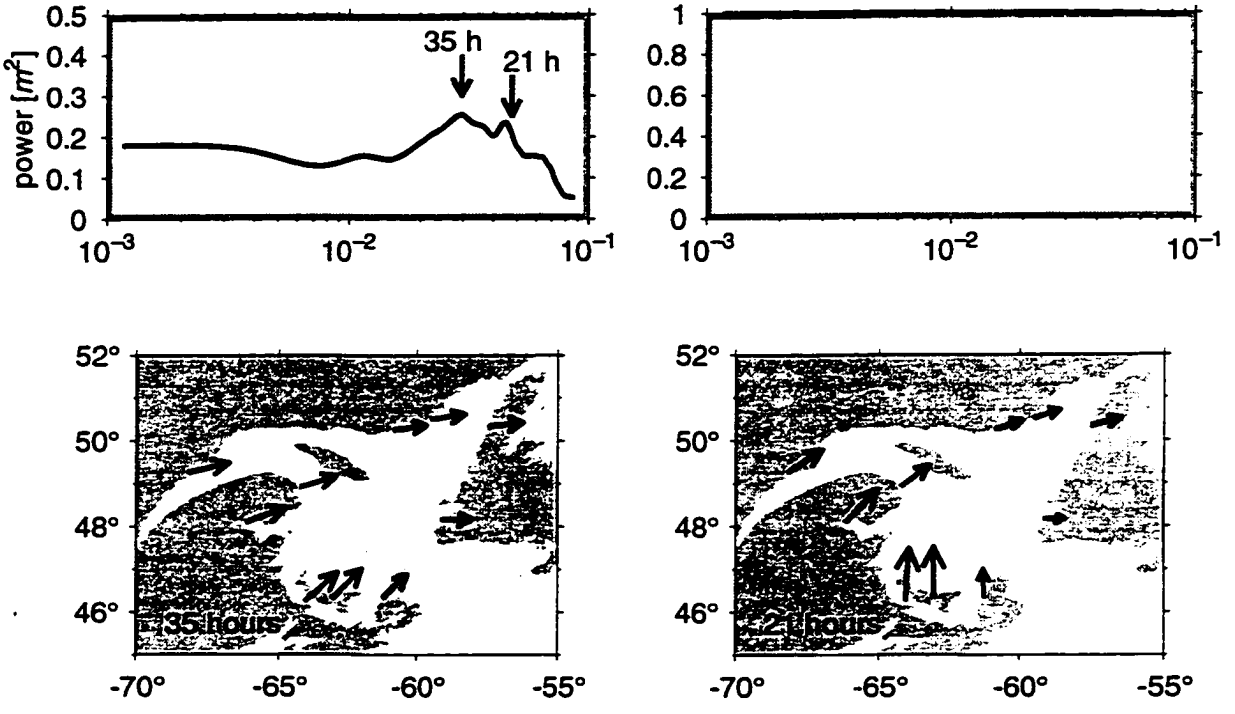

Figure 5.12: Complex empirical orthogonal functions for the sea level based on the model forced by the boundary forcing along the Newfoundland coast that changed randomly every 12 hours and was linearly interpolated. The upper left panel shows the trace of the cross-spectral matrix (thick line) and the first eigenvalue (thin line). The model was forced by one boundary condition, so thick and thin lines are identical. The lower row shows the eigenvector elements in the complex plane for periods of 35 and 21 hour.

ratio was reduced to around 0.2.

Data analysis showed evidence of resonances at periods of 35, 21 and 15 hours. The model was used to relate some of these periods to wind and boundary forcing. The model forced by a spatially uniform wind field, that changed randomly every 12 hours, showed that wind forcing could not explain the energy peaks found in the data. Theoretical calculations for a circular basin suggested that wind-induced resonances are more likely to appear at frequencies higher than the inertial. A similar experiment with the boundary forcing suggested that the oscillations with period of 35 hours could be the result of boundary forcing. The period is close to the theoretical estimate for the Helmholtz period, however it seems more likely that (because of its cyclonic propagation) this oscillation is due to topographic waves that propagate counter-clockwise around the basin. The model was also used to examine the response of the Gulf to a step change in the spatially uniform wind forcing. Both longitudinal and latitudinal wind components show responses at similar periods between 9 and 10 hours.

The results of this analysis show that local wind forcing cannot account for the synoptic variability in the sea level within the Gulf. The boundary forcing via Cabot Strait is the dominant source of sea level variability. The origin of the boundary forcing is however unknown. The data assimilation procedure, described in Chapter 3, provides us with the temporal evolution of the control boundary amplitudes. The boundary forcing (inflow at the boundary) is due to some distant effects and part of it is probably due to wind driven flow on the Newfoundland and Labrador Shelves. Here an attempt is made to relate the boundary forcing amplitude obtained by the assimilation model to the large scale wind field. Figure 5.13 shows correlation coefficients between boundary forcing and the longitudinal and the latitudinal components of the wind field for each of the three boundaries used to drive the model. For example, the longitudinal component of a vector corresponds to the correlation coefficient between the boundary inflow and the longitudinal component of the wind. The correlation maps show that a southward along-shore wind on the Labrador and Newfoundland Shelf is highly correlated with inflow along the Laurentian Channel and inflow along the southern Newfoundland coast. These results provide a basis for operational

modelling of the Gulf. The boundary forcing obtained by the assimilative model could be related to the data in the interior and(or) wind stress over distant areas (e.g. Labrador and Newfoundland shelves). Once the transfer function between the boundary and the data is known, we could predict the evolution of the open boundary condition, similarly to the suboptimal scheme tested for the Labrador Shelf.

The dynamics of the relationship between the distant wind forcing and the boundary forcing of the Gulf of Saint Lawrence can only be represented by a large scale dynamical model. That is also the only way to clearly determine the spatial structure of the boundaries that could be used in future modelling efforts in the Gulf of Saint Lawrence. Therefore, in the next chapter a large scale model, driven by winds and surface pressure, is used to hindcast the flow on the whole of the Canadian Atlantic Shelf.

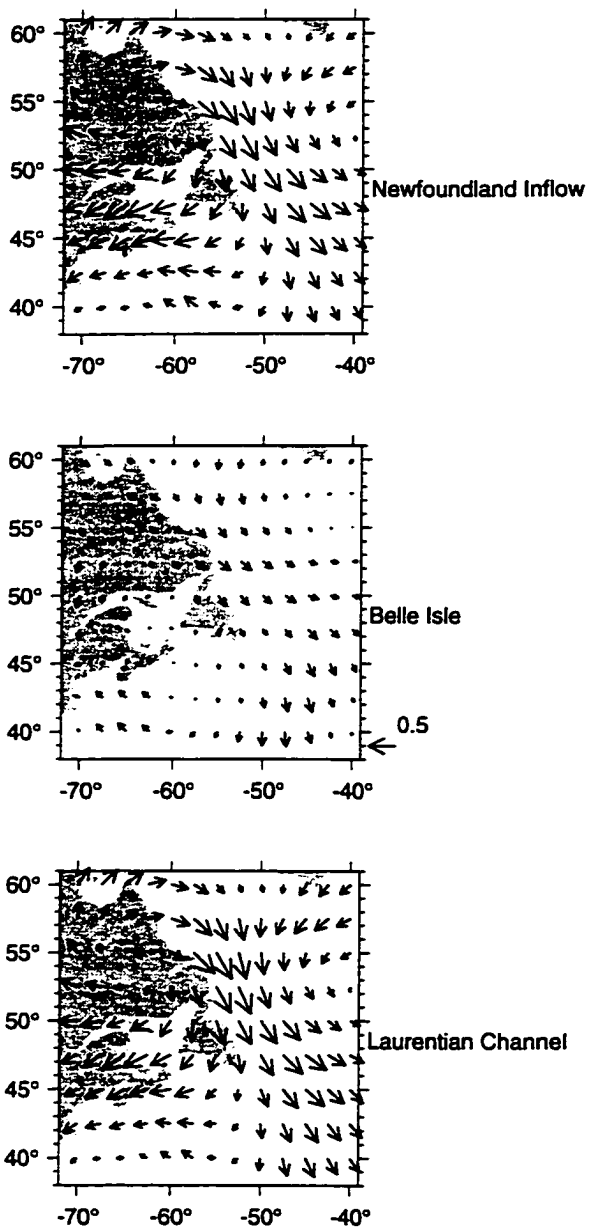

Figure 5.13: Correlation coefficients between the time varying boundary conditions for the Gulf of Saint Lawrence model and the large scale wind field. The boundary conditions were obtained from a data assimilative run. The arrows represent the correlation with longitudinal and latitudinal components of the wind field. First panel is for the inflow along the southern Newfoundland coast, second panel for the Strait of Belle Isle inflow and the third one for the inflow along the Laurentian Channel (as shown in Figure 5.5).

Chapter 6

Canadian Atlantic Shelf

In this chapter I focus on the whole of the Canadian Atlantic Shelf. The earlier subregional studies of the Labrador Shelf and the Gulf of Saint Lawrence indicated the relative importance of wind and boundary forcing. However, the dynamical mechanisms of the interactions between the subregions are still unknown. Only a large scale model that covers all of the Canadian Atlantic Shelf can address the questions related to the signal propagation from one area to another, the relative importance of the distant forcing that originates in a particular subregion for the downstream shelves, etc. In contrast to the earlier studies, in this chapter a wind and pressure driven model without data assimilation is used. The main goal of this study is to examine the connections between the individual shelves and develop a model that can be used operationally.

The data collected in the region are first used to analyse large scale patterns using principal component analysis. Statistical models are then used to estimate the relative importance of wind forcing over the Newfoundland Shelf and the Gulf of Saint Lawrence on the Scotian Shelf. Finally, the dynamical model is used to hindcast the flow on the shelf for two months. The model results are validated against independent oceanographic observations. The connections between the subregions are explored in detail by considering the transports through the virtual boundaries between the subregions of the model domain.

As discussed above, operational applications are usually associated with severe time constraints. Thus, timely information about the relative importance of the remote forcing

from a particular region is critical when trying to estimate the boundary flow of a limited area model. Therefore, the model is used to estimate the relative contribution of wind driven flow over one area for the downstream shelves. Once the effects of, for example, wind over the Newfoundland Shelf on the currents on the Scotian Shelf are known, the relationship can be used for operational prediction of the boundary conditions for limited area models, provided that meteorological forecasts are available. The operational aspects of this model are discussed at the end of the chapter and, in expanded form, in the last chapter.

6.1 Data Analysis

Current meter, bottom pressure and tide gauge data from the Scotian Shelf (Figure 6.1) were obtained during the CASP (Canadian Atlantic Storms Programme) experiment in 1985-86 (see Appendix A). The goal of the programme (Anderson and Smith, 1989) was to generate a comprehensive data set that would allow a detailed description of the response of the coastal ocean to severe winter weather. Additional tide gauge data from the Gulf of Saint Lawrence were collected at permanent tide gauge locations (not part of CASP).

I choose to concentrate on two winter months (January and February of 1986) that had the best data coverage in all regions. Sea level, bottom pressure and current-meter data were analysed for tides and filtered to remove all oscillations with periods less than 36 hours. The filtering was necessary for the consistency of statistical analysis because part of the data set (sea level and bottom pressures from the Scotian Shelf area) was obtained in filtered form. Sea level time series were isostatically adjusted to remove the inverse barometer effect.

Cross-spectra of the sea level time series (not shown here) with separation distance of about 800 kilometers (Port aux Basques (1) and Cape Sable (18) on Figure 6.1) show that these two signals are highly coherent. The records might be coherent simply because their forcing was coherent, but their coherence could also indicate that the signal forcing the Gulf of Saint Lawrence at Port aux Basques propagates southward along the Scotian Shelf. To

examine the spatial scales on which these interactions might occur the correlation matrix was formed. The matrix is based on adjusted sea level (12 locations around the Gulf of Saint Lawrence and 6 along the Scotian Shelf; Figure 6.1) and currents from the Scotian Shelf (both u and v components of the velocity at 10 locations). A principal component analysis was then performed on the correlation matrix. The observations were then projected on to the eigenvectors and modal amplitudes for the three modes with largest eigenvalues were calculated (Figure 6.2). The corresponding eigenvector elements for sea level are plotted in Figure 6.3 (left column), and for currents in Figure 6.4 (left column).

The first mode accounts for 36% of the variability. Spatially it corresponds to a large scale mean sea level and strong alongshore flow on the Scotian Shelf. The second mode corresponds to a NE-SW sea level gradient in the Gulf of Saint Lawrence that is associated with a strong alongshore gradient on the Scotian Shelf. The corresponding current components are weaker than in the first mode and show more spatial variability. The sea level pattern in the third mode is similar to the second one, with a weaker spatial gradient in the Gulf of Saint Lawrence. The currents associated with the third mode are similar to the first mode but the flow is reversed. The first and second modal amplitudes are highly coherent and in quadrature: the second mode lags by 90°. The physical interpretation is that after the mean sea level rises (or falls), local gradients are established, i.e. signal propagates through the Gulf of Saint Lawrence and downstream on the Scotian Shelf. Full interpretation based on the data is, of course, difficult, so this question will be addressed with the numerical model.

6.2 Statistical Model

In this section the linear statistical model described in Chapter 3 is used to estimate the relative importance of the wind forcing over different regions for the variability in the the Gulf of Saint Lawrence and on the Scotian Shelf. Modal analysis showed that the flow on the Scotian Shelf is dominated by the along-shore component of the flow. Hence, adjusted sea level, bottom pressure and the along-shore component of the flow are regressed

against wind stress from the Newfoundland Shelf and in the Gulf of Saint Lawrence. The alongshore axis is defined as being parallel to the coast for all current meter locations. The number of lags used was again chosen according to AIC and the optimal fit was found for a maximum number of lags (K) corresponding to 3 days.

To estimate the effect of wind over the Newfoundland Shelf, all oceanographic variables (Figure 6.1) were regressed against two representative wind series for the Newfoundland Shelf. The rationale here is that the wind driven flow over the Newfoundland Shelf could be an important source of the remote forcing for the Gulf of Saint Lawrence and could possibly have some impact on the Scotian Shelf. The regression results are shown in the first column of Tables 6.1, 6.2 and 6.3. The residual sea level variance around the Gulf of Saint Lawrence ranges from 0.37 to 0.58. Generally, the fit deteriorates in the shallower southern part of the Gulf where local wind forcing is probably more important. The best fit is realized for the northern part of the Scotian Shelf ($\gamma^2_{min} = 0.21$), but low values of γ^2_{min} are persistent all along the Scotian Shelf. Similar values are obtained for bottom pressure data across the Scotian Shelf (Table 6.2). The alongshore component of the currents on the Scotian Shelf shows a considerable variation in the fit, ranging from 0.27 to 0.73. The current meters close to shore generally fit better. This is likely a result of a strong coastal jet driven by remote forcing which may partly originate on the Newfoundland Shelf. The current meters away from the coast are probably more affected by nonlinear effects and baroclinic instabilities.

Next, the effect of the wind over the Gulf of Saint Lawrence is assessed by again taking two representative wind stress series (column GSL in Tables 6.1, 6.2 and 6.3). The wind stress now provides a local forcing for the data around the Gulf of Saint Lawrence and another source of the remote variability for the Scotian Shelf. The local wind stress seems to play a significant role in the Gulf of Saint Lawrence (γ^2_{min} between 0.24 to 0.60). The fit is better for the locations in the interior of the Gulf than for those in the Strait of Belle Isle or Cabot Strait. The results suggest that winds over the Newfoundland Shelf have more influence (γ^2_{min} around 0.25) on the Scotian Shelf variability than the Gulf of Saint Lawrence winds (γ^2_{min} around 0.39). This is even more evident in the bottom pressure and

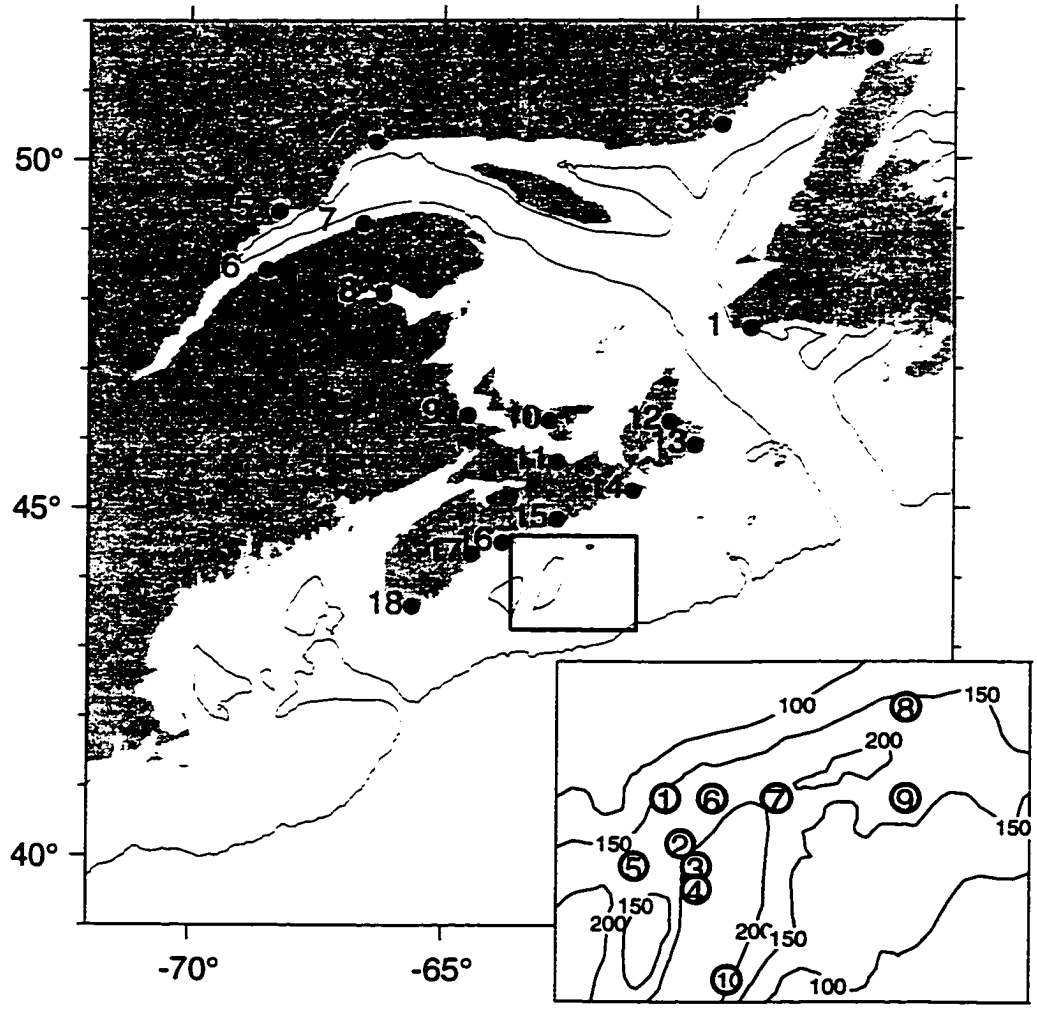

Figure 6.1: Observation locations. The dots mark coastal tide gauges (Table 6.1). The inset shows current meter and bottom pressure locations on the Scotian Shelf (For details see Appendix A).

along-shore current meter data where, typically, the Newfoundland Shelf winds account for about 10% more variability in the currents. At this point we can only speculate that the flow across the Laurentian Channel or the along-shelf-break flow may be responsible for the higher contribution of the Newfoundland Shelf to the Scotian Shelf data variability. This question will be addressed using the circulation model, as described in the next section. It should be noted that the two representative stresses in the Gulf are closer than those on the Newfoundland Shelf, which may, due to their higher correlation, result in poorer fits.

The last regression experiment integrates the previous two by regressing the oceanographic variables against both Newfoundland and Gulf of Saint Lawrence wind stresses. The statistical significance of the fit when the Gulf of Saint Lawrence winds are included is determined using the phase randomization procedure described in Chapter 3. The residual sea level variances for the Gulf are now below 25% (column All). The fit improvements are significant for all locations except West St. Modeste in the Strait of Belle Isle. This is not surprising because West St. Modeste together with Harrington Harbour showed the worst fit for the case with Gulf winds only, so the improvements in the fit when both Gulf and Newfoundland winds are considered could be attributed to over-fitting. Sea level at West St. Modeste is probably under the dominant influence of the Labrador Shelf flow, as indicated by the correlation with Labrador Shelf winds, shown in Chapter 5. (This remains to be confirmed with the dynamical model.) The bottom pressure fit improves at all locations (Table 6.2), so relative residual variances are now 15% or lower. The improvements are significant. The current meter fit improves as well, but those changes are not statistically significant. The reason for that might be the fact that four new series (two components for two locations) were added to the model. The phase randomisation test is only a rough estimate of the significance of the fit and it might not have much statistical power when a large number of forcing functions are added.

The statistical model used here was based on wind stress from the Newfoundland Shelf and the Gulf of Saint Lawrence. Although, the wind stress used could be taken as representative for most of the region, the conclusions from the statistical model are limited, for the reasons discussed earlier. Particularly, in this case, over-fitting might be a serious problem

because sea levels are regressed against wind stress from 4 locations that are correlated with each other. In the above analysis the statistical model helps us to understand the major effects that wind forcing over certain regions have on adjusted sea level, bottom pressure and currents on downstream shelves. It does not provide a clear result regarding the relative importance of the remote flow from a particular region, neither does it offer any dynamical explanation for how those interactions occur. The only way to address these questions is to use a numerical model that can provide clear answers about the origin and contribution of different forcing within the domain.

6.3 Dynamical Model Results

In this section results from a dynamical model that covers the whole Canadian Atlantic Shelf are presented. The goal is to assess the skill of a model driven by wind and pressure without data assimilation. By considering a larger domain I hope to account for the connections between the regions that were otherwise parameterized in some way. The model results are validated against the observations through both principal component analysis and comparison of predicted time series against statistical model predictions. The connections between the subregions are analysed by considering the transport variability through a number of sections that represent boundaries between subregions of the model domain.

6.3.1 Model Setup

The model domain (Figure 3.1) spans 38°N to 60°N and 72°W to 40°W. The resolution is $1/12^{o}$, which represents 9.3 km in the meridional direction. All boundaries are open and the radiation condition described in Chapter 3 is used. The model is forced by surface wind stress and pressure fields, that were linearly interpolated on the model grid both spatially and temporally. To increase computational efficiency the bathymetry of the deep ocean is flattened at 2000 m, so that all points deeper than 2000 m are set to that depth. This was necessary to do because the bathymetry in the Labrador Sea reaches the depth of over 4000 m that would require smaller model time steps to avoid numerical instability. With deep

Station	No.	NF	GSL	All	Wind	W+P
P.aux Basques	1	0.48	0.40	0.24	0.59	0.58
W.St. Modeste	2	0.37	0.60	0.25	0.35	0.33
Harrington H.	3	0.52	0.61	0.27	0.52	0.50
Baie Comeau	4	0.42	0.24	0.12	0.22	0.22
Rimouski	5	0.46	0.25	0.14	0.24	0.24
St.Anne	6	0.48	0.37	0.22	0.42	0.42
Riv au Renard	7	0.45	0.43	0.20	0.78	0.77
Dalhousie	8	0.39	0.25	0.10	0.24	0.24
Shediac Bay	9	0.51	0.24	0.12	0.22	0.22
Charlottetown	10	0.58	0.33	0.19	0.33	0.33
Pictou	11	0.58	0.30	0.17	0.37	0.36
North Sydney	12	0.49	0.52	0.23	0.61	0.61
Louisbourg	13	0.21	0.39	0.11	0.31	0.31
Temp-1	14	0.21	0.44	0.11	0.30	0.30
Temp-2	15	0.25	0.37	0.11	0.23	0.22
Sambro	16	0.27	0.39	0.11	0.25	0.25
Temp-3	17	0.27	0.33	0.09	0.17	0.17
Cape Sable	18	0.26	0.39	0.10	0.24	0.24

Table 6.1: Fit of regression of adjusted sea level on lagged winds, and the fit of the circulation model. The numbers are values of γ^2_{min} for the statistical model (NF, GSL and All) and γ^2 for the circulation model (Wind and W+P). The stations are listed anti-clockwise around the Gulf of Saint Lawrence and along the Scotian Shelf. The station numbers correspond to locations given in Figure 6.1. The regression fit is presented for Newfoundland Shelf winds (NF), Gulf of Saint Lawrence winds (GSL) and winds over both Newfoundland Shelf and Gulf of Saint Lawrence (All). The circulation model fit is presented for wind driven model (Wind) and for wind and pressure driven model (W+P).

Station	NF	GSL	All	Wind	W+P
p1	0.35	0.39	0.15	0.29	0.29
p2	0.29	0.40	0.12	0.26	0.26
p5	0.31	0.39	0.13	0.24	0.22
p6	0.30	0.39	0.12	0.23	0.22
p7	0.27	0.43	0.12	0.34	0.34
p8	0.26	0.42	0.11	0.27	0.27
p9	0.26	0.42	0.12	0.41	0.40
p10	0.33	0.42	0.14	0.38	0.36

Table 6.2: Fit of regression of bottom pressure gauges on lagged winds (NF, GSL and All) and the fit of the circulation model (Wind and W+P). The stations locations correspond to those given in Figure 6.1. The regression fit is presented for Newfoundland Shelf winds (NF), Gulf of Saint Lawrence winds (GSL) and winds over both Newfoundland Shelf and Gulf of Saint Lawrence (All). The circulation model fit is presented for wind driven model (Wind) and for wind and pressure driven model (W+P).

Station	NF	GSL	All	Wind	W+P
c1	0.42	0.56	0.30	0.48	0.48
c2	0.27	0.62	0.18	0.39	0.39
c3	0.46	0.57	0.23	0.55	0.56
c4	0.59	0.47	0.29	1.02	1.02
c5	0.73	0.69	0.45	1.44	1.43
c6	0.42	0.53	0.24	0.45	0.45
c7	0.38	0.53	0.23	0.50	0.50
c8	0.47	0.55	0.33	0.76	0.76
c9	0.44	0.52	0.25	0.92	0.92
c10	0.64	0.65	0.43	0.92	0.93

Table 6.3: Fit of regression of alongshore currents on lagged winds (NF, GSL and All) and the fit of the circulation model (Wind and W+P). The stations locations correspond to those given on Figure 6.1. The regression fit is presented for Newfoundland Shelf winds (NF), Gulf of Saint Lawrence winds (GSL) and winds over both Newfoundland Shelf and Gulf of Saint Lawrence (All). The circulation model was driven by the winds over the whole domain (Wind) and by wind and pressure (W+P).

water set to 2000 m a two month run of the model still took about two days.

6.3.2 Wind Driven Flow

The wind driven flow on the Canadian Atlantic Shelf is examined by driving the model by the wind over the two month period, January and February 1986. This is the same period as analysed in Section 6.2.

Using the same procedure as for the data, a correlation matrix of the model output is formed for 18 sea level data locations (12 around the Gulf of Saint Lawrence and 6 along the Scotian Shelf) and 10 current meter series on the Scotian Shelf. Principal component analysis was then performed on the correlation matrix. Modal amplitudes for the three largest eigenvalues are shown as thin lines on Figure 6.2. The corresponding eigenvector elements for sea level series are plotted in Figure 6.3 and for currents in Figure 6.4.

The modal analysis provides an overall comparison between the model and the data. It shows that general spatial patterns found in the data are captured by the model. The agreement for the first two sets of principal components is remarkable. The third mode starts to diverge from the observed pattern, particularly for the currents, but that is an expected result considering the simple dynamics represented in the model.

The first three modes account for 76% of the variability in the model, but only 58% in the data. The spectral analysis of the modal amplitudes associated with the first three modes (not presented here) shows that observations and model predictions are coherent and in phase for all periods for the first and second mode. For the third mode, observations and model predictions are coherent and in phase only in the synoptic band (2-10 days), but that is where most of the energy is concentrated. Let us now consider the individual eigenvectors and their elements for each of the modes.

The first mode, again, corresponds to a large scale mean sea level. It accounts for most of the variance (50% in the model vs. 36% in the observations). The current meter based components show a similar pattern as the data with a strong along-shore flow.

In the second mode the model reproduces the same NE-SW gradient in the sea level

in the Gulf of Saint Lawrence. However, while the data show the presence of the alongshore gradient on the Scotian Shelf, the model predicts relatively uniform sea level. The difference in the currents associated with this mode is probably related to the non-existing alongshore gradient in the model sea level.

The third mode shows the worst agreement between the data and the model predictions. The model predicts a strong gradient along the Scotian Shelf but the structure in the Gulf of Saint Lawrence differs from its data counterpart. The currents associated with this mode show correspondence to the data but much more spatial variability.

In section 6.2 the best fitting linear statistical model was used to assess the relative importance of the remote wind driven flow on a location specific basis. I now use the same approach to assess the fit of the dynamical model.

The fits to adjusted sea level are summarised in Table 6.1 (column Wind) and plotted in Figure 6.5. The values for γ^2 vary dramatically from 0.17 to 0.78 (Table 6.1). In general, sea level data along the Scotian Shelf fit better than those around the Gulf of Saint Lawrence (Figure 6.6). The spatial resolution of the wind field might play some role. Higher resolution of the wind field would probably improve the results in the areas of highly variable land topography around the Gulf of Saint Lawrence (Herfst, 1984).

Bottom pressure gauge results are presented in Table 6.2. The fit is generally better for the stations closer to the shore, but overall it is similar to that for coastal sea level.

For the currents the same alongshore axis as in Section 6.2 is defined. The fit for the current meter data is highly variable (Figure 6.7). The values for γ^2 range from 0.39 to 1.44 (Table 6.3). The stations closer to the shore tend to fit better. The worst fits are found for the stations that are in topographically variable areas. The current meters are clustered in a relatively small region, however the observed time series differ significantly. This is not the case with the model prediction where the flow is rather smooth and shows less spatial variability. Sheng and Thompson (1997) found similar problems with a 3-D limited area data assimilative model for the Scotian Shelf. As evidenced on the Labrador Shelf, the local bathymetry plays an important role that needs to be recognized when the fit of a barotropic model is assessed. The fit improves at three current meter locations if the local

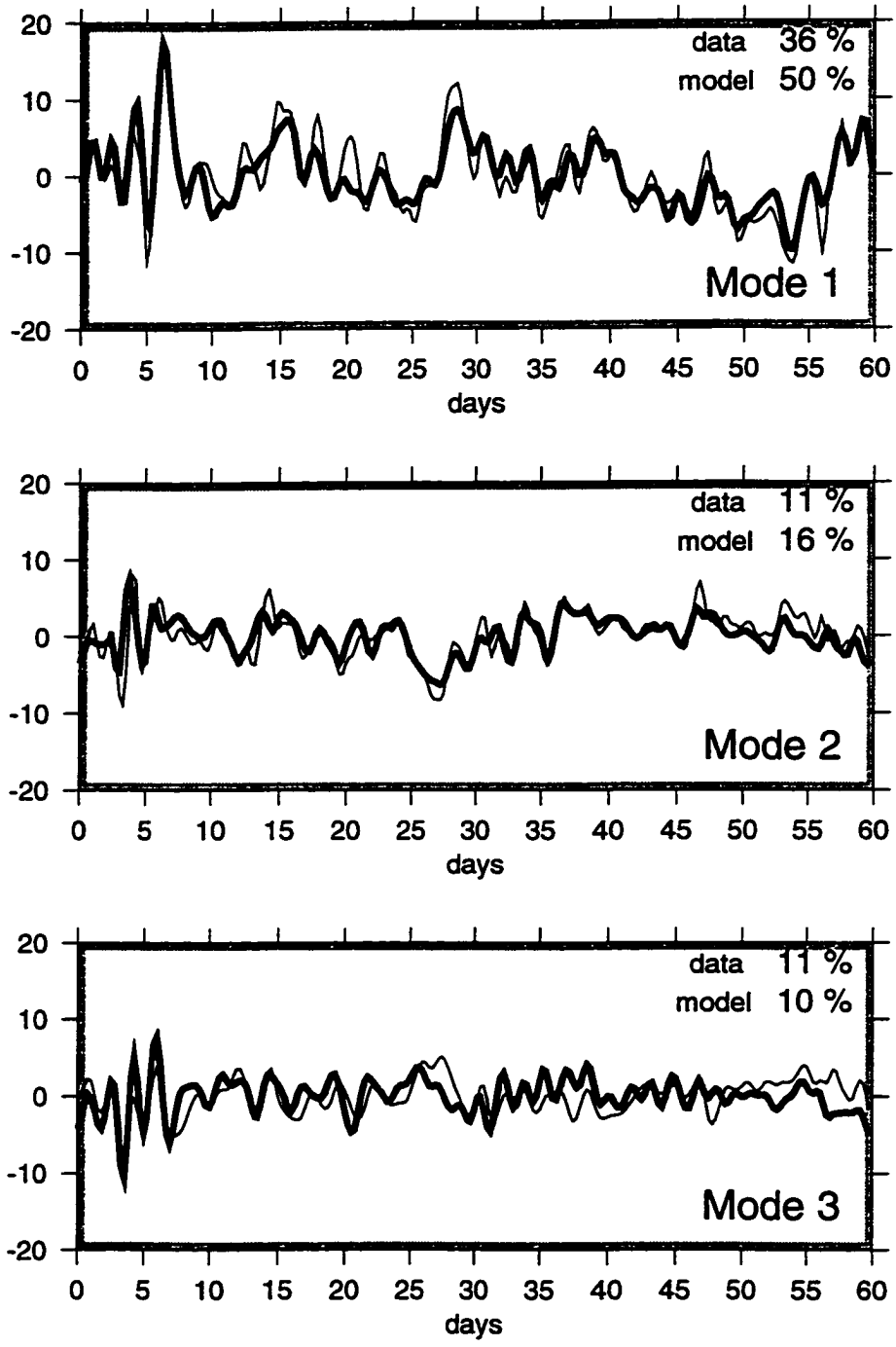

Figure 6.2: Time series of modal amplitudes for first three eigenvector modes based on 18 adjusted sea levels and 10 current meter records. The correlation matrix was used. Data based modes are shown by thick and model predicted modes by thin lines. Numbers in the upper right corner represent the amount of the variability accounted for by that mode.

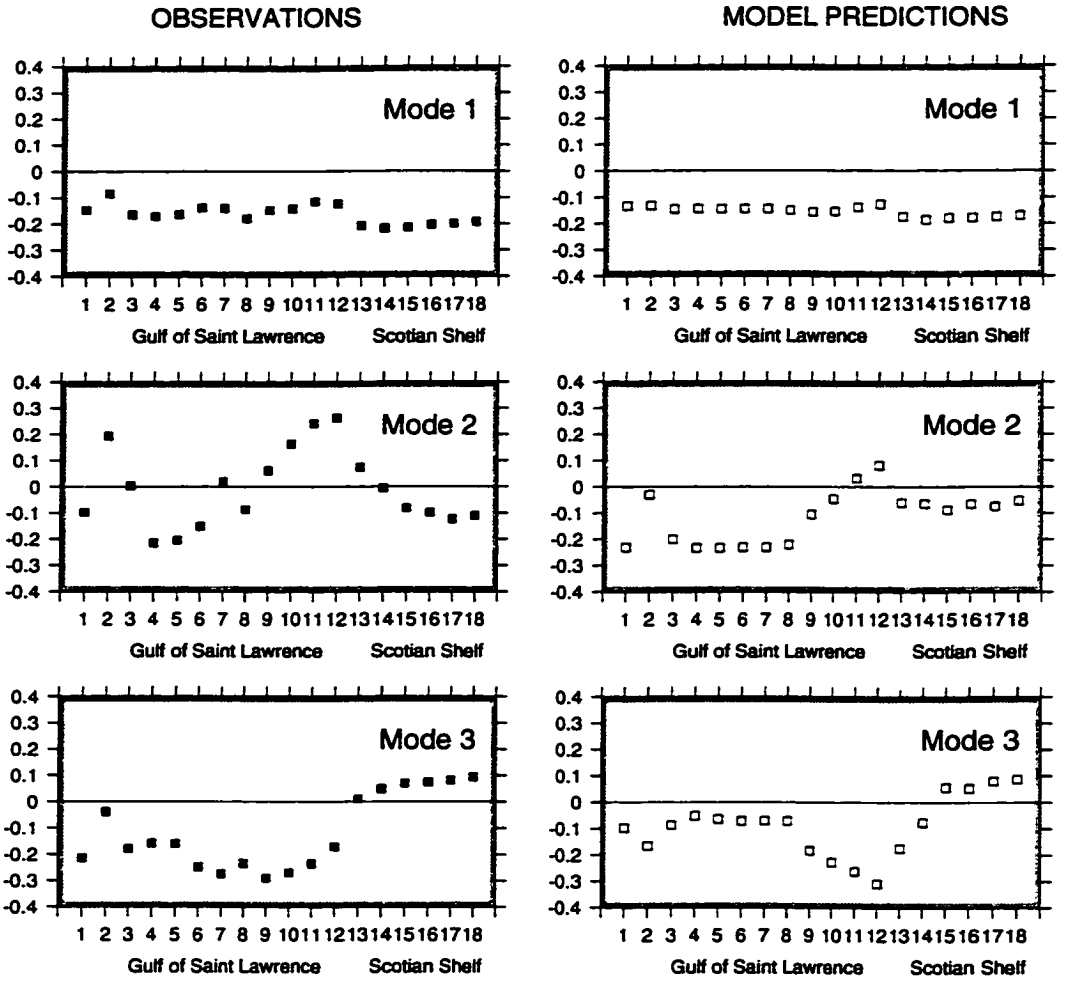

Figure 6.3: Eigenvector elements for adjusted sea level associated with the modes shown in Figure 6.2. Adjusted sea level stations are ordered anti-clockwise around the Gulf of Saint Lawrence and downstream along the Scotian Shelf (Table 6.1). The left (right) column shows eigenvectors based on observations (model predictions).

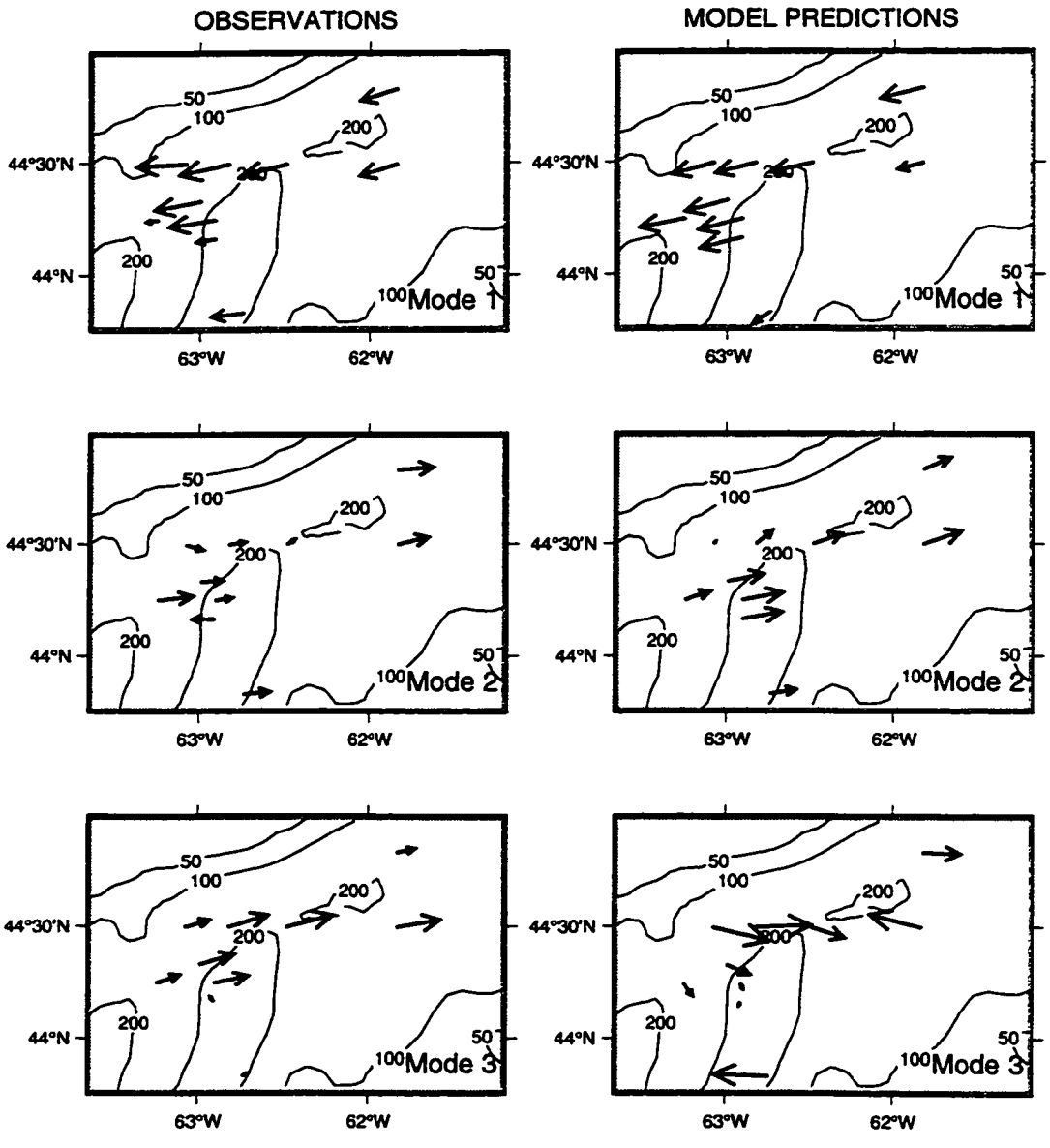

Figure 6.4: Eigenvector elements for currents on the Scotian Shelf associated with the modes shown in Figure 6.2. The left (right) column shows eigenvectors based on observations (model predictions). The locations correspond to those given by the inset of Figure 6.1.

along-isobath component is considered. At c4 γ^2 is reduced from 1.02 to 0.93, at c8 from 0.76 to 0.53 and at c9 from 0.92 to 0.84. This is consistent with the results obtained with the same kind of model on the Labrador Shelf. The rest of the variance not accounted for at the current-meter locations is probably due to other forcing mechanisms. Thompson and Sheng (1996) discuss the role of the baroclinic Nova Scotia Current that flows parallel to the shore between the 150 m and 200 m isobaths. It appears that the changes in its position might also have a significant effect on the predictions for some current meter locations.

Sheng and Thompson (1997) used a uniform wind field over the Scotian Shelf and data assimilation to infer the upstream boundary condition and got results of similar quality. Therefore, results from a large-scale model driven by a relatively coarse wind field are comparable to a study that assimilated sea level data to predict the variability on the Scotian Shelf.

The results presented show that a large scale wind driven model for the Canadian Atlantic Shelf has some predictive skill, particularly for the sea level. Moreover, they clearly demonstrate the importance of the connections between different regions. To further explore these connections four transects are defined that should be representative of the variability in transport between different subregions of the model domain (Figure 6.8). The transects are further partitioned into sections that should roughly represent different flow regimes. The first column of Table 6.4 shows the standard deviation of the transport through each of the sections defined on Figure 6.8. Here transport variability is presented because the model is depth averaged, but section averaged current variability can be easily calculated using transport variability from Table 6.4 and the cross-sectional area of each section from Figure 6.8.

The Strait of Belle Isle shows small transport variability. Although the current variability is large, the small cross-sectional area of the strait makes its total contribution to the Gulf of Saint Lawrence variability insignificant when compared to the Cabot Strait (Table 6.4, column Total). The analysis of model predicted sea level along the northern coast of the Gulf of Saint Lawrence showed that the Strait of Belle Isle signal stays confined to the northern coast and is quickly damped.

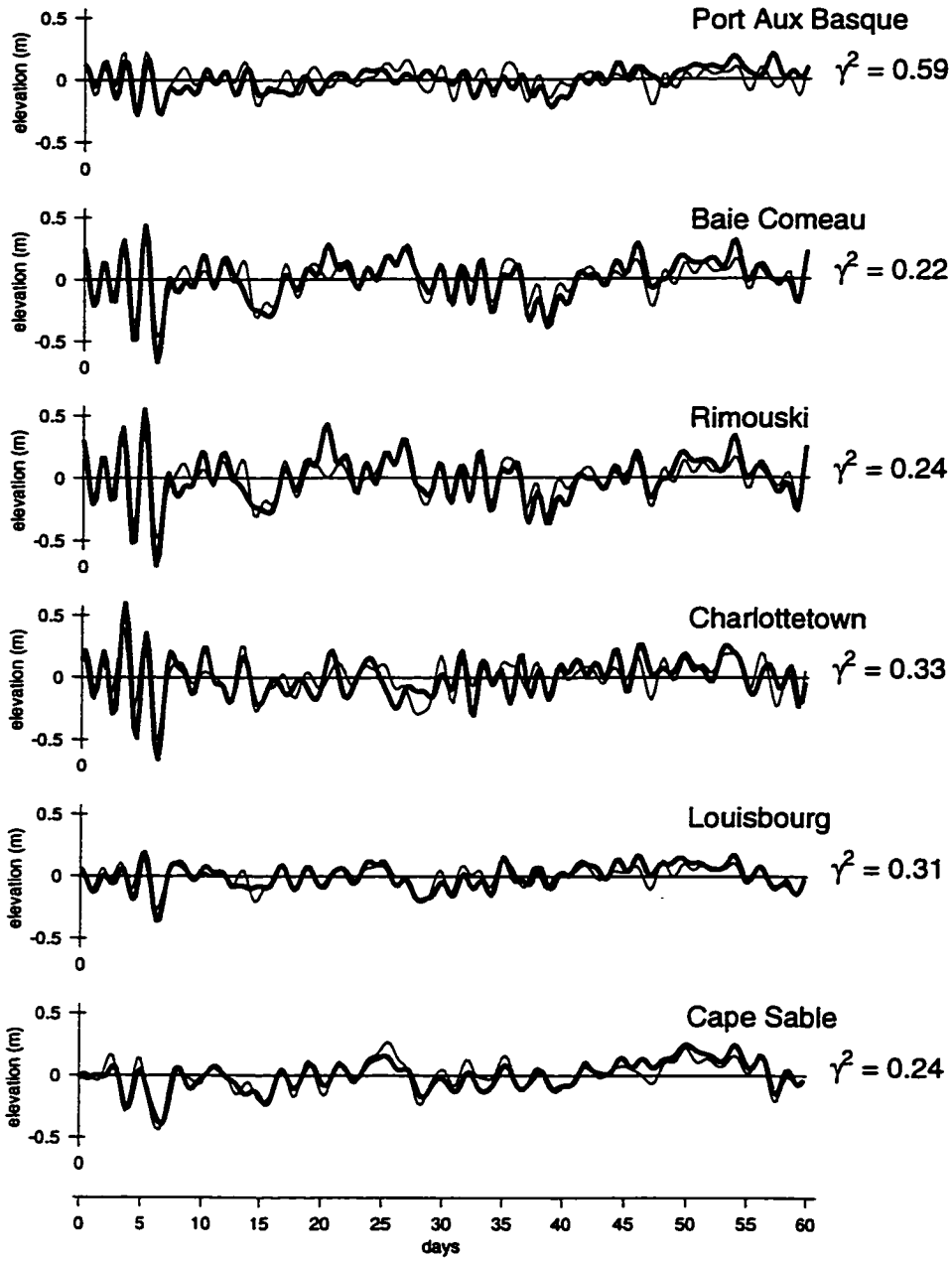

Figure 6.5: Comparison of observed adjusted sea level and predictions from the wind driven model. The thick (thin) line shows observed (predicted) adjusted sea level at 6 representative locations in the Gulf of Saint Lawrence and on the Scotian Shelf. The period covered is January and February 1986. The value of γ^2 shown to the right of each graph is the variance of the difference between observation and prediction divided by the observation variance (Table 6.1).

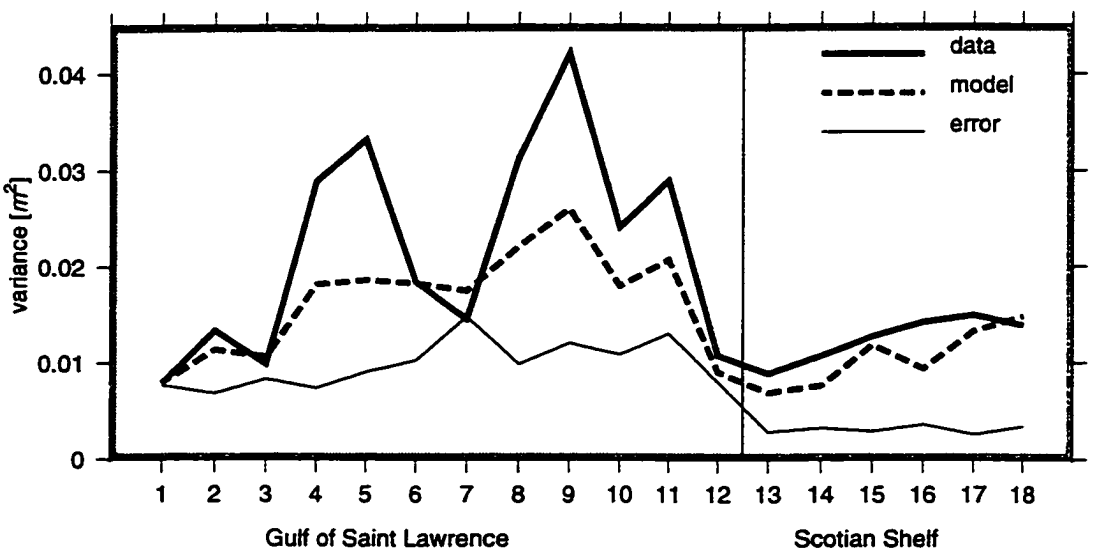

Figure 6.6: Proportion of adjusted sea level variance accounted for by the wind driven model. The thick (dashed) line shows the variance of the observed (predicted) adjusted sea level at 18 tide gauges in the Gulf of Saint Lawrence and on the Scotian Shelf. The thin line is the variance of the difference of the observations and model predictions. The ratio of the heights of thin and thick lines is the γ^2 value (Table 6.1).

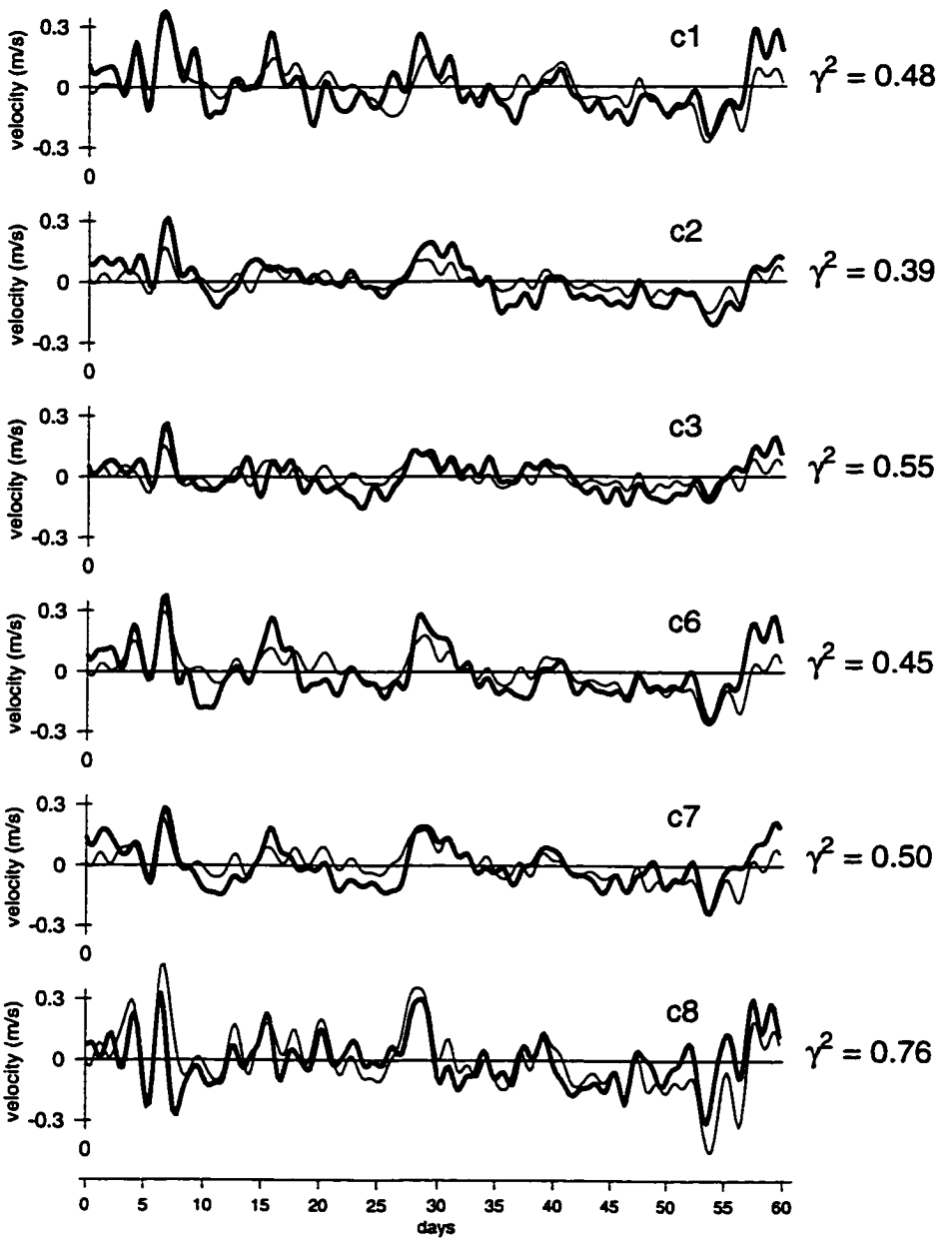

Figure 6.7: Comparison of observed alongshore currents and predictions from the wind driven model. The thick (thin) line shows observed (predicted) alongshore current at 6 representative locations on the Scotian Shelf. The locations correspond to those given by the inset of Figure 6.1. The period covered is January and February 1986. The value of γ^2 shown to the right of each graph is the variance of the difference between observation and prediction divided by the observation variance (Table 6.3).

The highest variability in the Newfoundland section is found in the shallow area over St. Pierre Bank (section N2). At this point we can only speculate that most of it is driven by local wind forcing. The coastal section (N1) shows smaller transport variability, but its cross-sectional area is much smaller. Depth averaged currents in sections N1 and N2 have very similar variability. The slope transport variability (N3) is $0.7 \cdot 10^6 m^3 s^{-1}$. In a steady state calculation Greatbatch et al. (1990) found that the flow around the Grand Bank follows f/h contours, but is highly influenced by friction.

In Cabot Strait the strongest variability is for section C3 along the Newfoundland coast. The shelf is relatively narrow here, so the topography-following flow from the Newfoundland Shelf enters the Gulf of Saint Lawrence in a narrow jet. Relatively strong transport variability is induced through the Laurentian Channel, i.e. the central deeper part of the Cabot Strait (C2). The southern part of the Cabot Strait (C1) is responsible for the outflow from the Gulf of Saint Lawrence. The major source of its variability is probably the wind driven flow in the southern shallow part of the Gulf (Magdalene Shallows). In terms of transport variability each of the Cabot Strait sections makes a similar contribution.

The flow from the Gulf of Saint Lawrence enters the Scotian Shelf as a coastal jet. However, the transport variability is equally strong in the central part of the shelf. The character of this remote forcing of the Scotian Shelf could depend on the frequency of the forcing. Power spectra of the model predicted along-shore current near the coast and in the central shelf is shown in Figure 6.9. It demonstrates that the lower frequency flow follows the topography. The flow at the central shelf has more variability at higher frequencies. A theoretical experiment with the model, where a spatially uniform wind field that varied at different frequencies was used, confirmed the result. This result is consistent with the speculation by Sheng and Thompson (1996) that the upstream forcing of the Scotian Shelf could be frequency dependent.

To supplement the transport analysis, I analysed the modes of interaction between Cabot Strait and the upstream boundary of the Scotian Shelf using the correlation matrix for the transports through the 6 sections. Modal amplitudes, spectral densities and a schematic representation of the three most important modes are shown in Figure 6.10. The dominant

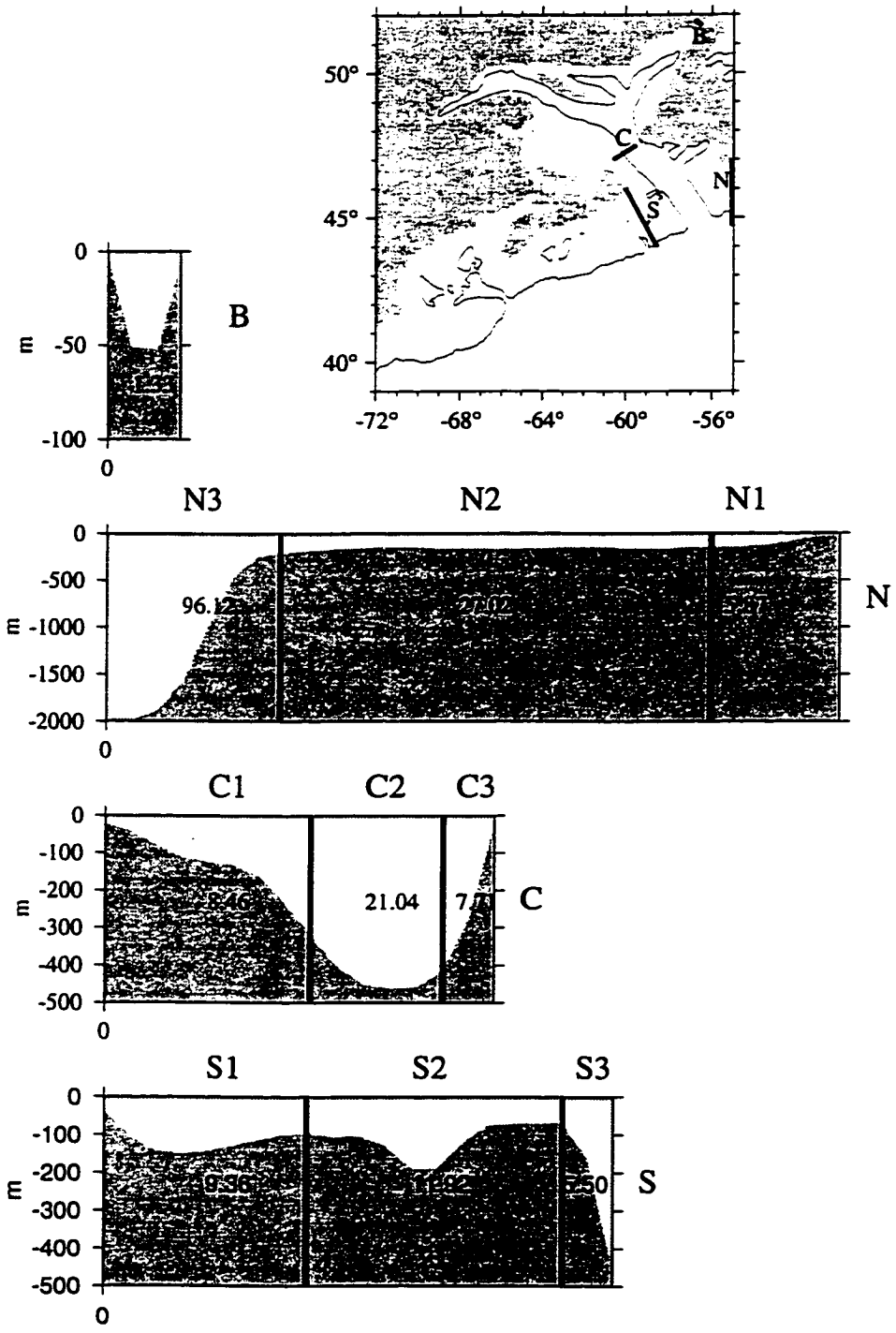

Figure 6.8: Bathymetry and partitioning of the transects defined by the map in the upper right corner. The transects represent boundaries between different subregions of the large-scale model. The transport variability through each of the sections is presented in Table 6.4. The number in each of the sections is its cross-sectional area in $10^6 m^2$. The panels are not equally scaled in depth.

mode accounts for 52% of the variability. It represents inflow at the northern side of Cabot Strait (C3) and outflow through the Laurentian Channel (C2) and along the northern coast of Nova Scotia (C1). The response along the Scotian Shelf upstream boundary is uniform. The second mode (18%) shows a shift towards higher frequency and is characterized by inflow at all locations along Cabot Strait and strongest variability along the shelf break of the Scotian Shelf. The third mode (15%) has similar spectral density to the second one, but these two modes are completely incoherent. The structure shows strong outflow at both sides of the Cabot Strait compensated by an inflow through the Laurentian Channel. On the Scotian Shelf the highest response is found in section S2. Spectral analysis of modal amplitudes shows that the first two modes are coherent at periods higher than 50 hours and in quadrature. Considering the spatial structure of the modes (Figure 6.10) this result is consistent with the modal analysis of the sea level data from section (6.1). The third mode is coherent with the first one only at periods between 24 and 50 hours and the modes are in phase. The spectra, however, do not show a clear shift in frequency for the coastal signal, as was shown in Figure 6.9. This is probably a consequence of smoothing that occurs when transport across the section is computed.

The analysis of the transport variability and the interactions between the regions offered some answers as to how they interact with each other. However, at this point we cannot offer clear explanation about the origin of the variability for the particular region. In section (6.4) a step further is taken by considering separately the effects of the wind forcing over different regions for the downstream shelves.

6.3.3 Pressure Forcing Contribution

The comparison of the adjusted sea level against wind driven model results shows that the model fits better on the Scotian Shelf than in the Gulf of Saint Lawrence. As mentioned, the resolution of the wind field in a semi-enclosed basin like the Gulf of Saint Lawrence might play some role, but the non-isostatic surface pressure forcing is another source of forcing that might explain the errors in the model prediction.

To explore the effect of pressure forcing the model was forced with wind and surface

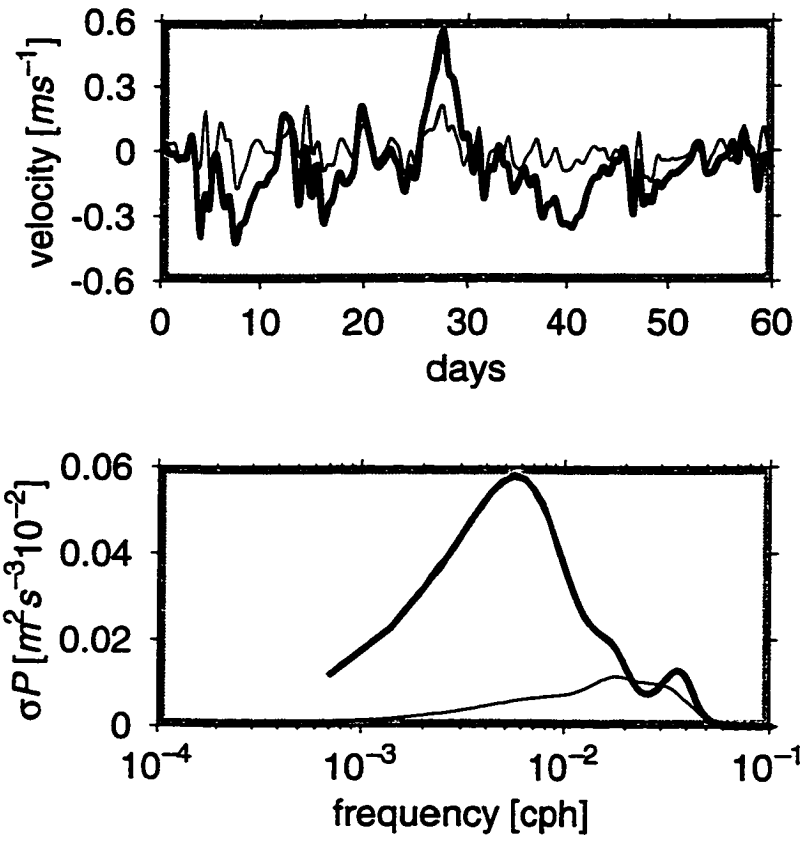

Figure 6.9: Scotian Shelf predicted currents time series and their power spectra. The first panel shows the along-shore current predicted at one location in Section S1 (thick line) and in Section S2 (thin line). The second panel shows power spectra of the current time series in variance preserving form. The thick line corresponds to the series from section S1 and the thin line to the series from section S2.

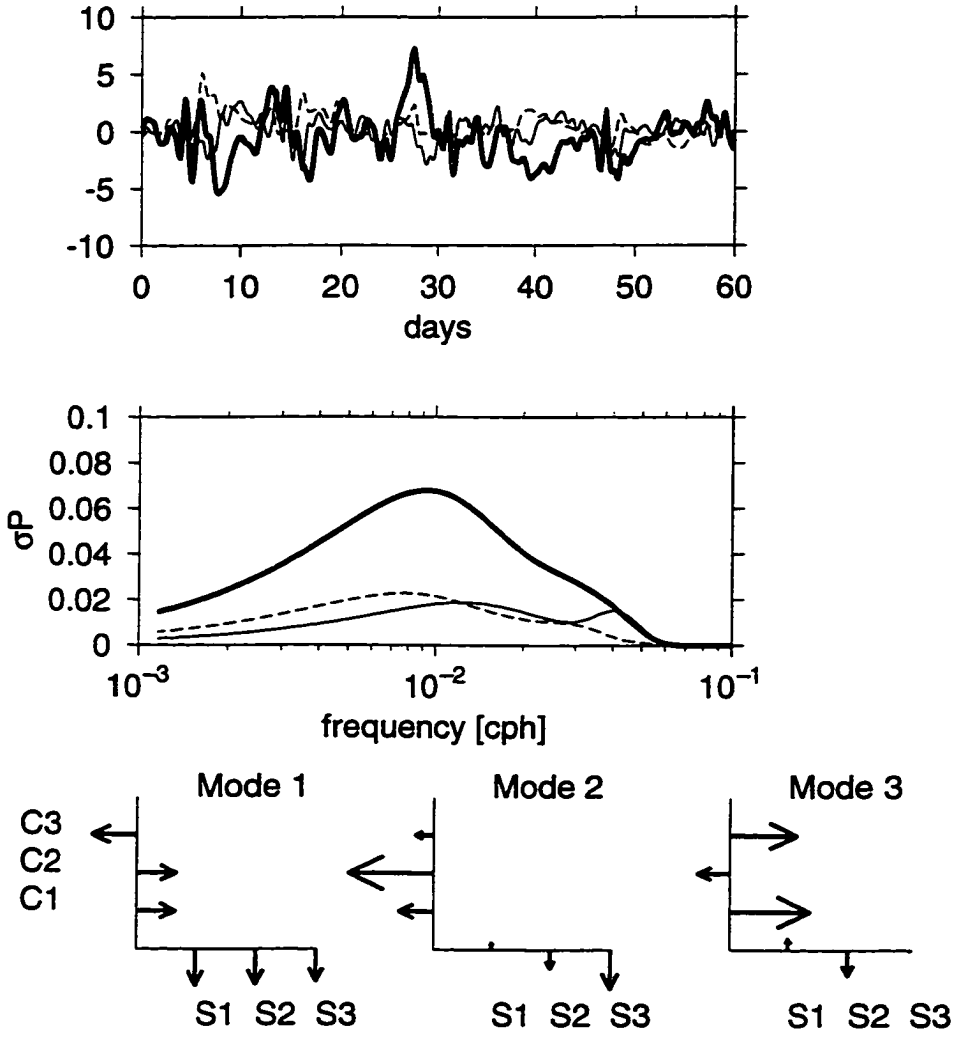

Figure 6.10: Principal component analysis of Cabot Strait and Scotian Shelf transport variability. The analysis is based on the correlation matrix of 6 transport time series for each of the sections defined on Figure 9. The top panel shows modal amplitudes associated with the three largest eigenvalues. Mode 1 (thick) accounts for 52% of the variability. Mode 2 (thin) accounts for 18% of the variability. Mode 3 (dashed) accounts for 15% of the variability. The second panel shows the spectral density of the modal time series. The line types correspond to those in the first panel. The third panel is a schematic representation of the Cabot Strait and the Scotian Shelf interaction. The arrows represent eigenvector elements for each of the sections in the Cabot Strait (C1, C2 and C3) and across the Scotian Shelf upstream boundary (S1, S2 and S3).

Sv	Total	LAB	NF	GSL	SS
B	0.10	0.05	0.02	0.01	0.00
N1	0.38	0.13	0.32	0.02	0.03
N2	1.88	0.57	1.60	0.06	0.08
N3	0.70	0.11	0.70	0.03	0.23
C1	0.39	0.03	0.07	0.45	0.28
C2	0.42	0.08	0.11	0.79	0.10
C3	0.60	0.07	0.28	0.55	0.10
S1	0.55	0.12	0.24	0.13	0.43
S2	0.64	0.15	0.36	0.10	0.42
S3	0.44	0.15	0.33	0.05	0.27

Table 6.4: Standard deviations of the transport (in Sv) through the sections defined in Figure 6.8. The columns are for the following wind driven cases: wind over the whole domain (Total), wind only over the Labrador Shelf (LAB), wind only over the Newfoundland Shelf (NF), wind only over the Gulf of Saint Lawrence (GSL) and wind only over the Scotian Shelf (SS).

pressure. The only difference from the previous, wind driven case, is the new forcing term $p_{at}/\rho g$ in the continuity equation, as described in Chapter 3.

The model was run over the same period of time and forced by wind and surface pressure. The resulting time series for the adjusted sea level are shown in Figure 6.11 and in Tables 6.1, 6.2 and 6.3 (Column W+P). The fact that the adjusted sea level is considered simply means that we are looking at the non-isostatic effect only. (The direct isostatic response to the surface pressure variations is not in the model results as it was removed from the data.) When non-isostatic surface pressure effects are included the model predictions do not change dramatically. Sea level predictions improve at some locations, but at most locations the changes are minimal. Similarly, bottom pressure and current meter predictions do not change.

Overall, the conclusion is that the role of non-isostatic pressure forcing is not very important. This is consistent with the speculation of Thompson and Sheng (1996) that the local and remote non-isostatic forcing do not affect the currents on the Scotian Shelf. Moreover, the model resuits show that, contrary to some suggestions (e.g. Koutitonsky

and Bugden, 1989), the Gulf of Saint Lawrence does not have the same effect for the Scotian Shelf, as Hudson Bay has for the Labrador Shelf, i.e. pressure variations over the Gulf do not appear to drive coastal trapped waves on the Scotian Shelf for the time period considered.

6.4 Interactions Between Subregions

The results from the statistical model indicate that the flow on the Scotian Shelf is better accounted for by the wind on the Newfoundland Shelf than by the wind forcing over the Gulf of Saint Lawrence. The circulation model captures most of the variability on the Scotian Shelf, but it does not allow us to separate the effect of local wind and that acting over other parts of the domain. As discussed in the introduction, this information becomes extremely valuable once operational modelling is considered. In the previous section I analysed the transport variability through the transects that connect different regions, but was not able to clearly distinguish the dominant forcing for the various signals.

To assess the relative importance of the wind driven flow over different regions of the model domain for the downstream shelves the model is run in the following way: The domain is partitioned into four different areas that define the Labrador Shelf, the Newfoundland Shelf, the Gulf of Saint Lawrence and the Scotian Shelf with the Gulf of Maine. The boundaries are defined along latitude and longitude lines so that the regions include both the shelf and the deep ocean. The model is then run four times and for each run I allow for wind forcing in one subregion and set the wind to zero in the remaining three regions. I recognize the fact that, by setting wind stress to zero, an artificial curl of the wind stress along the regions boundary is introduced, but, as discussed in Chapter 4, the experiments show that it does not result in a significant contribution to the model results.

The results from these four model runs are summarized in Table 6.4. The columns represent the standard deviations of the transport across the sections defined on Figure 6.8 for each experiment. The standard deviation of the predicted sea level and currents at selected locations for each of the four model runs is shown on Figures 6.12 and 6.13.

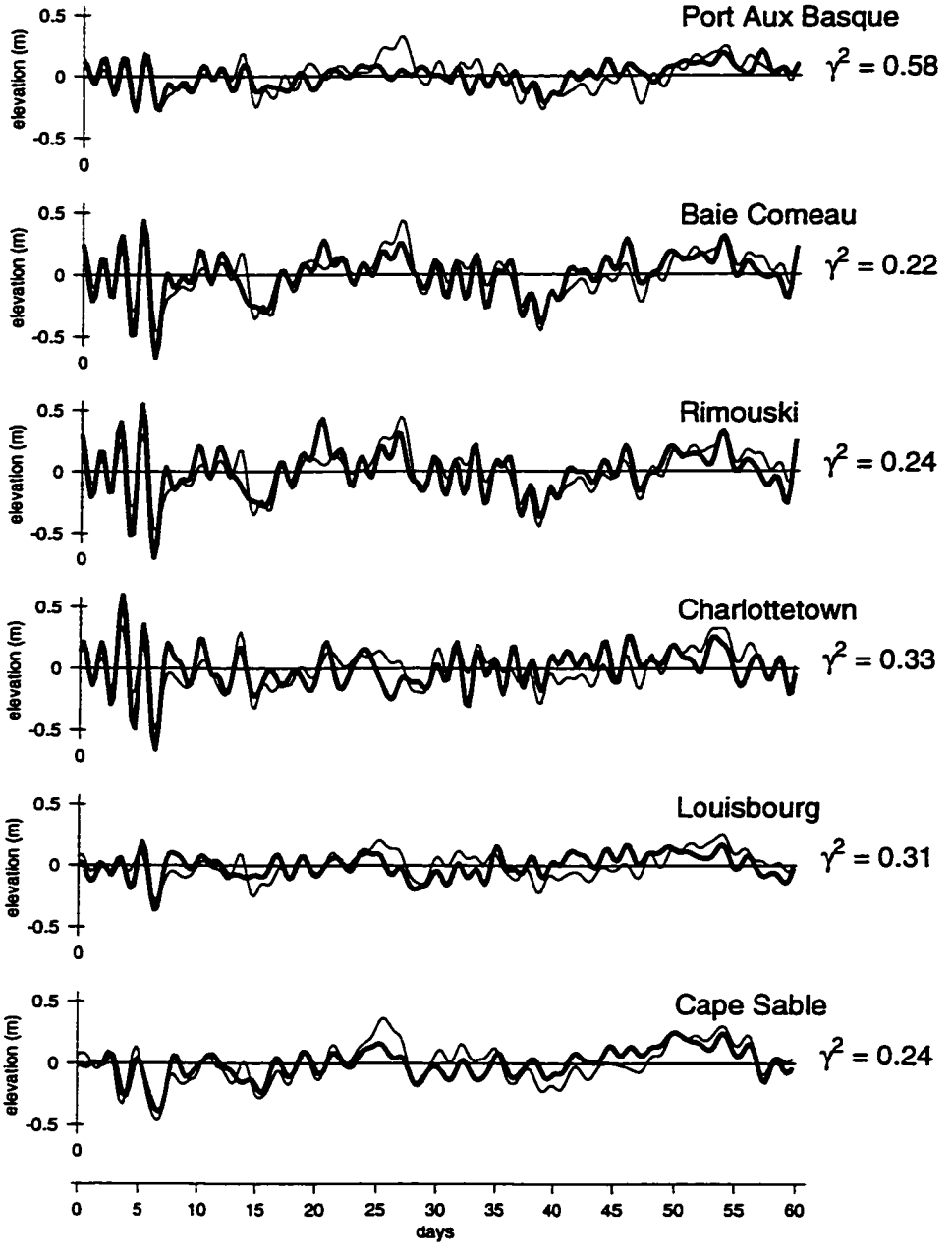

Figure 6.11: Comparison of observed adjusted sea level and predictions from the model driven by wind and pressure. The thick (thin) line shows observed (predicted) adjusted sea level at 6 representative locations in the Gulf of Saint Lawrence and on the Scotian Shelf. The period covered is January and February 1986. The value of γ^2 shown to the right of each graph is the variance of the difference between observation and prediction divided by the observation variance (Table 6.1).

Labrador Shelf flow

The Labrador Shelf influence is the most pronounced at West St. Modeste (location 2 on Figure 6.1) which is to be expected based on the statistical modelling and principal component analysis. At other locations, Labrador Shelf forcing is responsible for up to 10% of the variability.

Spectral analysis of the predicted sea level series around the Gulf of Saint Lawrence (not shown here) indicates that the remote signal from the Labrador Shelf enters the Gulf through the Strait of Belle Isle and the Cabot Strait. The Belle Isle portion influences the northern coast of the Gulf of Saint Lawrence, but is quickly damped. Most of its energy is at periods between 4-8 days. The Cabot Strait signal propagates around the Gulf with most energy at periods between 2-4 days.

The analysis of the previously defined transects (Table 6.4) shows that the transport variability induced by the Labrador Shelf winds (column LAB) is the largest in the section N2 of the Newfoundland transect. The ratio between the variability in section N2 and section N1 is similar to the case where the wind blows over the whole domain. The relative importance of the N3 section is much smaller than for the case with the winds over the whole domain. This means that the remote forcing along the shelf break, that originates on the Labrador Shelf, is probably damped by the friction before it reaches the southern part of the Newfoundland Shelf.

In Cabot Strait, the Laurentian Channel (section C2) and the flow along the Newfoundland coast (section C3) have similar transport variability. The flow along the coast comes from the Newfoundland Shelf coastal current. The Laurentian Channel flow is the result of the flow along the slope of the Grand Bank and eventually through Section N3. The current response in the Gulf at selected locations (not shown here) is coherent with signals from both sections C2 and C3. The most variability in currents in the Gulf (Figure 6.13) is present in the area close to the Strait of Belle Isle, as was for the sea level.

On the Scotian Shelf the variability is evenly distributed across sections. Spectral analysis of the results reveals frequency dependent structure of the response to remote forcing. The topography prevents low frequency variability from reaching the downstream shelves,

but a high frequency signal crosses f/h contours and the remote forcing is then equally distributed over the Scotian Shelf upstream boundary.

Newfoundland Shelf flow

The wind driven flow from the Newfoundland Shelf makes the most significant contribution to the remote variability of the downstream Gulf of Saint Lawrence and the Scotian Shelf (Table 6.4; column NF). At most sea level locations in the Gulf it is more important than the local wind forcing. It is also dominant at the northern sea level stations of the Scotian Shelf (Figure 6.12). A similar result is found for the currents. On the Scotian Shelf, away from the coast, the wind driven flow from the Newfoundland Shelf is equally important for the variability in the currents (e.g. locations 10 and 12 in Figure 6.13) as the local wind forcing.

The analysis of the Newfoundland sections (Table 6.4) shows larger variability than in the previous experiment. Part of the variability is probably induced locally (wind is blowing over that section), but part of it originates at the upper Newfoundland Shelf. The effects of locally generated forcing are particularly evident through larger contribution of the coastal section (N1) when compared to the Labrador Shelf winds. The relative importance of the along-shelf-break flow (N3) is also larger. The variability in that section is unlikely to be generated locally (because the section is very deep) and is probably the result of the upper Newfoundland Shelf flow that leaks out to the shelf break and is transmitted around the Grand Bank.

In Cabot Strait the highest variability is found in the northern section C3. This is a direct consequence of the stronger coastal flow through sections N1 and N2. The relative contribution of the Laurentian Channel (C2) to the total variability in Cabot Strait is smaller when compared to the flow that originated on the Labrador Shelf. It is interesting to note that although the variability in the upstream sections (N2 and N3) increased, the total variability introduced via the Laurentian Channel (C2) is not dramatically different for the cases of wind forcing over the Labrador or Newfoundland Shelves.

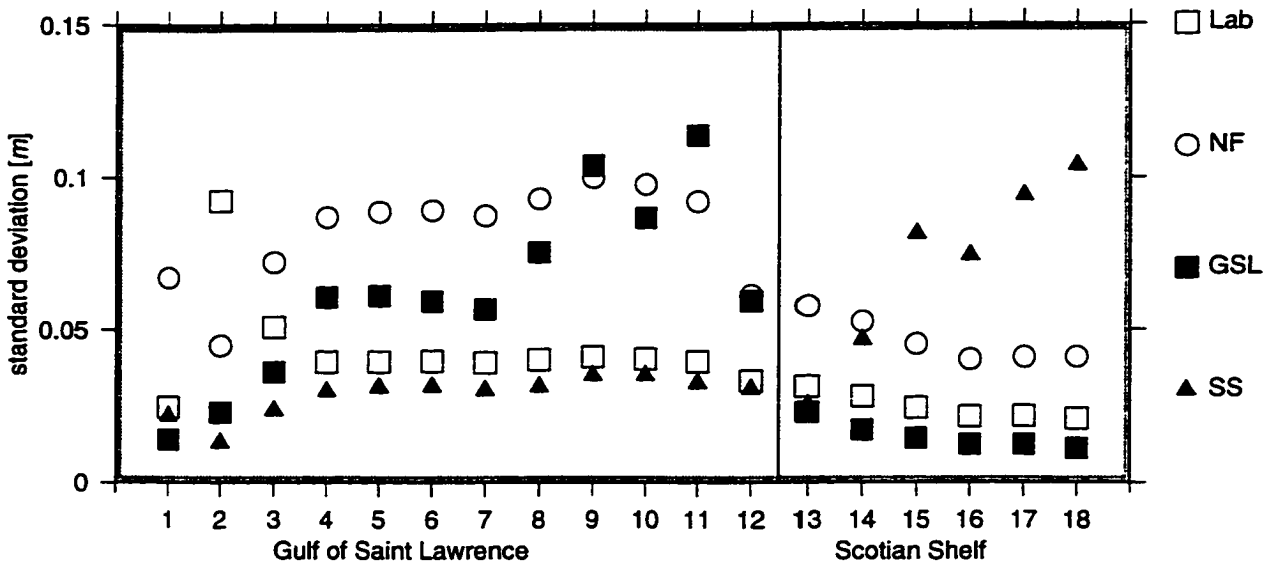

Figure 6.12: Effects on sea level of wind blowing over different parts of the model domain. The locations marked by the ticks on the x-axis refer to coastal tide gauges (Table 6.1). The ordinate of each symbol equals the standard deviation of the adjusted sea level predicted by the model. The different symbol types correspond to winds blowing over different subregions: empty squares - Labrador Shelf, empty circles - Newfoundland Shelf, full squares - Gulf of Saint Lawrence, triangles - Scotian Shelf.

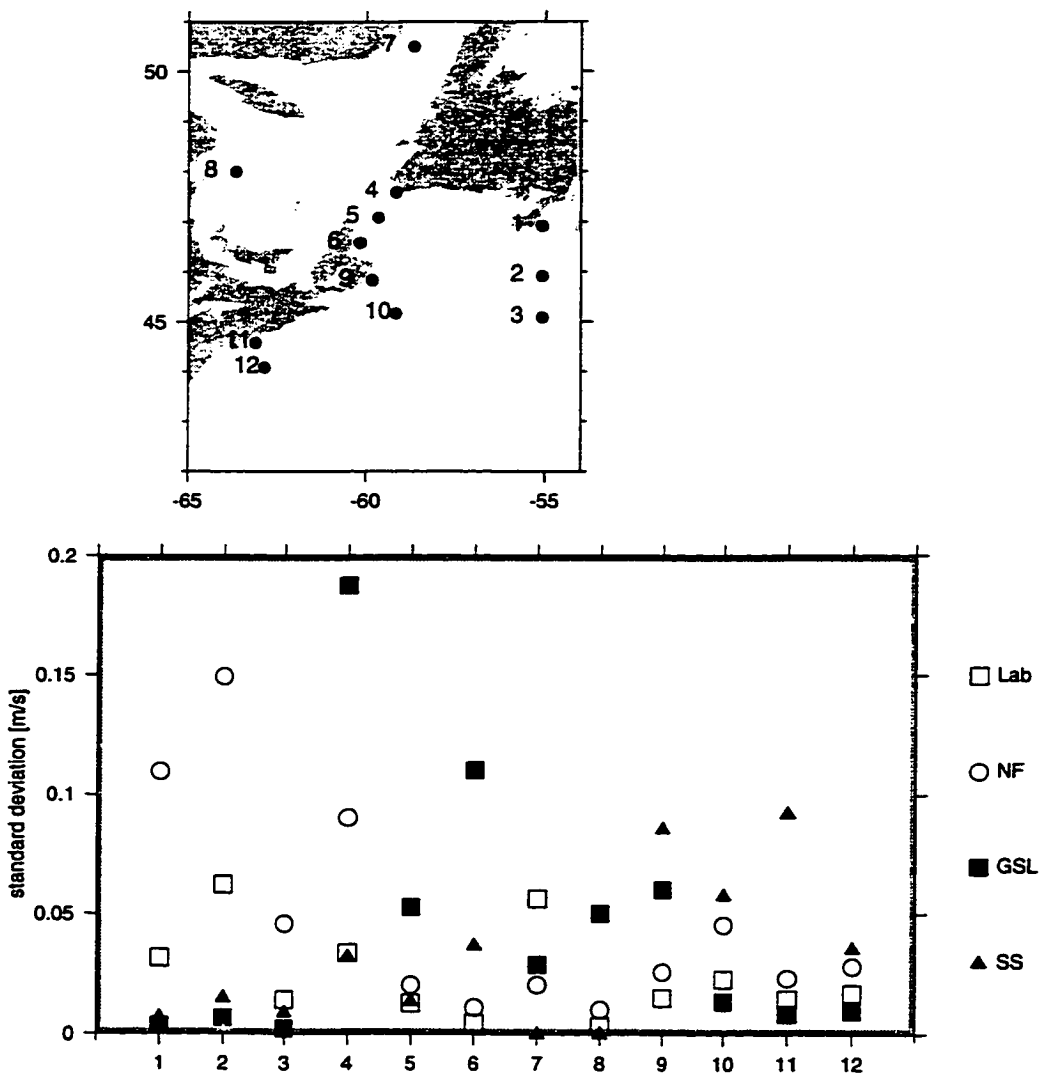

Figure 6.13: Effects on along-shore currents of wind blowing over different parts of the model domain. The locations marked by the ticks on the x-axis refer to locations given on the upper panel. The ordinate of each symbol equals the standard deviation of the along-shore current predicted by the model. The different symbol types correspond to winds blowing over different subregions: empty squares - Labrador Shelf, empty circles - Newfoundland Shelf, full squares - Gulf of Saint Lawrence, triangles - Scotian Shelf.

In the Scotian Shelf transect the variability is almost equally distributed over all sections. In general, it is stronger than the variability in Cabot Strait. This result is similar to the one when the wind was blowing over the Labrador Shelf. It seems that the remote forcing from either the Newfoundland or Labrador Shelf can force the Scotian Shelf directly without necessarily following the wave guide around the Gulf of Saint Lawrence. In the previous section, the difference in frequencies for the predicted currents in the coastal and mid-shelf location was shown. Thus, this "direct forcing" of the Scotian Shelf might also depend on frequency. The spectral analysis and principal component analysis (similar to the one presented in Figure 6.10) of the transports through N, S and C suggest that the lower frequency flow follows the topography. It appears to be propagating from the Newfoundland Shelf through Cabot Strait and around the Gulf of Saint Lawrence. On the other hand, power spectra suggest that flow at higher frequencies can cross the Laurentian Channel and 'directly' force the Scotian Shelf. This speculation is supported by the statistical model results where Newfoundland Shelf winds accounted for more variability on the Scotian Shelf than in the Gulf of Saint Lawrence.

Gulf of Saint Lawrence and Scotian Shelf flow

Wind forcing over the Gulf of Saint Lawrence (column GSL; Table 6.4) is a dominant source of the variability for both sea level and currents in the southern, shallower part of the Gulf. Wind forcing over the Gulf of Saint Lawrence did not induce much variability on the Scotian Shelf. For most locations, even the remote signal from the Labrador Shelf generated more variability on the Scotian Shelf than the signal from the adjacent Gulf of Saint Lawrence. The statistical model used in Section 6.2 indicated the weaker contribution of the Gulf of Saint Lawrence winds to Scotian Shelf circulation, so this experiment provides a dynamical demonstration of the relative unimportance of the Gulf of Saint Lawrence for the Scotian Shelf. Therefore, contrary to expectations, the Gulf of Saint Lawrence is not the major source of remote forcing for the Scotian Shelf. The most important source is the wind over the Newfoundland Shelf.

The variability in Cabot Strait induced by winds over the Gulf of Saint Lawrence is

locally generated and it does not propagate further downstream. The Scotian Shelf section shows the importance of the coastal signal (section S1) in contrast to the previous two cases (Newfoundland and Labrador Shelf winds). Outflow through the Laurentian Channel is responsible for the variability introduced on the central Scotian Shelf and along the shelf break.

The local wind driven flow on the Scotian Shelf dominates the coastal sea level and current variability (Figures 6.12 and 6.13). This influence gets stronger as we move downstream along the shelf. The importance of local wind forcing was recognized by Schwing (1989) and is consistent with Gill and Schumann's (1974) theory of wind driven shelf waves and Csanady's (1982) theory of arrested topographic waves.

6.5 Discussion

A linear, barotropic, depth-averaged circulation model of the eastern Canadian Shelf seas has been used to examine the synoptic variability of pressure and current field. The data analysis shows that the subregions of the model domain interact with each other and I have used the dynamical model to quantify those interactions.

The dynamical model driven by local wind stress can reproduce well the synoptic variability on the Canadian Atlantic Shelf. The principal component analysis of the model results, based on the correlation matrix, agrees well with the data indicating that the model captures the general patterns in sea level and currents. Hindcasts of coastal sea level show considerable variability (γ^2 between 0.2 and 1), but overall they approach the levels established by the statistical model. The quality of the current predictions is highly dependent on location. In general, the model has higher skill at the inshore locations where it typically leaves only 40% of the variability unaccounted for.

The introduction of non-isostatic air pressure forcing did not significantly change the model skill. Adjusted sea level predictions did not change at most locations which indicates that locally generated non-isostatic response in this area is not important for the period considered. Only small improvements to the currents' fits were observed when pressure

forcing was included. The results show that the Gulf of Saint Lawrence, due to the large cross-sectional area of Cabot Strait, does not act as a source of non-isostatic variability for the downstream shelves.

The analysis of the transport variability through different sections shows that there is a strong interaction between subregions of the model domain. Cabot Strait is responsible for the remote synoptic forcing of the Gulf of Saint Lawrence. Although most of the variability is induced along the Newfoundland coast, the model results suggest an important role for the Laurentian Channel in the communication of the Gulf of Saint Lawrence with the open shelves. The total Scotian Shelf remote variability is equally distributed over its upstream boundary, but there is frequency dependent structure. The low frequency flow tends to follow the topography close to shore while the higher frequency flow is more spread over the shelf.

By partitioning the wind forcing into four different regions, the relative importance of each of the regions as a source of remote wind driven flow for the downstream shelves was estimated. The model results show that the Newfoundland Shelf is the major source of the remote variability for both the Gulf of Saint Lawrence and the Scotian Shelf. This result is no surprise in the case of the Gulf of Saint Lawrence where data analysis shows that the northern coast and lower estuary stations are dominated by the remote signal. However, it was generally believed (e.g. Schwing, 1992) that the wind driven flow in the Gulf of Saint Lawrence is responsible for most of the Scotian Shelf variability. The present results indicate that most of the Scotian Shelf remote variability originates on the Newfoundland Shelf. Spectral analysis suggests that the remote signal from the Newfoundland Shelf can cross the f/h contours of the Laurentian Channel and introduce variability uniformly along the Scotian Shelf upstream boundary. The result seems to be in agreement with the general theory of shelf waves propagating over an abrupt change in the topography (e.g. Middleton and Wright, 1988). The theory strictly holds for very low frequencies (periods longer than 240 h; Middleton, 1991) where the low frequency flow is expected to follow the topography, while the higher frequency flow can cross the abrupt change in topography. The theory suggests that the energy of the transmitted wave decreases strongly as the frequency

approaches inertial frequency which is also consistent with the results obtained here (e.g. Figure 6.9).

The large scale model used here shows significant hindcast skill for sea level and inshore currents. The results are comparable to those realized with a similar model with data assimilation by Sheng and Thompson (1997). This is a highly encouraging result because it indicates that a simple large scale model could be used for operational purposes and overcome the problems of data assimilation in real time. An attractive feature of this model is that it is forced only by wind and(or) pressure forcing. Thus, it can be easily implemented operationally because wind and pressure forecasts for 2-3 days into the future can be obtained from meteorological agencies. The model could provide forecasts of the sea level and current field for a few days into the future. Considering the skill of the model when predicting sea level variability, this may be particularly useful for storm surge prediction, i.e. prediction of the extreme coastal sea levels.

Chapter 7

Conclusions

The goals of this thesis are to improve our understanding of the connections between the subregions of the Canadian Atlantic Shelf and to develop models that can be used operationally. The former goal was realized through three separate studies that provided insight to a number of open issues. First, two subregional studies were used to examine the importance of local and remote forcing of the Labrador Shelf and the Gulf of Saint Lawrence. Then, an integrated approach was taken and the whole of the Canadian Atlantic Shelf was studied with a large-scale model.

Major results have been summarised and discussed at the end of each chapter. Hence, only a list of major conclusions is provided here. They are presented in point form for each of the chapters. Possible operational extensions of this work are discussed in a separate section.

Labrador Shelf

- Currents on the southern Labrador Shelf show a lot of small scale synoptic variability which is not well represented by the barotropic model. A depth averaged barotropic model can account for part of the variability, but more than 50% of the variability remains unaccounted for.

- For the chosen model domain, boundary forcing is the dominant source of sea level

and bottom pressure variability. Local wind plays a significant role for both current and pressure variability on the southern Labrador Shelf.

- Offshore forcing effects can be removed from the sea level and bottom pressure data on the shelf. The removal leads to improved predictions for currents on the southern Labrador Shelf.

- A suboptimal prediction scheme based on data assimilative model runs has skill for predicting bottom pressure and currents.

Gulf of Saint Lawrence

- Local wind forcing can account for a small part of the sea level variability in the Gulf of Saint Lawrence. Most of the variability is introduced through the open boundaries.

- Cabot Strait is the dominant source of remote variability in the Gulf of Saint Lawrence. The Strait of Belle Isle, due to its small cross-sectional area and transport variability, has only a small influence on the synoptic variability in the Gulf.

- Boundary forcing can be related to the large scale wind field on the Labrador and Newfoundland Shelves.

- Sea level data show evidence of resonances at 35, 21 and 15 hours. Boundary forcing can induce resonant response in sea level at periods of 35 and 21 hours.

Canadian Atlantic Shelf

- A significant portion of the sea level and current variability is driven by the wind and air pressure. Part of the signal is generated locally, but the remote signal from other subregions of the Canadian Atlantic Shelf makes a significant contribution to the total variance.

- Non-isostatic pressure forcing within the domain is negligible during the period considered.

- The Newfoundland Shelf is a major source of remotely driven sea level and current variability for the Gulf of Saint Lawrence and the Scotian Shelf.
- The upstream forcing of the Scotian Shelf depends on frequency. Lower frequency flow follows the topography and is confined to the coast. Higher frequency flow is spread across the upstream boundary.

7.1 Operational Extension

One of the goals in this thesis was to develop models that are suitable for operational use. A forecasting scheme was developed and tested for the Labrador Shelf. It showed good skill when predicting coastal sea level, bottom pressure and along-isobath currents. The most encouraging result is the time invariant character of the transfer function between the observations and boundary conditions. Therefore, at any later time, if data from tidal gauges and wind field predictions were available, the model could provide reasonable predictions of the flow field. Based on the model results, a similar suboptimal scheme could have been developed for the Gulf of Saint Lawrence. It would rely again on the information from tide gauges and wind forecasts.

The skill of the large-scale model that did not use data assimilation to predict sea level, bottom pressure and currents is certainly the most encouraging result. The result showed that for this region the problems associated with data assimilation could be overcome by considering a large-scale model driven by surface winds.

The large-scale model can be used operationally in a number of ways. The most straightforward way is to run it with forecast winds and thereby provide sea level and current forecasts for the whole domain. The results could also be used to update the open boundary conditions of a limited area model. This could be done in two ways: The analysis of subregional boundaries has shown that the remote forcing through such a boundary could be related to the wind field acting over upstream subregions of the shelf. For example, a linear relationship could be established between the Scotian Shelf upstream boundary and the Newfoundland Shelf wind field. Thus, at some later time, the forecast wind field could be

used to predict the open boundary conditions for a limited area model of the Scotian Shelf without running a complete large-scale model. The second way to provide boundary conditions for a limited area model is to run a large-scale model in 'nested mode'. Using either of these approaches a limited area model that could have higher resolution, allow density to evolve with the flow, include turbulence, etc. would be driven by boundary conditions predicted by the large-scale model.

A separate operational application arises from the use of data assimilation techniques in two subregional studies. The models developed could be used to guide the design of observational arrays. Before the instruments are deployed the model could be used to check if the location chosen is sensitive to the specification of the open boundaries of the model. This can be done by running a series of twin experiments with the model. However, the problem with twin experiments is that they rely on artificial data generated by the model. Another way to test the observational array design is to run the adjoint model backwards forcing it by a delta function at the chosen location. The forcing vector θ_n, used in Appendix B to force the adjoint model, would be unity at one location and one time step. The information from the observation point would spread throughout the domain and eventually reach the model boundaries. This could be repeated for any location. This approach can be related to the representers solution described in detail by Bennett (1982) and applied to Massachusetts Bay by Bogden et al. (1996).

7.2 Future Work

Although a number of important questions have been addressed in this thesis, many problems remain unexplained. In my view, the most critical issue that needs to be addressed concerns the small scale variability in the currents. In general, the models used here could account for part of the variance in the along-shore or along-isobath flow, but for very little of the variance in the cross-isobath direction. The first problem to note is that the flow considered here was based on depth integrated equations of motion. Hence, it is possible

that a three dimensional extension of the model could provide some of the answers, particularly, on the Labrador Shelf, where all of the current meters were within 5 meters of the bottom. For example, Thompson and Sheng (1996) used a 3-D model of the Scotian Shelf and found that it could account for a significant part of the variability in the currents.

A possibly important effect could be attributed to small scale baroclinic variability generated locally. As discussed, temporal changes in the density field are probably critical when attempting to explain the small scale variability. Thus, it would be necessary to use a fully prognostic model that allows the density field to evolve with the flow. Currently, an attempt to use a prognostic model in the Gulf of Saint Lawrence and on the Scotian Shelf is underway (Sheng, personal communication).

The Gulf of Saint Lawrence, in many ways, still requires attention. In particular, field projects that are aimed at a better understanding of synoptic variability are necessary. Appropriate current meter observations are sparse and were collected as part of small-scale studies. A Gulf-wide effort to collect current meter data would be desirable. This would be the best way to validate the model results presented in Chapter 5 and it would enable us to get a better and more complete picture of the current variability in the Gulf. Particularly, an extensive observational effort in the Cabot Strait is necessary. It would provide a solid basis for understanding of the exchange between the Gulf and the open shelf.

The models used here were driven by relatively coarse resolution wind and pressure fields. Better wind fields are becoming available through re-analysis efforts at the European Center for Medium Range Weather Forecasts. Therefore, it would be interesting to use the same models with refined forcing fields to examine the limits of simple dynamical models. It is possible that higher resolution forcing would increase the predictive skill of the coastal ocean models. In that respect, a more interesting result would be obtained if a limited area ocean model was coupled with a meso-scale atmospheric model of the same area. For example, suboptimally predicted open boundary conditions could be used to run a prognostic Gulf of Saint Lawrence model coupled to an atmospheric model. The result of this coupling would be more realistic wind and surface heat flux fields that should certainly improve predictions of the flow field.

The models developed in this thesis could be used operationally. Therefore, one of the aspects of future activity is certainly their operational use. Wind forecasts are typically available on-line for 3-5 days into the future. Thus, large scale model could be used operationally and, for example, provide storm surge forecasts for the region. At present these forecasts are made using only statistical estimates.

Appendix A

Data Description

In this appendix details of the data sets used throughout the thesis are presented and examples of their time series shown. The observations presented here represent a compilation of various data sets from different sources. Some of the data have been previously processed and some were obtained "raw". In some cases this represented a problem because of different sampling intervals, filtering that was previously applied, etc. However, if different data sources were used, the observations were processed so that the time series for statistical analysis or assimilation are consistent.

A.1 Wind and Pressure Data

Surface wind and pressure data were obtained from the European Center for Medium Range Weather Forecasts (ECMWF). The wind and pressure fields were provided every 12 hours at 10 m above the sea surface with a spatial resolution of 2.5^o. The grid is shown in Figure A.1. The data covered a period of three years, starting on January 1st 1985 and ending on December 31st 1987.

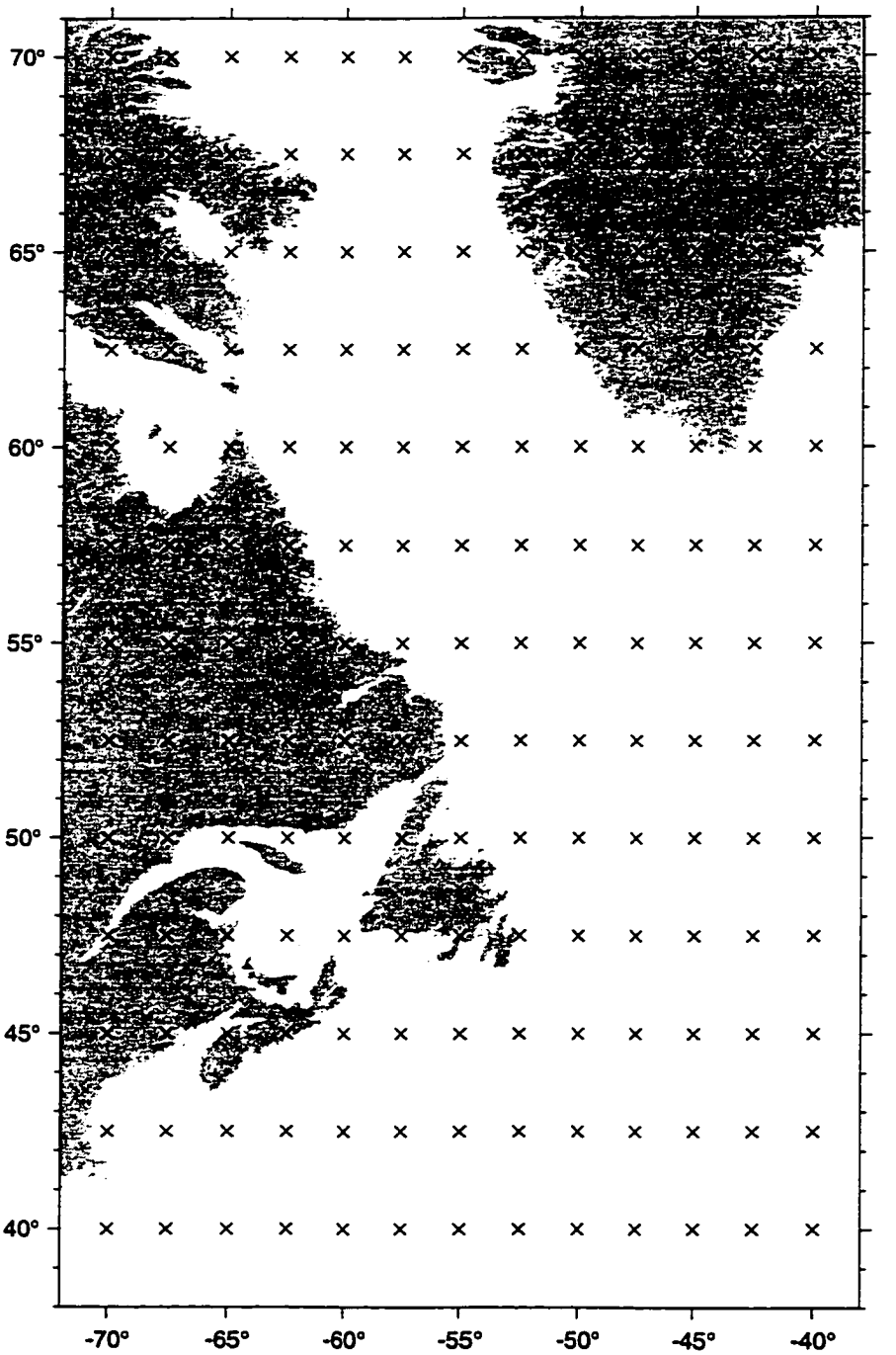

Figure A.1: Surface wind and pressure locations from ECMWF.

A.2 Labrador Shelf Data

Between the summer of 1985 and the summer of 1987 several field studies collected data over the Labrador Shelf (Wright et al., 1988). Figure A.2 shows periods of data availability on the Labrador Shelf. Coastal gauge data were collected on the northern part of the shelf. Bottom pressure gauges were deployed both cross-shore and along-shore. Finally, current meters were moored in the Hamilton Bank area, associated with a long term monitoring program of the Labrador Current. All current meters were within 5 meters of the bottom due to concerns about fishing pressures. Data locations are shown in Chapter 4; Figure 4.1.

All data were analysed for tides and residuals were calculated. Sea level data were also isostatically adjusted to remove the inverse barometer effect. An example of coastal sea level and bottom pressure time series is shown in Figure A.3.

A.3 Gulf of Saint Lawrence Data

Coastal sea level data from the Gulf of Saint Lawrence were obtained from the Marine Environmental Data Service (MEDS). The data were collected at permanent tide gauge locations. Tide gauge locations are listed in Table A.1 and shown in Figure 5.1 in Chapter 5. The observations covered a 3 year period from January 1st 1985 to December 31st 1987 with an hourly sampling interval. Most of the time series were not complete and the percentage of complete data for each of the locations is shown in the last column of Table A.1. Although most of the data have more than 90% valid records, there were a lot of short gaps in most of the time series. Consequently, it was not possible to find periods where a larger number of tide gauges returned uninterrupted records.

All data were analysed for tides and isostatically adjusted. An example of sea level time series is shown in Figure A.4.

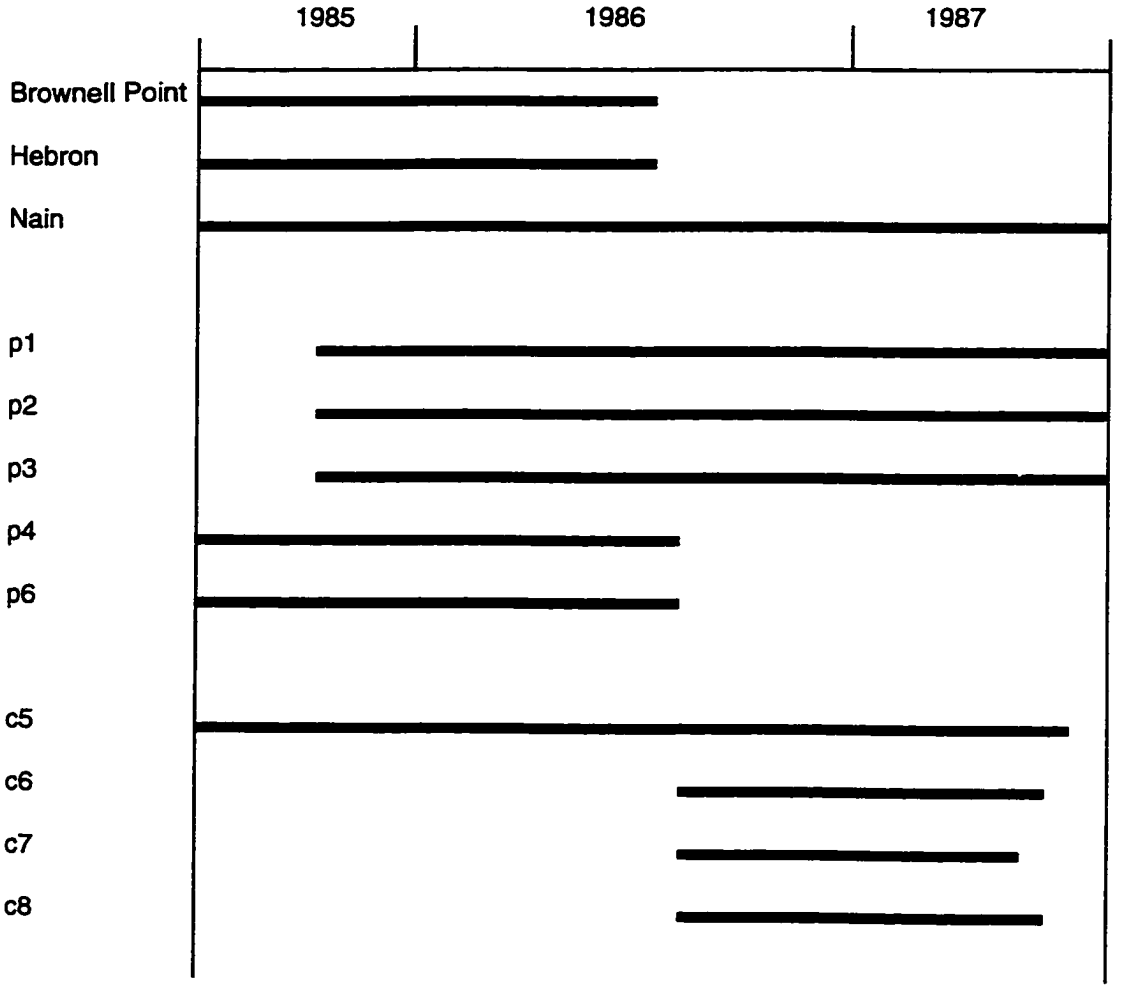

Figure A.2: Availability of data on the Labrador Shelf. Data locations are shown on Figure 4.1 in Chapter 4.

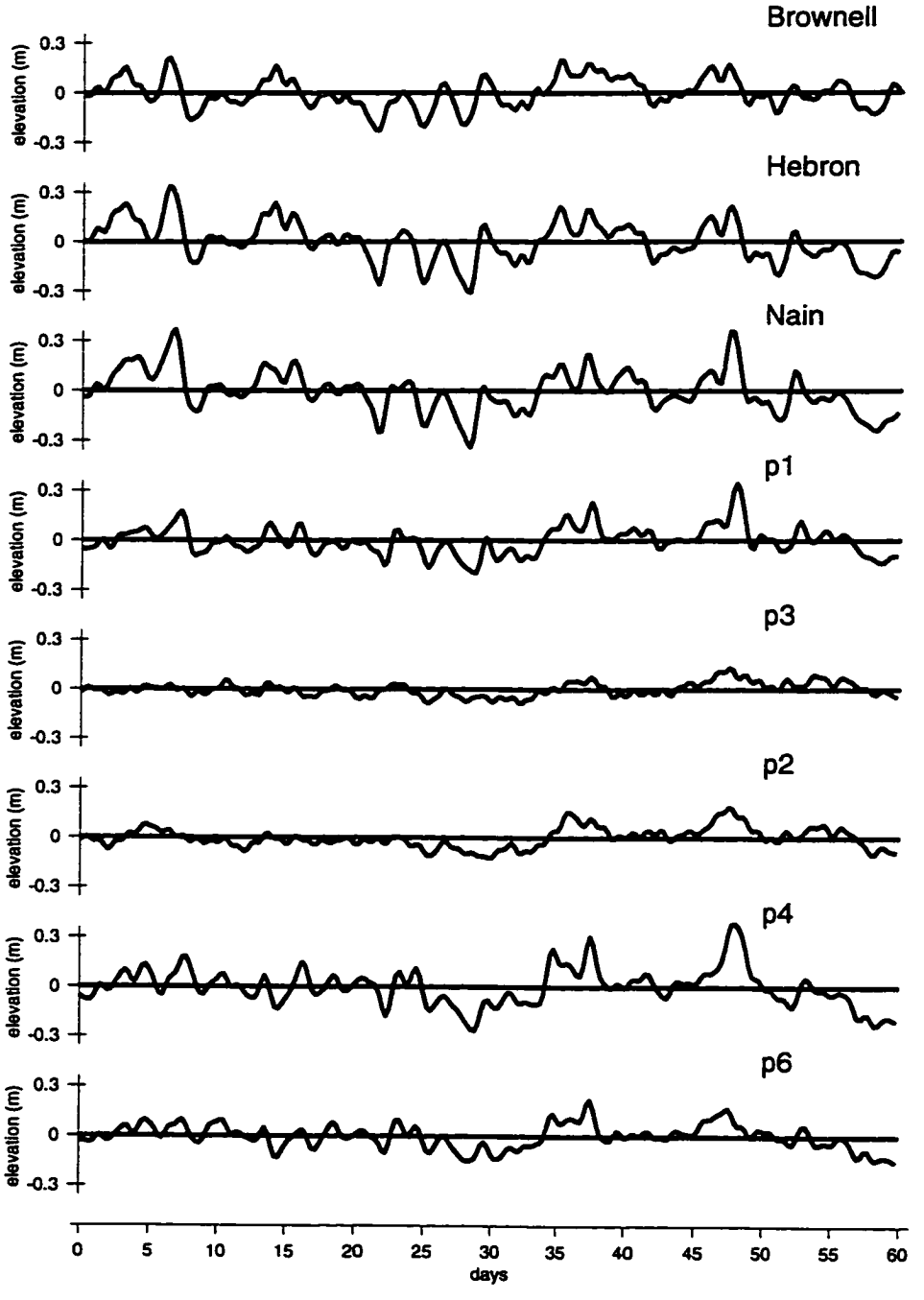

Figure A.3: Time series of adjusted sea level and bottom pressure observed on the Labrador Shelf for January and February 1986. The sampling interval is 6 hours and the data were filtered to remove all periods shorter than 2 days (Wright et al., 1988).

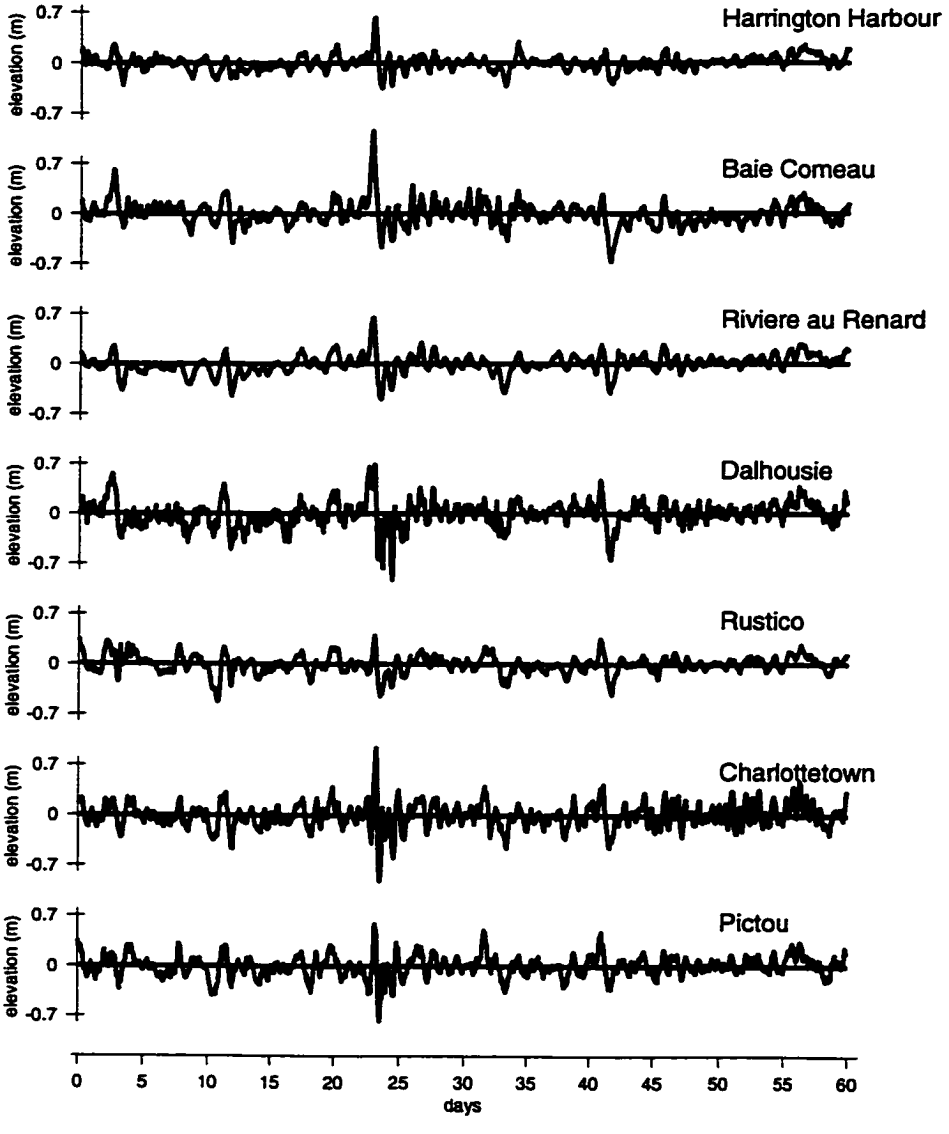

Figure A.4: Time series of adjusted sea level in the Gulf of Saint Lawrence for January and February 1987. The sampling interval is 1 hour and the tides were removed from the time series.

Location	No.	Latitude	Longitude	Complete (%)
P.aux Basque	1	-58.91	47.58	99
W.St. Modeste	2	-56.58	51.58	90
Harrington H.	3	-59.50	50.50	95
Baie Comeau	4	-66.33	50.25	93
Rimouski	5	-68.25	49.25	96
St.Anne	6	-68.50	48.41	61
Riv au Renard	7	-66.58	49.08	89
Dalhousie	8	-66.16	48.08	94
Shediac Bay	9	-64.50	46.33	98
Charlottetown	10	-62.91	46.25	100
Pictou	11	-62.75	45.66	98
North Sydney	12	-60.50	46.25	98

Table A.1: Tide gauge locations from the Gulf of Saint Lawrence. Columns are: station number, latitude, longitude and completeness. Completeness is ratio of the number of data available and the record length. The station numbers correspond to the ones used throughout the thesis (e.g. Figure 6.1).

A.4 Scotian Shelf Data

All data from the Scotian Shelf were collected during the Canadian Atlantic Storms Programme (CASP) experiment. The goal of the programme (Anderson and Smith, 1989) was to generate a comprehensive data set that would describe the response of the coastal ocean to severe winter weather. Coastal sea level, bottom pressure and moored current meter data were collected from late November 1985 to early April 1986. Here, only the two month period from the beginning of January to the end of February has been used. Table A.2 shows the tide gauge locations and the period that was covered. Table A.3 shows the bottom pressure and current meter locations. All of the locations listed in Table A.3 had moored current meters and bottom pressures. However, at locations 3 and 4, the pressure sensors did not work properly. An example of alongshore current meter records is shown in Figure A.5.

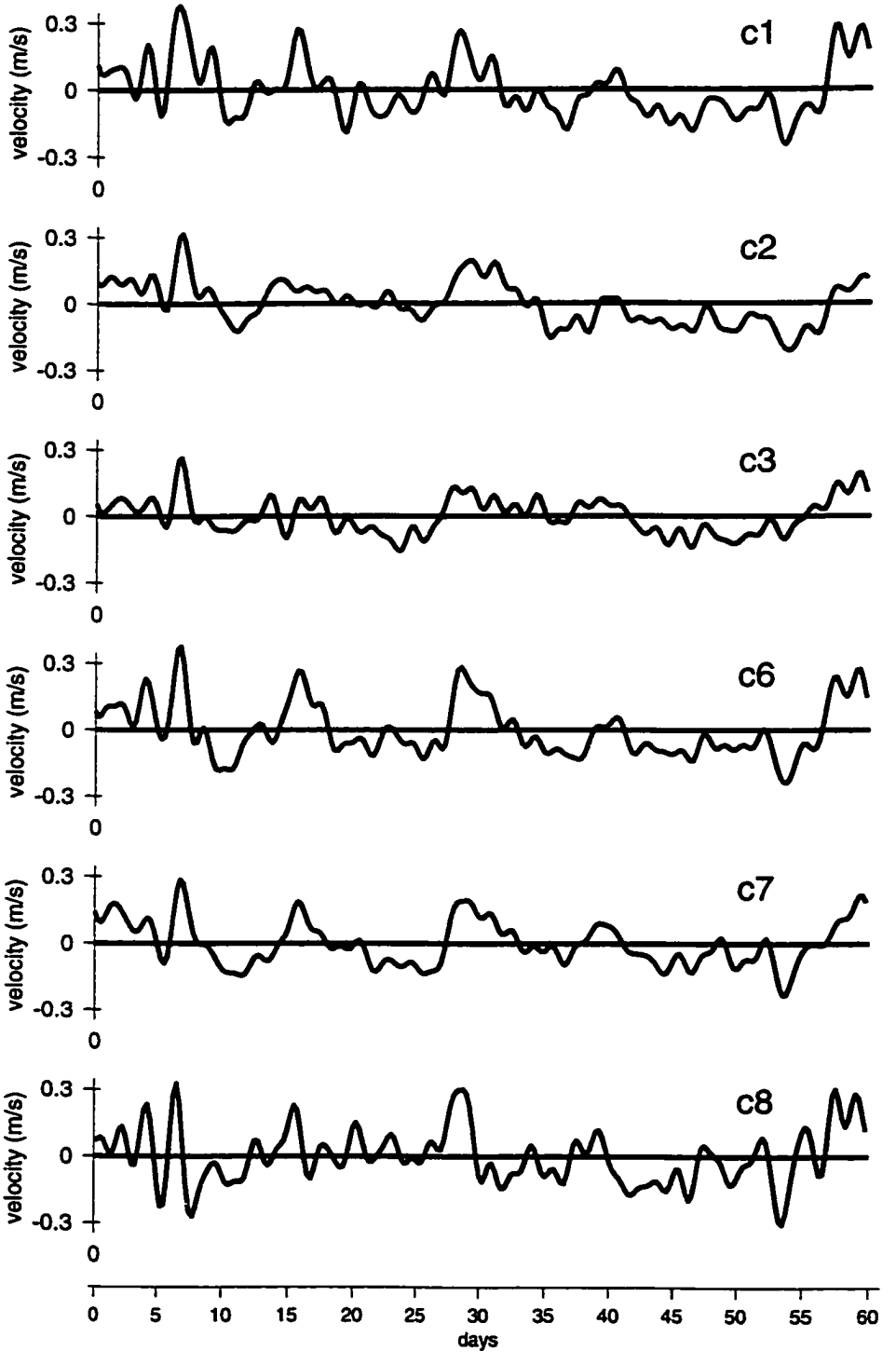

Figure A.5: Time series of observed alongshore (angle of 45°) currents on the Scotian Shelf. The period covered is January and February 1987.

Location	No.	Latitude	Longitude	Period
Louisbourg	13	-60.00	45.91	Nov 24 - Apr 6
Temp-1	14	-61.25	45.25	Nov 24 - Apr 6
Temp-2	15	-62.75	44.83	Nov 24 - Apr 6
Sambro	16	-63.83	44.50	Nov 24 - Apr 6
Temp-3	17	-64.41	44.33	Nov 24 - Apr 6
Cape Sable	18	-65.58	43.58	Nov 24 - Apr 6

Table A.2: Coastal sea level data locations from the Scotian Shelf. Columns are: station number, latitude, longitude and period covered.

Location	P/C	Latitude	Longitude	Period
1	P+C	-63.07	44.49	Nov 28 - Apr 4
2	P+C	-62.99	44.33	Nov 28 - Apr 4
3	C	-62.91	44.24	Nov 28 - Apr 4
4	C	-62.91	44.16	Nov 28 - Apr 4
5	P+C	-63.24	44.24	Nov 28 - Apr 4
6	P+C	-62.82	44.49	Nov 28 - Apr 4
7	P+C	-62.49	44.49	Nov 28 - Apr 4
8	P+C	-61.82	44.83	Nov 28 - Apr 4
9	P+C	-61.82	44.49	Nov 28 - Apr 4
10	P+C	-62.74	43.83	Nov 28 - Apr 4

Table A.3: Bottom pressure and current meter locations from the Scotian Shelf. Columns are: station number, pressure gauge or current meter, latitude, longitude and period covered.

Appendix B

Data Assimilation and Regression

This appendix provides an interpretation of data assimilation in terms of regression. In Chapter 3 the dynamical model is presented together with the assimilation scheme that is used to infer the open boundary conditions. The cost function that describes the discrepancy between the model results ($\hat{y}_i$) and the observations (y_i), weighted by w_{ij}, is defined by

$$J = \frac{1}{2}\sum_{i,j}(y_i - \hat{y}_i)w_{ij}(y_j - \hat{y}_j) \tag{B.1}$$

The sea level at a forcing boundary is defined by

$$\eta(t,\lambda,\phi) = \sum_i \alpha_i(t)\Psi_i(\lambda,\phi) \tag{B.2}$$

where Ψ_i is fixed in time, as discussed in Chapter 3. The amplitudes $\alpha_i(t)$ are defined by

$$\alpha_i(t) = \sum_p \beta_{ip}\omega_p(t) \tag{B.3}$$

The optimal choice of controls β minimizes the cost function J. Following the procedure described by Thompson and Griffin (1997), discretisation of the governing equations (3.13) leads to the following generalized time stepping form

$$x_n = \mathbf{B}_1 x_{n-1} + \mathbf{B}_2 \beta_n \tag{B.4}$$

where x_n is the state vector at time n, β_n is the forcing at the same time step, and $\mathbf{B}_1$ and $\mathbf{B}_2$ are dynamical matrices that depend on the governing equations (3.13). The model starts from rest ($x_0 = 0$), so it can be simplified to the following form

$$\mathbf{D}_1 x = \mathbf{D}_2 \beta \tag{B.5}$$

where x and β are vectors of stacked x_n and β_n vectors, respectively, and $\mathbf{D}_1$ and $\mathbf{D}_2$ are large sparse matrices that consist of $\mathbf{B}_1$ and $\mathbf{B}_2$ as diagonal and off-diagonal elements. If matrix $\mathbf{H}$ maps the state to the observations, the prediction vector $\hat{y}$ becomes

$$\hat{y} = \mathbf{H}\mathbf{D}_1^{-1}\mathbf{D}_2 \beta \tag{B.6}$$

If we define $\mathcal{X} = \mathbf{H}\mathbf{D}_1^{-1}\mathbf{D}_2$ then $\hat{y} = \mathcal{X}\beta$. In terms of classical regression, the observation vector y is represented by

$$y = \mathcal{X}\beta + \epsilon \tag{B.7}$$

and the optimal estimator in the least square sense for β is given by:

$$\hat{\beta} = (\mathcal{X}' \Sigma_\epsilon^{-1} \mathcal{X})^{-1} \mathcal{X}' \Sigma_\epsilon^{-1} y \tag{B.8}$$

where Σ_ϵ is the error covariance matrix. In principal, the problem is solved because β provides the solution that minimizes the discrepancy between the model and the observations, measured by J and Σ_ϵ^{-1}. The only technical problem are sizes of the matrices $\mathbf{D}_1$ and $\mathbf{D}_2$. Turning back to the cost function, the optimal choice for β minimizes J and its gradient at arbitrary β is given by

$$\frac{\partial J}{\partial \beta} = \mathbf{D}_2' a \tag{B.9}$$

where

$$\mathbf{D}_1' a = -\mathbf{H}' \Sigma_\epsilon^{-1} \tag{B.10}$$

The above expression can be written in time stepping form

$$a_{n-1} = \mathbf{B}_1' a_n + \theta_n \tag{B.11}$$

where the forcing θ_n is the appropriate column of the matrix $\mathbf{H}' \Sigma_\epsilon^{-1}$ and the a_n are generalized Lagrange multipliers at time n. The gradient of J with respect to β is thus calculated by running the model of the form (B.11) backwards in time to obtain a. The equation (B.11) or the, so called, adjoint model is usually derived using Lagrangian multipliers in the constrained minimization. (The details of the derivation of the adjoint system are given in the Appendix C.) Once the gradient of the cost function is obtained a minimization method is used to update the controls of the system. In this case I use the linear conjugate gradient algorithm (Gill et al., 1981) that requires one run of the dynamical model and one run of the adjoint model to update the controls (β) and the cost function (J). The procedure iterates as described and illustrated in Chapter 3.

Appendix C

Adjoint Model Derivation

In this appendix the derivation of the adjoint model is described. The adjoint model is used to minimize the cost function J subject to the strong constraint that model variables u, v and η obey the discretised form of the governing equations (3.13). This is done by appending the left-hand side of equations (3.13) multiplied by a set of Lagrangian multipliers U, V and E to the cost function J (Thacker, 1988) to form a Lagrangian L for every time step and grid point

$$
\begin{aligned}
L \;=\; & J + \sum_{n=1}^{Nt} \\
& [\sum_{i=1}^{Nl}\sum_{j=1}^{Nf} E^n_{i,j}[\eta^{n+1}_{i,j} - \eta^n_{i,j} + \frac{\Delta t}{R\cos\phi_j \Delta\lambda}(u^n_{i+1,j}h^{\lambda}_{i+1,j} - u^n_{i,j}h^{\lambda}_{i,j}) + \\
& \frac{\Delta t}{R\Delta\phi}(v^n_{i,j+1}h^{\phi}_{i,j+1}\cos\phi_{j+1} - v^n_{i,j}h^{\phi}_{i,j}\cos\phi_j)] + \\
& \sum_{i=1}^{Nl+1}\sum_{j=1}^{Nf} U^n_{i,j}[u^{t+1}_{i,j}\delta^{\lambda}_{i,j} - \Delta t[u^t_{i,j} - (f_j\overline{v^n_{i,j}} - \frac{g}{R\cos\phi_j\Delta\lambda}(\eta^{n+1}_{i,j} - \eta^{n+1}_{i-1,j}) + \frac{\tau^{\lambda,n}_{i,j}}{\rho h^{\phi}_{i,j}})]] + \\
& \sum_{i=1}^{Nl}\sum_{j=1}^{Nf+1} V^n_{i,j}[v^{t+1}_{i,j}\delta^{\phi}_{i,j} - \Delta t[v^t_{i,j} - (-\Delta t f_j\overline{u^n_{i,j}} - \frac{g\Delta t}{R\Delta\phi}(\eta^{n+1}_{i,j} - \eta^{n+1}_{i,j-1}) + \frac{\tau^{\phi,n}_{i,j}}{\rho h^{\phi}_{i,j}})]]]
\end{aligned}
\tag{C.1}
$$

and $h^{\lambda}_{i,j}, h^{\phi}_{i,j}, \delta^{\lambda}_{i,j}, \delta^{\phi}_{i,j}$ are defined by

$$h^{\lambda}_{i,j} = (h_{i,j} + h_{i-1,j})/2$$

$$h^{\phi}_{i,j} = (h_{i,j} + h_{i,j-1})/2$$

$$\delta^{\lambda}_{i,j} = (1 + \frac{r\Delta t}{h^{\lambda}_{i,j}})$$

$$\delta^{\phi}_{i,j} = (1 + \frac{r\Delta t}{h^{\phi}_{i,j}})$$

and $\overline{u^n_{i,j}}$ and $\overline{v^n_{i,j}}$ represent four point averaged velocities used to compute the Coriolis term in the momentum equations (details of the $\overline{u^n_{i,j}}$ and $\overline{v^n_{i,j}}$ computation are standard and therefore considered unimportant for this derivation). Subscripts denote longitudinal and latitudinal indices and superscripts denote time. Differentiating (C.1) with respect to U, V and E returns the original model equations (3.13). Differentiation with respect to u, v and η yields a new set of time stepping equations for U, V and E that form the adjoint model (B.11) that is integrated backwards in time. The differentiation with respect to dynamical variables (u, v, η) at interior points of the model yields:

$$U^{n-1}_{i,j}\delta^{\lambda}_{i,j} - [U^n_{i,j} - \frac{1}{R\cos\phi_j}\frac{\Delta t}{\Delta\lambda}[E^n_{i,j} - E^n_{i-1,j}]h^{\lambda}_{i,j} - \Delta t\overline{V^n_{i,j}}] + \frac{\Delta t}{\sigma_u^2}(u^n_{obsi,j} - u^n_{i,j}) = 0 \tag{C.2}$$

$$V^{n-1}_{i,j}\delta^{\phi}_{i,j} - [V^n_{i,j} - \frac{\Delta t}{R\Delta\phi}[E^n_{i,j} - E^n_{i,j-1}]h^{\phi}_{i,j} + \Delta t\overline{U^n_{i,j}}] + \frac{\Delta t}{\sigma_v^2}(v^n_{obsi,j} - v^n_{i,j}) = 0 \tag{C.3}$$

$$E^{n-1}_{i,j} - E^n_{i,j} + \frac{g}{R\cos\phi_j}\frac{\Delta t}{\Delta\lambda}[U^{n-1}_{i,j} - U^{n-1}_{i+1,j}] + \frac{g}{R}\frac{\Delta t}{\Delta\phi}[V^{n-1}_{i,j} - V^{n-1}_{i,j+1}] + \frac{\Delta t}{\sigma_\eta^2}(\eta^n_{obsi,j} - \eta^n_{i,j}) = 0 \tag{C.4}$$

where $\overline{U^n_{i,j}}$ and$\overline{V^n_{i,j}}$ are four point averages of the Lagrangian multipliers for U and V that come as a result of the Coriolis term averages in the momentum equations. As mentioned in Appendix A, the adjoint equations are forced by the model errors, i.e. terms like $\frac{\Delta t}{\sigma_\eta^2}(\eta^n_{obsi,j} - \eta^n_{i,j})$. The integration is carried backwards in time from Nt to 1, and the order of the equations is reversed, i.e. first $U^{n-1}_{i,j}$ and $V^{n-1}_{i,j}$ are updated and then $E^{n-1}_{i,j}$.

Once the Lagrangian multipliers (U,V and E) are obtained, the gradient of the cost function can be calculated using the procedure described in Appendix B.

References

Akaike, H., 1974, A new look at the statistical model identification, IEEE Transactions on Automatic Control, AC-19, 6, 716-723

Anderson, C., and P.C. Smith, 1989, Oceanographic observations on the Scotian Shelf during CASP, Atmosphere-Ocean, 27, 130-156

Bennett, A.F., and P.C. McIntosh, 1982, Open ocean modelling as an inverse problem: Tidal theory, Journal of Physical Oceanography, 12, 1004-1018

Bennett, A.F., 1992, Inverse methods in physical oceanography, Cambridge University Press, New York, 346 pp

Bogden, P.S., P. Malanotte-Rizzoli, and R. Signell, 1996, Open-ocean boundary conditions from interior data: Local and remote forcing of Massachusetts Bay, Journal of Geophysical Research, 101, 6487-6500

Brink, K., 1991, Coastal-trapped waves and wind-driven currents over the continental shelf, Annu. Rev. Fluid. Mech., 23, 389-412

Chapman, D.C., 1985, Numerical treatment of cross-shelf open boundaries in a barotropic coastal ocean model, Journal of Physical Oceanography, 15, 1060-1075

Church, J.A., H.J. Freeland, and R.L. Smith, 1986, Coastal-trapped waves on the east Australian continental shelf, I, Propagation of modes, Journal of Physical Oceanography, 16, 1929-1943

Csanady, G.T., 1982, Circulation in the coastal ocean, Reidel, Dordrecht, 280pp

Davies, A.M., and R.A. Flather, 1978, Application of numerical models of the North West European continental shelf and the North Sea to the computation of the storm surges of November to December 1973, Deutche Hydrographische Zeitschrift, 14, Hamburg

Davies, A.M., and G.K. Furnes, 1980, Observed and computed M_2 tidal currents in the North Sea, Journal of Physical Oceanography, 10, 237-257

Dawson, W.B., 1907, The currents in Belle-Isle-Strait, Department of Marine Fisheries, Ottawa, 43 p

DeYoung, B., L. Youyu, and R. Greatbatch, 1995, Synoptic bottom pressure variability on the Labrador and Newfoundland continental shelves, Journal of Geophysical Research, 100, 8639-8653

El-Sabh, M.I., 1977, Oceanic features, currents, and transport in Cabot Strait, Journal of Fisheries Research Board Canada, 34, 516-528

Farquharson, W.I., and W.B. Bailey, 1966, Oceanographic study of Belle-Isle Strait 1963, Rep. 66-9, Bedford Inst. Oceanogra. Dartmouth, N.S., 78p

Garrett, C., and B. Petrie, 1981, Dynamical aspects of the flow through the Strait of Belle Isle, Journal of Physical Oceanography, 11, 376-393

Garrett, C., F. Majaess, and B. Toulany, 1985, Sea-level response at Nain, Labrador, to atmospheric pressure and wind, Atmosphere-Ocean, 23, 95-117

Ghil, M. and P. Malanotte-Rizzoli, 1991, Data assimilation in meteorology and oceanography, Adv. Geophys., 33, 141-266

Gill, A.E., 1982, Atmosphere-ocean dynamics, Academic Press, San Diego, 662pp

Gill, A.E., and E.H. Schumann, 1974, The generation of long shelf waves by the wind, Journal of Physical Oceanography, 4, 83-90

Gill, P., W. Murray, and M. Wright, 1981, Practical Optimization, Academic Press, San Diego, 401pp

Godin, G., 1972, The analysis of tides, University of Toronto Press, Toronto, Canada, 246pp

Gratton, Y. Low-frequency vorticity waves over strong topography, Ph.D. Thesis, University of British Columbia, 143 pp.

Gratton, Y., and P.H. LeBlond, 1986, Vorticity waves over strong topography, Journal of Physical Oceanography, 16, 151-166

Greatbatch, R.J., and A. Goulding, 1989, Seasonal variations in a linear barotropic model of

the North Atlantic driven by the Hellerman and Rosenstein wind stress field, Journal of Geophysical Research, 19, 572-595

Greatbatch, R.J., B. deYoung, A. Goulding, and J. Craig, 1990, On the influence of local and North Atlantic wind forcing on the seasonal variation of sea level on the Newfoundland and Labrador Shelf, Journal of Geophysical Research, 95, 5279-5289

Greenberg, D.A., and B.D. Petrie, 1988, The mean barotropic circulation on the Newfoundland Shelf and Slope, Journal of Geophysical Research, 93, 15541-15550

Griffin, D.A. and K.R. Thompson, 1996, The adjoint method of data assimilation-used operationally for shelf circulation, Journal of Geophysical Research, 101, 3457-3472

Heaps, N.S., 1969, A two-dimensional numerical model, Phil. Trans. Roy. Soc. London, 265, 93-137

Hellerman, S., and M. Rosenstein, 1983, Normal monthly wind stress over the world ocean with error estimates, Journal of Physical Oceanography, 13, 1093-1104

Herfst, F.J., 1984, Wind regimes in the St.Lawrence river valley, MSc. thesis, University of Toronto, Toronto, 152 p.

Hukuda, H., R.J. Greatbatch, and A.E. Hay, 1989, A simple three-dimensional model of the circulation off Newfoundland, Journal of Geophysical Research, 94, 12607-12618

Huntsman, A.G., W.B. Bailey, and H.B. Hachey, 1954, The general oceanography of the Strait of Belle Isle, J. Fish. Res. Board. Can, 11, 198-260

Huthnance, J.M., 1975, On trapped waves over a continental shelf, J. Fluid. Mech., 69, 689-704

Koutitonsky, V.G., and G.L. Bugden, 1991, The physical oceanography of the Gulf of St. Lawrence: A review with emphasis on the synoptic variability of the motion, Canadian Special Publication of Fisheries and Aquatic Sciences, 113, 57-90

Lamb, H., 1932, Hydrodynamics, 6th edition, Dover, New York, 738pp

Large, W.G., and S. Pond, 1981, Open ocean momentum flux measurements in moderate strong winds, Journal of Physical Oceanography, 11, 324-336

Lazier, J.R.N., and D.G. Wright, 1993, Annual velocity variations in the Labrador Current, Journal of Physical Oceanography, 23, 659-678

LeBlond, P.H., 1982, Satellite observations of Labrador Current undulation, Atmosphere-Ocean, 20, 129-142, 1982

LeBlond, P.H. and L.A. Mysak, 1978, Waves in the Ocean, 2nd edition, Elsevier, New York, 602pp

Lynch, D.R., Naimie C.E., and Werner F.E., 1996, Comprehensive coastal circulation model with application to the Gulf of Maine, Continental Shelf Research, 16, 875-906

Middleton, J.F., 1991, Coastal-trapped wave scattering into and out of straits and bays, Journal of Physical Oceanography, 21, 681-694

Middleton, J.F., and D.G. Wright, 1988, Shelf wave scattering due to a longshore jump in topography, Journal of Physical Oceanography, 18, 230-242

Middleton, J.F., and D.G. Wright, 1989, Coastally trapped waves on the Labrador Shelf, Can. Tech. Rep. Hydrog. Ocean Sci., 116, Department of Fisheries and Oceans, Ottawa

Middleton, J.F., and D.G. Wright, 1991, Coastally trapped waves on the Labrador Shelf, Journal of Geophysical Research, 96, 2599-2617

Miles, J.W., 1971, Resonant response of harbours: An equivalent-circuit analysis, J. Fluid. Mech., 46, 241-265

Murty, T.S., and J.D. Taylor, 1970, A numerical calculation of the wind-driven circulation in the Gulf of St. Lawrence, J. Oceanogr. Soc. Japan, 26, 203-214

Murty, T.S., 1984, Storm surges: meteorological ocean tides, Can. Bull. Fish. Acquat. Sci., 212, 897pp

Mysak, L.A., 1980, Topographically trapped waves, Annu. Rev. Fluid. Mech., 12, 45-78

Mysak, L.A., 1986, Elliptical topographic waves, Geophys. Astrophys. Fluid Dynamics, 31, 91-135

Nechaev, D.A. and M.I. Yaremchuk, 1994, Conductivity-temperature-depth data assimilation into a three-dimensional quasi-geostrophic open ocean model, Dynamics of Atmospheres and Oceans, 21, 137-165

Narayanan, S., Prinsenberg S., and Smith, P.C., 1996, Current meter observations from the

Labrador and Newfoundland Shelves and comparisons with barotropic model predictions and IIP surface currents, Atmosphere-Ocean, 34, 227-255

Petrie, B., B.J. Topliss, and D.G. Wright, 1987, Coastal upwelling and eddy development off Nova Scotia, Journal of Geophysical Research, 29, 12979-12991

Petrie, B., B. Toulany, and C. Garrett, 1988, The transport of water, heat and salt through the Strait of Belle Isle, Atmosphere-Ocean, 26, 234-251

Platzman, W.G., 1972, Two-dimensional free oscillations in natural basins, Journal of Physical Oceanography, 2, 117-138

Rao, D.B., 1966, Free gravitational oscillations in rotating rectangular basins, J. Fluid Mech., 25, 523-555

Sarkisyan, A.S., and V.F. Ivanov, 1971, The combined effect of baroclinicity and bottom relief as an important factor in the dynamics of ocean currents, Izv. Acad. Sci. USSR, Atmos. Oceanic Phys., 173-188 (AGU translation)

Saunders, P.M., 1977, Wind stress on the ocean over the eastern continental shelf of North America, Journal of Physical Oceanography, 7, 555-566

Schwing, F.B., 1989, Subtidal response of the Scotian Shelf bottom pressure field to meteorological forcing, Atmosphere-Ocean, 27, 157-180

Schwing, F.B., 1992, Subtidal response of Scotian Shelf circulation to local and remote forcing. Part II: Barotropic model, Journal of Physical Oceanography, 22, 542-563

Scott, J.T., and G.T. Csanady, 1976, Nearshore currents off Long Island, Journal of Geophysical Research, 81, 5401-5409

Sheng, J., and K.R. Thompson, 1993, A modified Galerkin-spectral model for three dimensional, barotropic, wind-driven shelf circulation, Journal of Geophysical Research, 98, 7001-7022

Sheng, J., and K.R. Thompson, 1996, Summer surface circulation on the Newfoundland Shelf and Grand Banks: The roles of local density gradients and remote forcing, Atmosphere-Ocean, 34, 257-284

Sheng, J., and K.R. Thompson, 1997, 3-D data assimilative model for the Scotian Shelf, in preparation

Smith, E.H.F., M. Soule, and O. Mosby, 1937, The Marion and General Green expeditions to Davis Strait and Labrador Sea, Bull. U.S. Coast Guard, 19, 259 pp

Smith, P.C., 1983, The mean and seasonal circulation off southwest Nova Scotia, Journal of Geophysical Research, 4079-4096

Smith, P.C., B. Petrie, and C.R. Mann, 1978, Circulation, variability and salinity off southwest Nova Scotia, Canadian Journal of Fisheries and Aquatic Sciences, 46 (Suppl. 1), 4-20

Smith, P.C., and F.B. Schwing, 1991, Mean circulation and variability on the eastern Canadian continental shelf, Continental Shelf Research, 11, 977-1012

Thacker, W.C., 1988, Fitting models to inadequate data by enforcing spatial and temporal smoothness, Journal of Geophysical Research, 93, 10655-10665

Thacker, W.C., and R.B. Long, 1988, Fitting dynamics to data, Journal of Geophysical Research, 93, 1227-1240

Thompson, K.R., J.R.N. Lazier, and B. Taylor, 1986, Wind-forced changes in Labrador Current transport, Journal of Geophysical Research, 91, 14261-14268

Thompson, K.R., and J. Sheng, 1996, Subtidal circulation on the Scotian Shelf: Assessing the performance of a linear barotropic model, Journal of Geophysical Research, submitted

Trites, R.W., 1972, The Gulf of St. Lawrence from a pollution point of view, p. 59-72, In: Marine pollution and Sea life, FAO, Fishing News Books, London

Wang, D-P., 1982, Effects of continental slope on the mean shelf circulation, Journal of Physical Oceanography, 12, 1524-1526

Webster, I., and S. Narayanan, 1988, Low-frequency current variability on the Labrador Shelf, Journal of Geophysical Research, 93, 8163-8173

Wright, D.G., D.A. Greenberg, and F.G. Majaess, 1987, The influence of bays on adjusted sea level over adjacent shelves with application to the Labrador Shelf, Journal of Geophysical Research, 92, 14610-14620

Wright, D.G., J.R.N. Lazier, and W. Armstrong, 1988, Moored current and pressure data from the Labrador/Newfoundland Shelf, June 1985 - July 1997, Can. Tech. Rep.

Hydrog. Ocean Sci. 62, Department of Fisheries and Oceans, Ottawa, 258pp

Wright, D.G., D.A. Greenberg, and J.F. Middleton, 1991, Statistical estimates and dynamical interpretations of bottom pressure variability over the Labrador/Newfoundland Shelf, Can. Tech. Rep. Hydrog. Ocean Sci. 131, Department of Fisheries and Oceans, Ottawa, 60pp

IMAGE EVALUATION
TEST TARGET (QA-3)

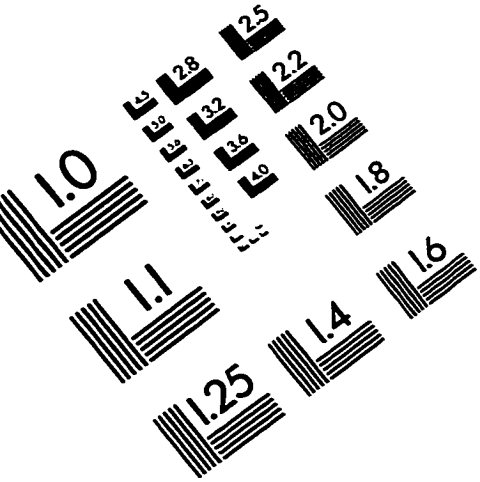

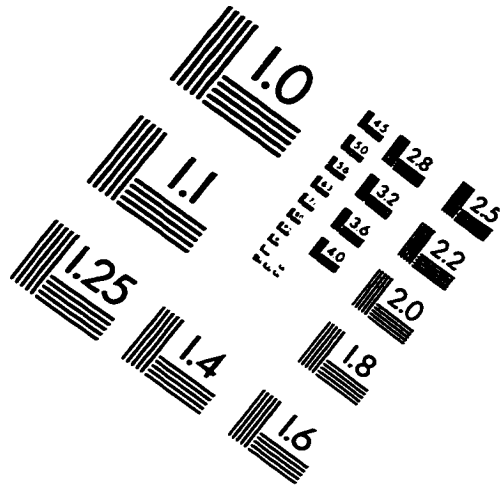

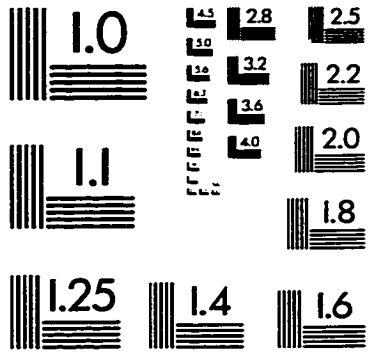

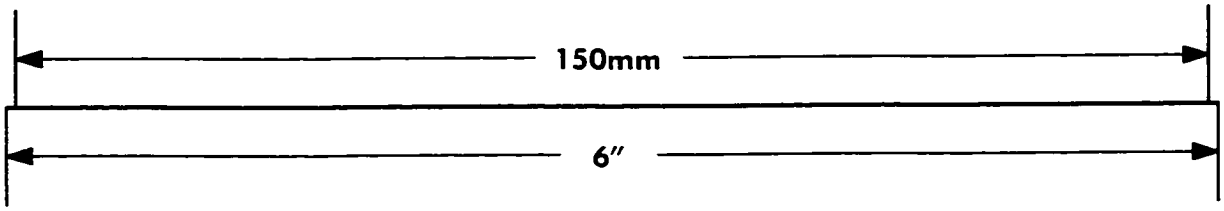

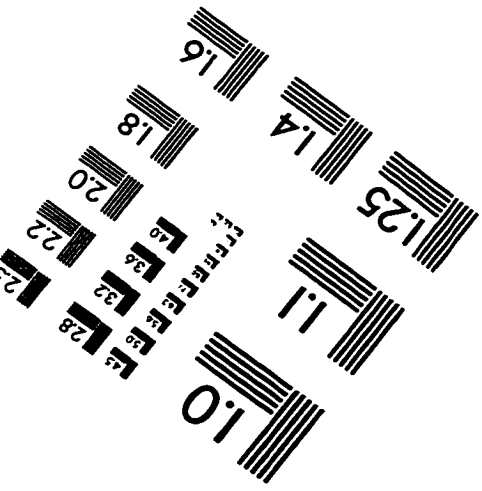

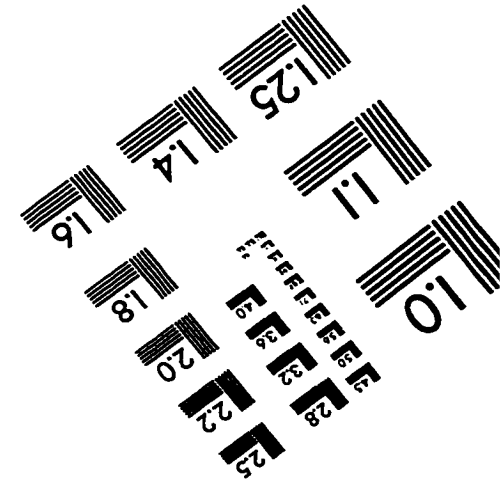

APPLIED IMAGE, Inc
1653 East Main Street
Rochester, NY 14609 USA
Phone: 716/482-0300
Fax: 716/288-5989

© 1993, Applied Image, Inc., All Rights Reserved